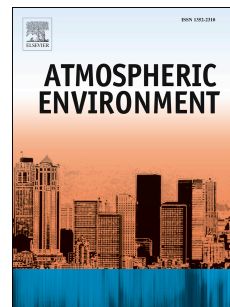


# Journal Pre-proof



The contribution of global aviation to anthropogenic climate forcing for 2000 to 2018

D.S. Lee, D.W. Fahey, A. Skowron, M.R. Allen, U. Burkhardt, Q. Chen, S.J. Doherty, S. Freeman, P.M. Forster, J. Fuglestedt, A. Gettelman, R.R. De León, L.L. Lim, M.T. Lund, R.J. Millar, B. Owen, J.E. Penner, G. Pitari, M.J. Prather, R. Sausen, L.J. Wilcox

PII: S1352-2310(20)30568-9

DOI: <https://doi.org/10.1016/j.atmosenv.2020.117834>

Reference: AEA 117834

To appear in: *Atmospheric Environment*

Received Date: 9 February 2020

Revised Date: 2 July 2020

Accepted Date: 30 July 2020

Please cite this article as: Lee, D.S., Fahey, D.W., Skowron, A., Allen, M.R., Burkhardt, U., Chen, Q., Doherty, S.J., Freeman, S., Forster, P.M., Fuglestedt, J., Gettelman, A., De León, R.R., Lim, L.L., Lund, M.T., Millar, R.J., Owen, B., Penner, J.E., Pitari, G., Prather, M.J., Sausen, R., Wilcox, L.J., The contribution of global aviation to anthropogenic climate forcing for 2000 to 2018, *Atmospheric Environment* (2020), doi: <https://doi.org/10.1016/j.atmosenv.2020.117834>.

This is a PDF file of an article that has undergone enhancements after acceptance, such as the addition of a cover page and metadata, and formatting for readability, but it is not yet the definitive version of record. This version will undergo additional copyediting, typesetting and review before it is published in its final form, but we are providing this version to give early visibility of the article. Please note that, during the production process, errors may be discovered which could affect the content, and all legal disclaimers that apply to the journal pertain.

© 2020 Published by Elsevier Ltd.

**Author Contributions**

**D. S. Lee, D. W. Fahey**

Role: Investigation, Methodology, Writing–review & editing, Data curation; Formal analysis, Project administration, Supervision

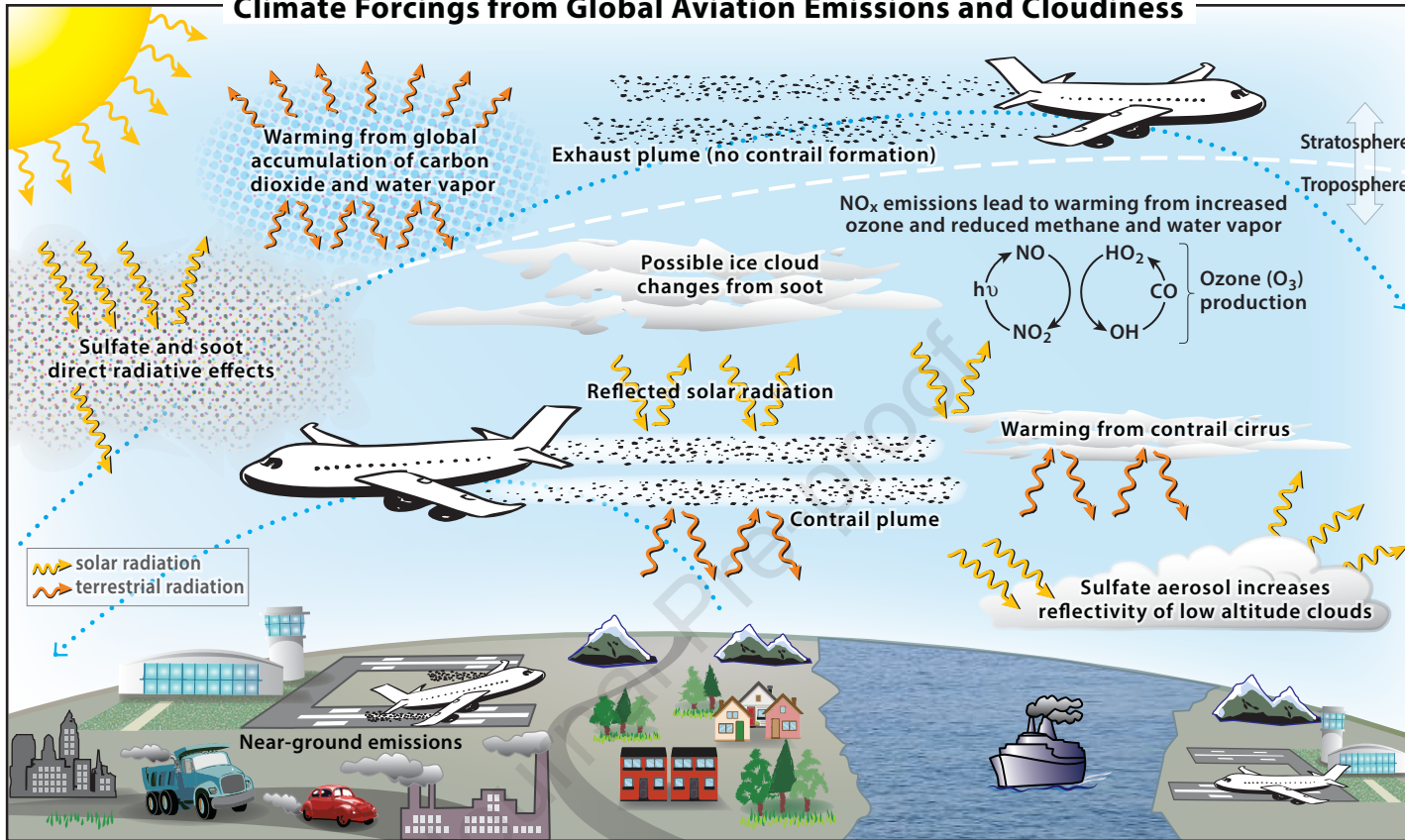
**A. Skowron**

Role: Investigation, Methodology, Writing–review & editing, Data curation, Formal analysis; Software

**M. R. Allen, U. Burkhardt, Q. Chen, S. J. Doherty, S. Freeman, P.M. Forster, J. Fuglestedt, A. Gettelman, R. R. De León, L. L. Lim, M. T. Lund, R. J. Millar, B. Owen, J. E. Penner, G. Pitari, M. J. Prather, R. Sausen, L. J. Wilcox**

Role: Writing–review & editing, Investigation, Methodology, Writing–original draft, Data curation; Formal analysis;

### Climate Forcings from Global Aviation Emissions and Cloudiness



Jet Engine Combustion	Exhaust Plumes	Plume Composition	
<p><b>Air:</b> nitrogen (N<sub>2</sub>) + oxygen (O<sub>2</sub>)</p> <p><b>Kerosene fuel:</b> carbon (C<sub>n</sub>), hydrogen (H<sub>x</sub>), sulfur, aromatics</p>	<p><b>No contrail formation</b></p> <p><b>Contrail formation in low-temperature ice-supersaturated air</b></p>	<p><b>Gases</b></p> <p>Carbon dioxide (CO<sub>2</sub>)</p> <p>Nitrogen oxides (NO<sub>x</sub>)</p> <p>Carbon monoxide (CO)</p> <p>Water vapor (H<sub>2</sub>O)</p> <p>Sulfur compounds</p> <p>Unburned hydrocarbons (HC)</p>	<p><b>Aerosol Particles</b></p> <p>Cloud condensation nuclei</p> <p>Ice nuclei</p> <p>Contrail ice</p> <p>Others</p>

1 July 2020 Revised

1 The contribution of global aviation to anthropogenic climate forcing for 2000 to  
2 2018

3  
4 D. S. Lee<sup>a,1</sup>, D. W. Fahey<sup>b</sup>, A. Skowron<sup>a</sup>, M. R. Allen<sup>c,n</sup>, U. Burkhardt<sup>d</sup>, Q. Chen<sup>e</sup>, S. J. Doherty<sup>f</sup>, S.  
5 Freeman<sup>a</sup>, P.M. Forster<sup>g</sup>, J. Fuglested<sup>h</sup>, A. Gettelman<sup>i</sup>, R. R. De León<sup>a</sup>, L. L. Lim<sup>a</sup>, M. T. Lund<sup>h</sup>, R. J.  
6 Millar<sup>c,o</sup>, B. Owen<sup>a</sup>, J. E. Penner<sup>j</sup>, G. Pitari<sup>l</sup>, M. J. Prather<sup>k</sup>, R. Sausen<sup>d</sup>, L. J. Wilcox<sup>m</sup>

7  
8 <sup>a</sup>Faculty of Science and Engineering, Manchester Metropolitan University, John Dalton Building, Chester Street,  
9 Manchester M1 5GD, United Kingdom;

10 <sup>b</sup>NOAA Chemical Sciences Laboratory (CSL), Boulder, CO USA;

11 <sup>c</sup>School of Geography and the Environment, University of Oxford, Oxford, UK;

12 <sup>d</sup>Deutsches Zentrum für Luft- und Raumfahrt (DLR), Institut für Physik der Atmosphäre, Oberpfaffenhofen,  
13 Germany;

14 <sup>e</sup>State Key Joint Laboratory of Environmental Simulation and Pollution Control, College of Environmental Sciences  
15 and Engineering, Peking University, Beijing 100871, China;

16 <sup>f</sup>Cooperative Institute for Research in Environmental Sciences (CIRES), University of Colorado, Boulder, CO,  
17 USA;

18 <sup>g</sup>School of Earth and Environment, University of Leeds, Leeds LS2 9JT, United Kingdom;

19 <sup>h</sup>CICERO—Center for International Climate Research—Oslo, PO Box 1129, Blindern, 0318 Oslo, Norway;

20 <sup>i</sup>National Center for Atmospheric Research, Boulder, CO, USA;

21 <sup>j</sup>Department of Climate and Space Sciences and Engineering, University of Michigan, 2455 Hayward St., Ann  
22 Arbor, MI 48109-2143, USA;

23 <sup>k</sup>Department of Earth System Science, University of California, Irvine, 3329 Croul Hall, CA 92697-3100, USA;

24 <sup>l</sup>Department of Physical and Chemical Sciences, Università dell'Aquila, Via Vetoio, 67100 L'Aquila, Italy;

25 <sup>m</sup>National Centre for Atmospheric Science, Department of Meteorology, University of Reading, Earley Gate,  
26 Reading RG6 6BB, UK;

27 <sup>n</sup> also at the Department of Physics, University of Oxford, Oxford, UK;

28 <sup>o</sup> also at the Committee on Climate Change, 151 Buckingham Palace Road, London, SW1W 9SZ, UK.

29  
30 <sup>1</sup>To whom correspondence should be addressed. Email: [d.s.lee@mmu.ac.uk](mailto:d.s.lee@mmu.ac.uk) Tel: +44 161 247 3663

31

1 July 2020 Revised

## 32 **Highlights**

- 33 • Global aviation warms Earth's surface through both CO<sub>2</sub> and net non-CO<sub>2</sub> contributions.
- 34 • Global aviation contributes a few percent to anthropogenic radiative forcing.
- 35 • Non-CO<sub>2</sub> impacts comprise about 2/3 of the net radiative forcing.
- 36 • Comprehensive and quantitative calculations of aviation effects are presented.
- 37 • Data are made available to analyze past, present and future aviation climate forcing.

## 39 **Abstract**

40 Global aviation operations contribute to anthropogenic climate change via a complex set of processes that  
41 lead to a net surface warming. Of importance are aviation emissions of carbon dioxide (CO<sub>2</sub>), nitrogen  
42 oxides (NO<sub>x</sub>), water vapor, soot and sulfate aerosols, and increased cloudiness due to contrail formation.  
43 Aviation grew strongly over the past decades (1960–2018) in terms of activity, with revenue passenger  
44 kilometers increasing from 109 to 8269 billion km yr<sup>-1</sup>, and in terms of climate change impacts, with CO<sub>2</sub>  
45 emissions increasing by a factor of 6.8 to 1034 Tg CO<sub>2</sub> yr<sup>-1</sup>. Over the period 2013–2018, the growth rates  
46 in both terms show a marked increase. Here, we present a new comprehensive and quantitative approach  
47 for evaluating aviation climate forcing terms. Both radiative forcing (RF) and effective radiative forcing  
48 (ERF) terms and their sums are calculated for the years 2000 to 2018. Contrail cirrus, consisting of linear  
49 contrails and the cirrus cloudiness arising from them, yields the largest positive net (warming) ERF term  
50 followed by CO<sub>2</sub> and NO<sub>x</sub> emissions. The formation and emission of sulfate aerosol yields a negative  
51 (cooling) term. The mean contrail cirrus ERF/RF ratio of 0.42 indicates that contrail cirrus is less  
52 effective in surface warming than other terms. For 2018 the net aviation ERF is +100.9 milliwatts (mW)  
53 m<sup>-2</sup> (5–95% likelihood range of (55, 145)) with major contributions from contrail cirrus (57.4 mW m<sup>-2</sup>),  
54 CO<sub>2</sub> (34.3 mW m<sup>-2</sup>), and NO<sub>x</sub> (17.5 mW m<sup>-2</sup>). Non-CO<sub>2</sub> terms sum to yield a net positive (warming) ERF  
55 that accounts for more than half (66%) of the aviation net ERF in 2018. Using normalization to aviation  
56 fuel use, the contribution of global aviation in 2011 was calculated to be 3.5 (4.0, 3.4) % of the net  
57 anthropogenic ERF of 2290 (1130, 3330) mW m<sup>-2</sup>. Uncertainty distributions (5%, 95%) show that non-  
58 CO<sub>2</sub> forcing terms contribute about 8 times more than CO<sub>2</sub> to the uncertainty in the aviation net ERF in  
59 2018. The best estimates of the ERFs from aviation aerosol-cloud interactions for soot and sulfate remain  
60 undetermined. CO<sub>2</sub>-warming-equivalent emissions based on global warming potentials (GWP\* method)  
61 indicate that aviation emissions are currently warming the climate at approximately three times the rate of  
62 that associated with aviation CO<sub>2</sub> emissions alone. CO<sub>2</sub> and NO<sub>x</sub> aviation emissions and cloud effects  
63 remain a continued focus of anthropogenic climate change research and policy discussions.

64 **Key words:** | aviation | contrail cirrus | climate | radiative forcing | CO<sub>2</sub> | NO<sub>x</sub> |

65 **Dedication:** This paper is dedicated to the memory of Professor Ivar S. A. Isaksen of the University of  
66 Oslo, whose scientific excellence, friendship, and mentorship is sorely missed.

## 68 **1. Introduction**

69 Aviation is one of the most important global economic activities in the modern world. Aviation emissions  
70 of CO<sub>2</sub> and non-CO<sub>2</sub> aviation effects result in changes to the climate system (**Figure 1**). Both aviation  
71 CO<sub>2</sub> and the sum of quantified non-CO<sub>2</sub> contributions lead to surface warming. The largest contribution to  
72 anthropogenic climate change across all economic sectors comes from the increase in CO<sub>2</sub> concentration,  
73 which is the primary cause of observed global warming in recent decades (IPCC, 2013; 2018). Aviation  
74 contributions involve a range of atmospheric physical processes, including plume dynamics, chemical  
75 transformations, microphysics, radiation, and transport. Aggregating these processes to calculate changes  
76 in a greenhouse gas component or a cloud radiative effect is a complex challenge for contemporary

1 July 2020 Revised

77 atmospheric modeling systems. Given the dependence of aviation on burning fossil fuel, its significant  
78 CO<sub>2</sub> and non-CO<sub>2</sub> effects, and the projected fleet growth, it is vital to understand the scale of aviation's  
79 impact on present-day climate forcing.

80 Historically, estimating aviation non-CO<sub>2</sub> effects has been particularly challenging. The primary  
81 (quantified) non-CO<sub>2</sub> effects result from the emissions of NO<sub>x</sub>, along with water vapor and soot that can  
82 result in contrail formation. Aviation aerosols are small particles composed of soot (black and organic  
83 carbon (BC/OC)) and sulfur (S) and nitrogen (N) compounds. The largest positive (warming) climate  
84 forcings adding to that of CO<sub>2</sub> are those from contrail cirrus and from NO<sub>x</sub>-driven changes in the chemical  
85 composition of the atmosphere (Lee et al., 2009 (L09)). L09 estimated that in 2005, aviation CO<sub>2</sub>  
86 radiative forcing (RF (Wm<sup>-2</sup>)) was 1.59% of total anthropogenic CO<sub>2</sub> RF and that the sum of aviation CO<sub>2</sub>  
87 and non-CO<sub>2</sub> effects contributed about 5% of the overall net anthropogenic forcing.

88 Understanding of aviation's impacts on the climate system has improved over the decade since the last  
89 comprehensive evaluation (L09), but remains incomplete. Published studies of aviation contributions to  
90 climate change generally focus on one or a few ERF terms. For example, about 20 studies are cited here  
91 that quantify the contribution from global NO<sub>x</sub> emissions. In contrast, only a few studies have addressed  
92 the net RF from global aviation (IPCC, 1999; Sausen et al., 2005; L09). A more recent study updated  
93 some aviation terms without providing a net RF (Brasseur et al., 2016). Here, a comprehensive analysis of  
94 individual aviation ERFs is undertaken in order to provide an overall ERF for global aviation, along with  
95 the associated uncertainties, which is an analysis unavailable elsewhere. This step updates and improves  
96 the analysis of L09. Best estimates of individual aviation ERF terms are derived here for the first time and  
97 combined to provide a net ERF for global aviation. Quantifying the terms required new analyses of CO<sub>2</sub>  
98 and NO<sub>x</sub> ERFs and recalibration of other individual ERFs accounting for factors not previously applied in  
99 a common framework.

100 In L09, the net RF was calculated with and without the full contrail cirrus term but including an estimate  
101 for linear contrails. The exclusion was based on the lack of a best estimate derived from existing studies.  
102 At that time radiative forcing estimates were limited to linear or line-shaped contrails since the modelling  
103 approaches required scaling contrail formation frequency to observed coverage and only satellite  
104 observations of linear contrails existed (Burkhardt et al., 2010). The contrail cirrus term requires the  
105 simulation of the whole contrail cirrus life cycle, starting from persistent linear contrails which spread and  
106 often become later indistinguishable from natural cirrus. Persistent contrail formation requires ice-  
107 supersaturated conditions along a flight track, which are variable in space and time in the troposphere and  
108 tropopause region (Irvine et al., 2013). Estimating the RF from contrail cirrus requires knowledge of  
109 complex microphysical processes, radiative transfer, and the interaction with background cloudiness  
110 (Burkhardt et al., 2010). Contrail cirrus forcing dominates that of persistent linear contrails with the latter  
111 on the order of 10% of the combined forcing (Burkhardt and Kärcher, 2011). In the present study, we  
112 present a best estimate and uncertainty based on the results from global climate models employing  
113 process-based contrail cirrus parameterizations.

114 Emissions of NO<sub>x</sub> from aviation lead to photochemical changes that increase global ozone (O<sub>3</sub>) formation  
115 while decreasing the lifetime and abundance of methane (CH<sub>4</sub>). The changes result in positive and  
116 negative (cooling) RF contributions, respectively. Since L09, improved understanding and modeling  
117 capabilities have emerged, as well as additional RF terms in response to NO<sub>x</sub> emissions, namely a longer-  
118 term decrease in background O<sub>3</sub> and a reduction in H<sub>2</sub>O in the stratosphere in response to decreased CH<sub>4</sub>.  
119 Here, model results are used to calculate the additional RF terms, and to incorporate the updated CH<sub>4</sub>  
120 forcing as assessed by Etminan et al. (2016) and the equilibrium-to-transient corrections for the CH<sub>4</sub> term  
121 (see A4). Finally, aviation-specific efficacies (Appendix C) of the individual NO<sub>x</sub> components are used to  
122 estimate a net NO<sub>x</sub> ERF for the first time.

123 L09 includes best estimates for the RFs resulting from the aerosol-radiation interactions (previously  
124 called direct effects) of soot and sulfate aerosols from aviation. However, no best estimates of RFs from  
125 aerosol-cloud interactions (previously called indirect effects) were available in 2009. Subsequent studies  
126 discussed here have yet to provide a basis for best estimates of ERFs from aviation aerosol-cloud  
127 interactions that may be significant.

128 The primary motivations for the present study are to provide an updated, comprehensive evaluation of  
129 aviation climate forcings in terms of RF and ERF based on new calculations and the normalization of  
130 values from published modeling studies, and to combine the resulting best estimates via a Monte-Carlo  
131 analysis to yield a best estimate for the net ERF for global aviation for the years 2000 to 2018. The three  
132 years 2018, 2011, and 2005 are notable because the year 2018 is the latest year for which air traffic and  
133 fuel use datasets are available, 2011 is the most recent year evaluated for net anthropogenic climate  
134 forcing by the IPCC (IPCC, 2013), and 2005 is the year evaluated in the latest comprehensive aviation  
135 and climate evaluation (L09). By normalizing the calculations across these years, more specific and self-  
136 consistent comparisons can be made of the changes in aviation contributions over time. The normalization  
137 step requires addressing in each study, for example, the choice of air traffic inventory, the integration of  
138 emissions along flight tracks, and the assumed jet-engine emission indices. The new best estimates of  
139 aviation ERF, for example, show that the 2018 value is about 48% larger than the updated 2005 value.

140 In general, previous global aviation climate assessments have made different assumptions concerning  
141 emissions, cloudiness effects, and aviation operations (e.g., IPCC, 1999). Here, our self-consistent set of  
142 component and net aviation ERFs for 2000 to 2018 allows historical and scenario projections of aviation  
143 climate impacts to be assessed in context with other sectors, such as maritime shipping, ground  
144 transportation and energy generation. This updated understanding is especially important given the  
145 potential role of international aviation in meeting the goals of the Paris Agreement (Section 2) on limiting  
146 future temperature increases.

147 The remaining sections address global aviation growth statistics (Section 2); a brief summary of methods  
148 used in the analysis (Section 3); results for the ERF estimates of CO<sub>2</sub>, NO<sub>x</sub>, water vapor, contrail cirrus,  
149 and aerosol-radiation and aerosol-cloud interactions with soot and sulfate (Section 4); results for the net  
150 ERF of global aviation (Section 5); emission metrics (Section 6); and aviation CO<sub>2</sub> vs non-CO<sub>2</sub> forcings  
151 (Section 7). The appendices contain additional detailed information on trends in aviation emissions (App.  
152 A); aviation CO<sub>2</sub> radiative forcing calculations (App. B); radiative forcing, efficacy and ERF definitions  
153 (App. C); aviation NO<sub>x</sub> RF calculations (App. D); contrail cirrus RF scaling factors and uncertainty (App.  
154 E); and emission equivalency metric calculations (App. F). A Supplemental Data (SD) file is provided  
155 containing the interactive spreadsheet used to calculate RFs and ERFs for each aviation term.

## 156 2. Global aviation growth

157 Global aviation fuel use and CO<sub>2</sub> emissions have increased in the last four decades with large growth  
158 occurring in Asia and other developing regions due to the rapid expansion of civil aviation (**Figure 2** and  
159 Appendix A). Looking forward, this pattern of growth is expected to be maintained—for example, of the  
160 1229 orders of Airbus and 1031 orders of Boeing in 2017, 20.3% and 37.5%, respectively, are for airlines  
161 in the Asia region (Airbus, 2017; Boeing, 2018). Airbus projects 41% of orders over the next two decades  
162 to be from the Asia-Pacific region (Airbus, 2017). The uncertainty in this expectation has increased due to  
163 the slowdown in aviation operations in the early months of 2020 due to the COVID-19 pandemic (Le  
164 Quéré et al., 2020). Annual aviation emissions in 2020 are now expected to be below recent projections  
165 that are based on historical growth.

166 A striking feature of **Figure 2a** is the sustained multi-decade growth in CO<sub>2</sub> emissions; the average rate  
167 for the period 1960–2018 is 15 Tg CO<sub>2</sub> yr<sup>-1</sup>. The growth rate for 2013 through 2018 is much larger (44 Tg  
168 CO<sub>2</sub> yr<sup>-1</sup>). The annually averaged growth rate over the period 1970 to 2012 is 2.2% yr<sup>-1</sup> and for 2013 to  
169 2018 is 5% yr<sup>-1</sup> (increase of 27%). In 2018, global aviation CO<sub>2</sub> emissions exceeded 1000 million tonnes

170 per year for the first time (see methodology for scaling 2016 IEA data in Appendix A). The cumulative  
171 emissions of global aviation (1940 to 2018) are 32.6 billion ( $10^9$ ) tonnes of CO<sub>2</sub>, of which approximately  
172 50% were emitted in the last 20 years. Current (2018) CO<sub>2</sub> emissions from aviation represent  
173 approximately 2.4% of anthropogenic emissions of CO<sub>2</sub> (including land use change) (**Figure 2c**).

174 Aviation has grown strongly over time (**Figure 2b**) in terms of available seat kilometers (ASK, a measure  
175 of capacity) and revenue passenger kilometers (RPK, a measure of transport work). Fuel usage and hence  
176 CO<sub>2</sub> emissions have grown at a lesser rate than RPK, reflecting increases in aircraft efficiency derived  
177 from changes in technology, larger average aircraft sizes and increased passenger load factor. Aviation  
178 transport efficiency has improved by approximately eightfold since 1960, to 125 gCO<sub>2</sub> (RPK)<sup>-1</sup>.

179 At present and for some considerable time into the future, aviation growth is likely to be largely  
180 dependent upon the combustion of kerosene fossil fuel (Jet A-1/A) (OECD, 2012), resulting in emission  
181 of CO<sub>2</sub>. Renewable biofuels partially offset fossil fuel emissions but these have yet to be produced in  
182 sufficient quantities to offset growth of fossil fuel use. Furthermore, considerable uncertainties remain  
183 regarding the life-cycle emissions of biofuels, which determine the reductions in net CO<sub>2</sub> emissions (e.g.,  
184 Hari et al., 2015). There are current regulations regarding aviation emissions of CO<sub>2</sub>, NO<sub>x</sub>, and soot mass  
185 and number based on decisions by the International Civil Aviation Organization (ICAO). Under the 2016  
186 Paris climate agreement, nations are committing to limiting future increases in global temperatures with  
187 Nationally Determined Contributions (NDCs) (UNFCCC). Whereas domestic aviation CO<sub>2</sub> emissions are  
188 included in the NDCs, CO<sub>2</sub> emissions from international aviation are not mentioned in the agreement. It  
189 remains open as to whether emissions from international aviation or global emissions beyond greenhouse  
190 gases (e.g., short-lived (non-CO<sub>2</sub>) climate forcers) will be included in future international agreements.

### 191 **3. Methods**

192 The methodologies used to calculate ERF and RF for individual aviation terms are described in this  
193 section, and results of these calculations are given in Section 4. Common to the methodologies is a  
194 comprehensive multi-page spreadsheet (see SD) that begins with a user's guide. The spreadsheet pages  
195 include those for contrail cirrus, CO<sub>2</sub>, NO<sub>x</sub>, H<sub>2</sub>O, and sulfate and soot aerosol, along with CO<sub>2</sub>-equivalent  
196 metrics, ERF probability distributions, ERF time series, and estimates of forcings from aerosol-cloud  
197 effects. The spreadsheet displays the results of aviation forcings provided by individual published studies.  
198 ERF and RF values were calculated for 2018 and other years based on the normalized values of ERF or  
199 RF per unit emission or distance, choice of appropriate emission indices, and times series data on fuel use  
200 and distance travelled. In the case of the contrail cirrus forcing, the flight-track distance was chosen as the  
201 proxy over fuel usage. Annual global emissions are derived from fuel burn by multiplying by the average  
202 emission indices (**Table 1**). The combined and normalized results are used to create sets of RF and ERF  
203 aviation terms for the years 2000 to 2018. In addition to facilitating the present study, the spreadsheet also  
204 provides a quantitative framework for follow-on analyses.

205 Calculations of radiative forcing are expanded here beyond the approach in L09 to include ERF values in  
206 addition to the traditional RF values (**Tables 2 and 3 and Figure 3**). The distinction between ERF and  
207 RF is presented in Appendix C. ERF is the preferred metric for comparing the expected impacts of  
208 climate forcing terms (Myhre et al., 2013). Its use derives from the stronger correlation between ERF and  
209 the change in the equilibrium global-mean surface temperature for some forcing agents than for the  
210 corresponding RF. ERF is calculated as the change in net top-of-the-atmosphere (TOA) downward  
211 radiative flux after allowing for rapid adjustments in atmospheric temperatures, water vapor and clouds  
212 with globally-averaged sea surface and/or land surface temperatures unchanged. ERF is preferred over RF  
213 estimates because the imposed forcing and rapid responses to the forcing cannot always be separately  
214 evaluated, especially for aerosols. In general, the largest differences between ERF and RF are expected  
215 for aerosol-cloud interactions and contrail cirrus (Myhre et al., 2013; Boucher et al., 2013). In calculating  
216 ERF values for 2000-2018, the ERF/RF ratio is assumed to be constant with time.



1 July 2020 Revised

217 Most of the results for the non-CO<sub>2</sub> terms have associated statistics from which the median was chosen as  
218 the best estimate, including the net aviation ERF and RF, and the net non-CO<sub>2</sub> ERF and RF. For CO<sub>2</sub> and  
219 contrail cirrus, for which the sample sizes are small (3, in both cases), the mean was used as the best  
220 estimate. The best estimates of the non-CO<sub>2</sub> terms except contrail cirrus have associated uncertainties  
221 expressed as 5% and 95% confidence intervals calculated from 5, 95% percentile statistics. The  
222 uncertainty distributions for all forcing terms other than CO<sub>2</sub> and contrail cirrus are lognormal and that for  
223 net NO<sub>x</sub> has a discrete probability distribution function (PDF). The uncertainties for the ERF and RF of  
224 CO<sub>2</sub> were taken from IPCC (2013) and fitted with a Monte Carlo analysis with a normal distribution (see  
225 Section 5). The uncertainties for contrail cirrus were estimated partly from expert judgement of the  
226 underlying processes, as described in Appendix E, again fitted with a Monte Carlo analysis with a normal  
227 distribution.

## 228 4. Calculations of ERFs for aviation terms

### 229 4.1. CO<sub>2</sub>.

230 The time series of aviation CO<sub>2</sub> emissions is shown in **Figure 2** as derived from combined kerosene and  
231 avgas usage (UKDS, 2016). Calculating CO<sub>2</sub> concentrations from emissions requires use of a global  
232 carbon-cycle model, which has a range of complexity from a comprehensive Earth system model (ESM)  
233 to a simple climate model (SCM), with the latter being based on a box model or impulse response  
234 function (IRF) model. Three SCMs were used here: LinClim, an IRF model based on Sausen and  
235 Schumann (2000) (Appendix B); the Finite-amplitude Impulse Response (FaIR) model (Millar et al.,  
236 2017); and the CICERO-SCM (Fuglestedt and Berntsen, 1999; Skeie et al., 2017). The performance of  
237 LinClim and CICERO-SCM with respect to aviation emissions is documented in the multi-model  
238 comparison of Khodayari et al. (2013). The CO<sub>2</sub> concentrations attributable to aviation in 2018 based on  
239 LinClim, CICERO-SCM and FaIR are 2.9, 2.4 and 2.4 ppm, respectively, with concentrations nearly  
240 doubling in the last 20 years (see SD spreadsheet). The ERF/RF ratio for CO<sub>2</sub> is assumed to be unity. The  
241 resulting CO<sub>2</sub> ERFs, as derived from global concentrations using standard IPCC expressions (IPCC,  
242 2001), are 38.6, 32.0 and 32.4 mW m<sup>-2</sup>, respectively. With only three model estimates, the average of 34.3  
243 mW m<sup>-2</sup> (5 and 95% percentiles of 29 and 40 mW m<sup>-2</sup>), is chosen as the CO<sub>2</sub> RF best estimate.

### 244 4.2. NO<sub>x</sub>

245 The photochemical effects of aviation NO<sub>x</sub> emissions on the atmospheric abundances of O<sub>3</sub>, CH<sub>4</sub>, carbon  
246 monoxide (CO) and reactive hydrogen (HO<sub>x</sub>) are well established (Fuglestedt et al., 1999). Earlier  
247 studies assessed the short-term increase of O<sub>3</sub> and the longer-term reduction in CH<sub>4</sub> lifetime and  
248 abundance, which yield positive and negative RFs, respectively (IPCC, 1999; Sausen et al., 2005). L09  
249 introduced the concept of the ‘net NO<sub>x</sub>’ effect by combining the two components, extending and updating  
250 the study of Sausen et al. (2005). Later studies expanded the analysis of NO<sub>x</sub> effects to include the long-  
251 term decreases in both O<sub>3</sub> and stratospheric water vapor (SWV) resulting from the CH<sub>4</sub> reduction. Both  
252 effects yield negative RFs (Holmes et al., 2011; Myhre et al., 2011). In the present study, an ensemble of  
253 20 NO<sub>x</sub> studies is assessed to provide NO<sub>x</sub> forcing best estimates based on a wide range of global  
254 atmospheric chemistry/climate models and a broad range of present-day aviation emission inventories  
255 (details in Appendix D and SD spreadsheet). Results from 6 of the studies were adopted from Holmes et  
256 al. (2011).

257 The study ensemble represents various model methodologies in calculating and treating both the short-  
258 term and the long-term NO<sub>x</sub> components. In order to avoid gaps and additional uncertainties, standardized  
259 ERFs were developed that estimated disparate elements (e.g., CH<sub>4</sub> mediated decreases in SWV and long-  
260 term O<sub>3</sub>). Moreover, most of the studies were based upon a parameterization of the CH<sub>4</sub> response that  
261 assumed a full equilibrium response. In order to calculate the transient response for a specific year more  
262 accurately, a correction factor is needed (Myhre et al., 2011). Here, the CH<sub>4</sub> responses for individual  
263 years were calculated (see Appendix D) using the difference between two simulations with differing

1 July 2020 Revised

264 aviation  $\text{NO}_x$  emissions. A number of transient and equilibrium simulations were conducted with a 2D  
265 chemical-transport model to find that the requirement for a correction factor is well supported and that the  
266 2018 value is 0.79 (see Transient vs. equilibrium in Appendix D and Appendix Table D.2). In addition, a  
267 scaling factor (1.23) is applied to derived  $\text{CH}_4$  ERF numbers to account for the effect of shortwave  $\text{CH}_4$   
268 forcing, following Etminan et al. (2016) (see Appendix D). The existence and nature of correlations  
269 between the  $\text{NO}_x$  RF components were also explored (see Correlations in Appendix D and Appendix  
270 Figure D.1) since the degree of correlation between short-term  $\text{O}_3$  and  $\text{CH}_4$  terms was a source of  
271 uncertainty in the calculation of the net- $\text{NO}_x$  forcing in L09. The work of Holmes et al. (2011) supports  
272 the prior assumption of correlation, which is greatly expanded here. Regardless of inter-model  
273 differences, significant correlations are observed; for example, a significant negative correlation ( $p = -0.7$ )  
274 exists between the short-term and the long-term  $\text{NO}_x$  RF components.

275 The normalized sensitivity results for net  $\text{NO}_x$  in units of  $\text{mW m}^{-2} (\text{Tg (N) yr}^{-1})^{-1}$  for the individual  
276 modeling studies are shown in **Figure 4** along with statistical parameters (see Ensemble values in  
277 Appendix D). Given the diversity of studies conducted over nearly two decades, the standard deviations  
278 of the distributions are reasonably small. In contrast, the sign of the net- $\text{NO}_x$  RF obtained from summing  
279 over the 4 component values varies from positive to negative. The spread in  $\text{NO}_x$  RF values is caused by  
280 various factors (e.g., emissions inventories, experimental design or inter-model differences) and is  
281 particularly sensitive to the  $\text{NO}_x$  distribution in the model background troposphere (Holmes et al., 2011).  
282 The  $\text{NO}_x$  efficacies are 1.37 for the short-term ozone increases and 1.18 for methane decreases (Ponater et  
283 al., 2006). The efficacies do not equal the ERF/RF ratios, in general (Ponater et al., 2020; Appendix C);  
284 nonetheless, in the present study, we assume the efficacies and the ERF/RF ratios are equal, in the  
285 absence of better information. The factor of 1.18 was similarly adopted for the  $\text{CH}_4$ -mediated decreases in  
286 long-term ozone and SWV. It is noted that these ratios are from one study and that, in general, the ratio of  
287 ERF to RF for  $\text{CH}_4$  and tropospheric  $\text{O}_3$  are currently the subject of some debate (Smith et al., 2018; Xie  
288 et al., 2016; Richardson et al., 2019). Given the strength of the net effect of the ERF adjustment on the net  
289  $\text{NO}_x$  forcing (more than doubling over its stratosphere-adjusted RF), these ratios warrant further study.

290 The net- $\text{NO}_x$  ERF sensitivity of  $5.5 \pm 8.1 \text{ mW m}^{-2} (\text{Tg (N) yr}^{-1})^{-1}$  yields a 2018 best estimate of 17.5 (0.6,  
291 28.5)  $\text{mW m}^{-2}$ . This best estimate includes the correction factor for non-steady state conditions as well as  
292 the revised formulation of  $\text{CH}_4$  RF (Appendix D).

293 Other potential short-term effects from  $\text{NO}_x$  emissions involve the direct formation of nitrate aerosol and  
294 indirect enhancement of sulfate aerosol. These effects, addressed in a few modelling studies, are  
295 associated with large uncertainties (Righi et al., 2013; Pitari et al., 2017; Unger, 2011). The effects of  
296  $\text{NO}_x$  on aerosol abundances are not further considered here owing to the limited number of studies and the  
297 large associated uncertainties.

#### 298 *4.3. Water vapor emissions.*

299 A large fraction of annual aircraft emissions from the global fleet occurs in the stratosphere, primarily in  
300 the northern hemisphere (Forster et al., 2003). The accumulation of water vapor emissions perturbs the  
301 low background humidity in the lower stratosphere and changes the water vapor radiative balance.  
302 Calculating the water vapor RF is complicated by the sensitivity to the vertical and horizontal distribution  
303 of emissions, seasonal changes in tropopause heights, and short stratospheric residence times. Some  
304 earlier studies do not include the water vapor effect.

305 The water vapor effects were explored in detail (see SD) using results from nine studies: IPCC (1999),  
306 Marquart et al. 2001, Gauss et al. (2003), Ponater et al. (2006), Frömming et al. (2012), Wilcox et al.  
307 (2012), Lim et al. (2015), Pitari et al. (2015) and Brasseur et al. (2016). The reported RFs from these  
308 studies vary from  $0.4 \text{ mW m}^{-2}$  (Wilcox et al., 2012) through  $1.5 \text{ mW m}^{-2}$  (Frömming et al. 2012, Lim et  
309 al., 2015) to  $3.0 \text{ mW m}^{-2}$  (IPCC, 1999). The differences are attributed to the different transport models  
310 used, with some contribution from the different meteorologies in different studies. Normalizing to the

1 July 2020 Revised

311 same emissions and averaging these reported estimates yields a water vapor sensitivity of  $0.0052 \pm$   
312  $0.0026 \text{ mW m}^{-2} (\text{Tg} (\text{H}_2\text{O}) \text{ yr}^{-1})^{-1}$ . Scaling this value linearly to emissions of 382 Tg  $\text{H}_2\text{O}$  yields an ERF  
313 best estimate of 2.0 (0.8, 3.2)  $\text{mW m}^{-2}$  for 2018, which is well within the uncertainty range of the 2005  
314 L09 value of 2.8 (0.39, 20.3)  $\text{mW m}^{-2}$ . The ERF/RF ratio for stratospheric water increases is assumed to  
315 be unity. We have greater confidence in the new estimate and its smaller uncertainty since it is based on  
316 detailed physical studies, rather than a scaling of the earlier IPCC (1999) estimate. The new best estimate  
317 is also in good agreement with the earlier results of Gauss et al. (2003) and Ponater et al. (2006), after  
318 scaling their results to account for emissions differences.

#### 319 4.4. Contrail cirrus.

320 The aviation fleet increases global cloudiness through the formation of persistent contrails when the  
321 ambient atmosphere is supersaturated with respect to ice (IPCC, 1999). Contrail cirrus, consisting of  
322 linear contrails and the cirrus cloudiness arising from them, have cooling (short-wave) and warming  
323 (long-wave) effects, with the effect at night being exclusively warming. In past assessments (e.g., IPCC,  
324 1999; L09), a best estimate was only available for the RF of linear persistent contrails, in part because of  
325 the difficulty of quantifying the cloudiness contribution of aging and spreading contrails (Minnis et al.,  
326 2013). The ERF of contrail cirrus was estimated for 2011 as 50 (20, 150)  $\text{mW m}^{-2}$  by Boucher et al.  
327 (2013). Results of a recent assessment of contrail cirrus and other aviation effects are included here,  
328 although the study did not propose new best estimates (Brasseur et al., 2016).

329 A persistent contrail requires ice-supersaturated conditions along the flight track. Contrail cirrus life  
330 cycles are dependent on the temporal and spatial scales of the ice supersaturated areas, which are highly  
331 variable in the troposphere and tropopause region (e.g., Lamquin et al., 2012; Irvine et al., 2013; Bier et  
332 al., 2017). Estimating the impact of contrail cirrus on upper tropospheric cloudiness requires the  
333 simulation of complex microphysical processes, contrail spreading, overlap with natural clouds, radiative  
334 transfer, and the interaction with background cloudiness (Burkhardt et al., 2010). We present new best  
335 estimates based on the results of global climate models employing process-based contrail cirrus  
336 parameterizations (Appendix E). Due to the small number of independent estimates the uncertainty must  
337 be estimated from the sensitivities of the respective processes and the uncertainty in the underlying  
338 parameters and fields.

339 Here, we consider RF and ERF estimates from global climate models (Burkhardt and Kärcher, 2011;  
340 Bock and Burkhardt, 2016; Chen and Gettelman, 2013; Schumann et al., 2015; Bickel et al., 2019) to  
341 ultimately produce an ERF best estimate. For the present study, the Chen and Gettelman study was  
342 repeated with lower prescribed initial ice-crystal diameters, thereby bringing assumptions in line with  
343 measurements (e.g., Schumann et al., 2017a). Since the RF estimates differ regarding the air traffic  
344 inventory, the measure of air traffic distance (i.e., taking only surface-projected or overall flight distances  
345 into account) and the temporal resolution of the air traffic data, the estimates were homogenized using  
346 known sensitivities (Bock and Burkhardt, 2016) (see Appendix E). Furthermore, the estimates were  
347 corrected to account for the underestimation of the contrail cirrus RF, as calculated by climate models that  
348 use frequency bands, relative to more detailed line-by-line radiative transfer calculations (Myhre et al.,  
349 2009). The Chen and Gettelman (2013) study is closer to a calculation of an ERF, since it accounts for  
350 fast feedbacks on natural clouds, which Bickel et al. (2019) show in their model explains most of the  
351 differences between an ERF and an RF calculation. Bickel et al. (2019) presents an explicit calculation of  
352 the contrail cirrus ERF and uses the same basic model formulation of Bock and Burkhardt, so the ERF  
353 calculation was not used here directly but rather the estimation of the ERF/RF ratio was used.

354 The RF best estimate for 2011 was calculated here for comparison to the most recent IPCC estimate  
355 (Boucher et al., 2013). With each study weighted equally, the resulting 2011 RF best estimate for contrail  
356 cirrus (excluding any adjustments) is approximately 86 (25, 146)  $\text{mW m}^{-2}$  (see **Table 3**). The IPCC best  
357 estimate of 50 (20, 150)  $\text{mW m}^{-2}$  (including the natural cloud feedback) was derived from scaling and

1 July 2020 Revised

358 averaging two studies. IPCC assigned a large uncertainty and low confidence to reflect important aspects  
359 with incomplete knowledge (e.g., spreading rate, optical depth, and radiative transfer). The RF best  
360 estimate derived here for 2018 is 111 (33, 189) mW m<sup>-2</sup>. The uncertainties in the present study are  
361 reduced due to the development of process-based approaches simulating contrail cirrus in recent years.  
362 The uncertainty in the new RF estimate, excluding the uncertainty in the ERF/RF scaling of individual RF  
363 values, is ±70%, a value substantially lower than the factor of three stated in IPCC.

364 The ±70% uncertainty was derived differently than for the NO<sub>x</sub> forcing due to the smaller number of  
365 available studies. Instead, the uncertainty was derived from the combined uncertainties associated with  
366 the processes involved (see Appendix E). The processes fall into two groups: those connected with the  
367 upper tropospheric water budget and the contrail cirrus scheme itself, and those associated with the  
368 change in radiative transfer due to the presence of contrail cirrus. We considered uncertainty in upper  
369 tropospheric ice-supersaturation frequencies and their simulation in global models and the uncertainty of  
370 ice-crystal numbers due to uncertainty in soot-number emissions, ice nucleation within the plume, and  
371 loss processes in the contrail's vortex phase. Finally, an important uncertainty comes from the adjustment  
372 of natural clouds (Burkhardt and Kärcher, 2011). There is also a small uncertainty associated with the  
373 contrail cirrus life cycle, which affects the difference in nighttime and daytime contrail cirrus cover  
374 (Stuber et al., 2006) based on work analyzing the diurnal cycle (Chen and Gettelman, 2013; Newinger  
375 and Burkhardt, 2012).

376 Uncertainty connected with the radiative response to contrail cirrus is largely due to the differences in the  
377 radiation schemes across climate models and the approximations made therein (Myhre et al., 2009;  
378 Gounou and Hogan, 2007); the background cloud field and its vertical overlap with contrail cirrus; and  
379 assumptions about the homogeneity of the contrail cirrus field. Furthermore, the presence of very small  
380 ice crystals (<5µm) (Bock and Burkhardt, 2016) and unknown ice-crystal habits (Markowicz and Witek,  
381 2011) add to the uncertainty.

382 Our best estimate of the contrail cirrus uncertainty does not include the impact of contrails forming within  
383 natural clouds, which was recently shown to be observable from space (Tesche et al., 2016), or the change  
384 in radiative transfer due to soot cores in contrail cirrus ice crystals (Liou et al., 2013), which decreases the  
385 albedo at solar wavelengths and increases the top of atmosphere net RF. Both effects are very likely to  
386 lead on average to an increase in contrail cirrus RF, causing our best estimate to be conservative. The  
387 estimated uncertainty relates to the average contrail cirrus RF. In specific synoptic situations,  
388 uncertainties may be much larger and correlated with each other.

389 In contrast to other aviation forcing terms, the average ERF/RF ratio for contrail cirrus is estimated to be  
390 0.42, much less than unity. The associated uncertainty is thought to be very large and dependent on  
391 prevailing aviation traffic and its geographic distribution. The low ERF/RF value is largely due to the  
392 reduction in natural cloudiness caused by increased contrail cirrus similar to the reduction in natural cirrus  
393 cloudiness as reported by Burkhardt and Kärcher (2011). The ERF/RF value is the average of three global  
394 climate model studies: two that estimated climate efficacies of 31% and 59% (Ponater et al., 2005; Rap et  
395 al., 2010) and a third that gave a direct estimate of the ERF of contrail cirrus that is 35% of the  
396 corresponding RF (Bickel et al., 2019). These studies conclude that efficacies equal to that of CO<sub>2</sub>  
397 overstate the role of cirrus changes due to aviation on global mean surface temperatures. The average  
398 ERF/RF ratio was applied to the homogenized estimates of RF, while the RF of Chen and Gettelman  
399 (2013) was interpreted as an ERF (see above). Weighting each study equally, the resulting ERF for  
400 contrail cirrus is 57 (17, 98) mW m<sup>-2</sup> for 2018. It is important to note that the uncertainty does not include  
401 any contribution coming from the ERF/RF estimate. Despite the large ERF/RF adjustment, this ERF term  
402 is the largest for global aviation in 2018 and is comparable in magnitude to the CO<sub>2</sub> term in the  
403 normalized results for 2000 to 2018 (**Figure 6**). While comparable in magnitude, these ERFs have  
404 different implications for future climate change (Section 6).

405 *4.5. Aerosol-radiation interaction.*

406 Aircraft engines directly emit soot, defined as mixture of BC and OC, and precursors for sulfate ( $\text{SO}_4^{2-}$ )  
407 and nitrate ( $\text{NO}_3^-$ ) aerosol along flight tracks. Soot aerosol is formed from the condensation of unburnt  
408 aromatic compounds in the combustor (e.g. Ebbinghaus and Wiesen, 2001) and sulfate aerosol from the  
409 oxidation of sulfur in the fuel (Dstan 91-91, 2015). Most of the sulfur is emitted as  $\text{SO}_2$ , whilst a small  
410 fraction (~3%) is emitted as oxidized  $\text{H}_2\text{SO}_4$  (Petzold et al., 2005). Most of the sulfate aerosol is produced  
411 after emission from sulfur precursor compounds by oxidation in the ambient atmosphere. Both aerosol  
412 types create RFs from aerosol-radiation interactions: soot absorbs short-wave radiation leading to net  
413 warming and sulfate aerosol scatters incoming short-wave radiation leading to net cooling (IPCC, 1999).  
414 As figures of merit, year 2000 global aviation emissions increase aerosol mass for both soot and sulfate  
415 by a few percent and aerosol number by 10–30% near air traffic flight corridors in the northern  
416 extratropics (Righi et al., 2013).

417 Past calculations of aerosol-radiation RF values using a variety of global aerosol models have yielded  
418 values of a few  $\text{mW m}^{-2}$  and with large uncertainties (e.g., Righi et al., 2013; Gettelman and Chen, 2013;  
419 L09). In the present study, 10 estimates across 8 models were used to evaluate soot and sulfate aerosol  
420 normalized RFs (IPCC, 1999; Sausen et al., 2005; Fuglestedt et al., 2008; Balkanski et al., 2010;  
421 Gettelmann and Chen, 2013; Unger et al., 2013; Pitari et al., 2015; Brasseur et al., 2016) (see SD  
422 spreadsheet). Averaging the normalized values yields a 2018 best estimate of the soot aerosol-radiation  
423 RF of 0.9 (0.1, 4.0)  $\text{mW m}^{-2}$  for 0.0093 Tg soot emitted. The corresponding best estimate for sulfate  
424 aerosol is -7.4 (-19, -3)  $\text{mW m}^{-2}$  for 0.37 Tg  $\text{SO}_2$  emitted. The uncertainties are derived from the standard  
425 deviation of the model values. The ERF/RF ratios for soot and sulfate are assumed to be unity in the  
426 absence of any estimates of this ratio.

427 *4.6 Aerosol-cloud interaction.*

428 Aerosol-cloud interactions are those processes by which aerosols influence cloud formation. For example,  
429 cloud droplets and ice crystals nucleate on aerosol particles. Thus, aerosol-cloud interactions involving  
430 aviation aerosol potentially result in an ERF. Aviation soot and sulfate particles are the predominant  
431 primary and secondary aerosol from aircraft. The uncertainties in evaluating the aerosol-cloud  
432 interactions of aviation soot and sulfate preclude best estimates of ERF contributions. Given the potential  
433 importance of these ERF terms, placeholders are included in **Figure 3**. Furthermore, to promote progress  
434 towards future best estimates, the results of relevant modeling studies were compiled and normalized to  
435 global aviation fuel usages in 2005, 2011, 2018, to a soot emission index, and to a fuel S content of 600  
436 pm (except in the cases of low fuel-S content tests) (see **Figure 5** and spreadsheet). As noted in the  
437 caption of **Figure 5**, some earlier wide-ranging values for the soot aerosol-cloud interaction have been  
438 superseded by a more recent study (Penner et al., 2018).

439 *4.6.1 Sulfate aerosol.*

440 Aviation sulfate aerosol primarily affects liquid clouds in the background atmosphere. Sulfate aerosol is  
441 very efficient as a cloud condensation nuclei (CCN) for liquid clouds, and for promoting homogeneous  
442 freezing of solution particles at cold temperatures, thus nucleating ice clouds. Two integrated model  
443 simulations (Kapadia et al., 2016; Gettelman and Chen, 2013) found large impacts on liquid clouds from  
444 aviation sulfate aerosol that is transported to liquid clouds at lower altitudes over oceans, which have low  
445 albedo. The reported RF values in these studies, when scaled appropriately, are -37 to -76  $\text{mW m}^{-2}$  in  
446 2018, excluding a low fuel-sulfur case. Note that the study of Righi et al. (2013) that yields an RF of -213  
447  $\text{mW m}^{-2}$  in 2018 includes sulfate aerosol-cloud interactions but cannot be directly compared with Kapadia  
448 et al. (2016) and Gettelman and Chen (2013), since the former treats the combined effects of sulfate,  
449 nitrate and particulate organic matter (POM) rather than isolating the effects of sulfate as done in the  
450 latter studies. While these RF estimates do not support a best estimate at present, they do suggest that the  
451 sign of the sulfate aerosol-cloud effect on low-level clouds is likely to be negative (i.e., a cooling), similar

1 July 2020 Revised

452 to the ERF for the aerosol-cloud interactions of other anthropogenic sources of sulfate aerosol (IPCC,  
453 2013).

454 Sulfate aerosol-cloud interaction forcing estimates are highly dependent on the sensitivity (or  
455 susceptibility) of the cloud radiative field to aerosol perturbations, which is dependent on uncertain model  
456 processes and the model background aerosol state. Clouds that form with small CCN number  
457 concentrations in the background atmosphere are more sensitive to CCN perturbations. Forcing by these  
458 cloud effects are largely concentrated near flight corridors over oceans because the high albedo contrast  
459 between the ocean surface and clouds increases forcing sensitivity to CCN perturbations.

460 A large uncertainty was also reported for the magnitude of the aerosol-cloud ERF from all anthropogenic  
461 activities, estimated for 2011 to be  $-450$  ( $-1200$ ,  $0.0$ )  $\text{mW m}^{-2}$  (Myhre et al., 2013). A more recent estimate  
462 of the aerosol-cloud RF from all anthropogenic activities has a 68% confidence interval of  $-650$  to  $-1600$   
463  $\text{mW m}^{-2}$  (Bellouin et al., 2019). In general, aerosol-cloud interactions contribute the largest uncertainty in  
464 calculations of anthropogenic ERF (IPCC, 2013).

#### 465 4.6.2 Soot.

466 The magnitude and the sign of the global RF from aviation soot effects on background cloudiness remain  
467 highly uncertain. The uncertainties center on the difficulties in accurately simulating homogeneous and  
468 heterogeneous ice nucleation in the background atmosphere, variations in the treatment of updraft  
469 velocities during cirrus formation, and the lack of knowledge of the ice nucleating (IN) ability of aviation  
470 soot particles during their atmospheric lifetime (Zhou and Penner, 2014; Penner et al., 2018).

471 Two studies find moderate effects of soot aerosol on ice clouds, depending on the ice nucleating  
472 efficiency and the size distribution. RF values of about  $11$  to  $13$   $\text{mW m}^{-2}$  (normalized to 2018 emissions)  
473 are calculated in some studies for moderate ice-nucleating efficiencies (Pitari et al., 2015, Gettelman and  
474 Chen, 2013).

475 In sensitivity tests, if soot processed within contrails is assumed to be an efficient IN particle, then the RF  
476 may be negative by up to  $-330$   $\text{mW m}^{-2}$  due to reductions in ice crystal number in regions dominated by  
477 homogeneous freezing (Penner et al., 2018; see Figure 5). The RF could be significantly smaller (less  
478 negative) if additional ice-forming particles, such as secondary organic aerosol (SOA), are already present  
479 in the background atmosphere (Penner et al., 2018; Gettelman and Chen, 2013). In addition, increases in  
480 ice crystal numbers occur when the background atmosphere has much lower sulfate or haze-forming  
481 aerosol number concentrations and is dominated by heterogeneous freezing, causing forcings near zero or  
482 even positive (Zhou and Penner, 2014). Other studies predict decreases in cirrus number for smaller  
483 numbers of larger soot particles (Hendricks et al., 2011), resulting in a slight warming (Gettelman and  
484 Chen, 2013).

485 A dominant uncertainty for the aerosol-cloud effect from soot is the IN properties of aviation soot aerosol.  
486 Some laboratory studies indicate soot particles are not efficient ice nuclei (DeMott et al., 1999), while  
487 other studies indicate higher efficiencies (Möhler et al., 2005; Hoose and Möhler, 2012). The possibility  
488 that contrail-processed soot particles would show enhanced IN activity after sublimation in the  
489 background atmosphere was addressed in the laboratory (Mahrt et al., 2020). The effect was limited to  
490 large soot particles, suggesting that the impact of aviation soot on cloudiness may be overestimated in  
491 previous studies that assume soot processed through contrails and not covered by a sulfate coating is an  
492 efficient IN (Penner et al., 2018).

493 Another source of uncertainty is soot number concentrations. For individual engines, the soot number can  
494 vary by two orders of magnitude (Agarwal et al., 2019). Soot number concentrations from aviation vary  
495 with the assumed size of the particles emitted as well as the mass emissions. Soot emissions from aircraft  
496 are set as a regulatory parameter for the landing/take-off (LTO) cycle by ICAO and are measured in terms  
497 of mass. Robust conversion factors from mass to number have recently been developed for the ICAO-

1 July 2020 Revised

498 LTO cycle (Agarwal et al., 2019) but have not yet been made for cruise, although other methodologies  
499 exist (Teoh et al., 2019).

## 500 5. Calculated net aviation ERF and RF values

501 ERF and RF values for the terms associated with global aviation emissions and cloudiness are given in  
502 **Tables 2 and 3**, respectively, for the years 2018, 2011, and 2005, along with uncertainties, sensitivities to  
503 emissions and the ERF/RF ratio for selected terms. ERF values are shown for all years in **Figure 6**. All  
504 ERF and RF values are available in the analysis spreadsheet (SD). Through normalization and scaling, all  
505 2000 to 2018 values are self-consistent. The sensitivity of each term to emission magnitudes or flight  
506 track distances is derived in the normalization process. ERF best estimates and uncertainties (95%  
507 confidence limits) are highlighted for year 2018 in **Figure 3** along with their assessed confidence levels.  
508 No best estimates are included for sulfate and soot aerosol-cloud interactions because of the substantial  
509 uncertainties noted above. However, placeholder spaces are included in both the **Tables 2 and 3** and  
510 **Figure 3** to indicate the potential importance of these terms and to flag the associated knowledge gaps for  
511 consideration in future research and assessment activities. The confidence levels and their justifications  
512 shown in **Figure 3** are obtained by employing the methodology of Mastrandrea et al. (2011), which is  
513 based on evidence and agreement in accordance with IPCC guidance (**Table 4**).

514 In **Figure 3**, contrail cirrus formation yields the largest positive (warming) ERF term, followed by CO<sub>2</sub>  
515 and NO<sub>x</sub> emissions. For the 1940 to 2018 period, the net aviation ERF is +100.9 mW m<sup>-2</sup> (5–95%  
516 likelihood range of (55, 145)) with major contributions from contrail cirrus (57.4 mW m<sup>-2</sup>), CO<sub>2</sub> (34.3  
517 mW m<sup>-2</sup>), and NO<sub>x</sub> (17.5 mW m<sup>-2</sup>). The aerosol and water vapor terms represent minor contributions. The  
518 formation and emission of sulfate aerosol yields the only significant negative (cooling) term. Non-CO<sub>2</sub>  
519 terms sum to yield a positive (warming) ERF that accounts for 66% of the aviation net ERF in 2018 (66.6  
520 (21, 111) mW m<sup>-2</sup>). The application of ERF/RF ratios more than halves the RF value of contrail cirrus  
521 while approximately doubling the NO<sub>x</sub> value. ERF/RF ratios were not included in the L09 analysis.  
522 Uncertainty distributions (5%, 95%) show that non-CO<sub>2</sub> forcing terms contribute about 8 times more than  
523 CO<sub>2</sub> to the uncertainty in the aviation net ERF in 2018. The best estimates of the ERFs from aviation  
524 aerosol-cloud interactions remain undetermined.

525 The time series of ERF values for individual terms is shown in **Figure 6** for the 2000–2018 period.  
526 Through normalization and scaling the terms are self-consistent over this period. The increase in all of the  
527 terms with time is consistent with the growth of aviation fuel burn and CO<sub>2</sub> emissions over the same  
528 period (**Figure 2**). Note that net ERF values shown for each year are not linear sums over the component  
529 terms due to the separate probability distributions associated with each component term in the sum, and  
530 instead are calculated with a Monte Carlo sampling method described below.

531 A comparison of updated RF estimates with L09 values for 2005 is given in **Table 3**. The large increase  
532 in the contrail cirrus RF between 2005 and 2018 results in part because the 2005 value only includes  
533 linear contrails. In L09, only an estimate of 2005 contrail cirrus was provided rather than a best estimate.  
534 The present study now includes a process-based model estimate of the contrail cirrus term (Section 4.4).  
535 The NO<sub>x</sub> treatment in L09 did not include the negative forcing contributions of the long-term O<sub>3</sub> decrease  
536 or the SWV decrease, the updated treatment of CH<sub>4</sub> of Etminan et al. (2016), nor an equilibrium-to-  
537 transient correction. As a result, the updated RF values for NO<sub>x</sub> are approximately a factor of 2 smaller.  
538 Incorporating all the updated information in the RF calculations of the NO<sub>x</sub> and contrail cirrus terms  
539 yields an approximately 30% increase in the net aviation RF for 2005, from 78.0 to 95.2 mW m<sup>-2</sup>. In the  
540 ERF evaluation for 2005 the net aviation forcing is reduced from 95.2 to 66.9 mW m<sup>-2</sup> because the  
541 ERF/RF ratios for NO<sub>x</sub> and contrail cirrus are different than unity.

542 In seeking comparison of net aviation ERF with net anthropogenic ERF, we note that IPCC (Myhre et al.,  
543 2013) provides a value for 1750–2011 of 2290 (1130, 3330) mW m<sup>-2</sup>. The percentage contributions of  
544 aviation to the net ERF in 2011 are 3.5% (4.0, 3.4%) and 1.59% (1.65, 1.56%) for the sum of all terms

1 July 2020 Revised

545 and the CO<sub>2</sub> term alone, respectively. The 2005 and 2018 percentages are likely the same because the  
546 fraction of aviation CO<sub>2</sub> emissions of total anthropogenic CO<sub>2</sub> emissions has averaged 2.1% ( $\pm 0.15$ ) for  
547 the last two decades (see **Figure 2**). Normalized relative probabilities of CO<sub>2</sub> and non-CO<sub>2</sub> ERFs for 2018  
548 as derived from the Monte Carlo simulations show that non-CO<sub>2</sub> uncertainties are the predominant  
549 contribution to the uncertainty in the aviation net ERF (**Figure 7**). IPCC also separately estimated the  
550 contrail cirrus term for 2011 as 50 (20, 150) mW m<sup>-2</sup> as discussed above, which compares well with the  
551 updated value of 44.1 (13, 75) mW m<sup>-2</sup>.

552 The determination of net aviation ERFs and their uncertainties shown in **Figure 3** and accompanying  
553 tables required a Monte Carlo approach to summing over terms with discrete probability distributions. A  
554 similar method was employed in L09. PDFs of each term were constructed from the respective individual  
555 studies as normal, lognormal or discrete distributions (see SD spreadsheet). Monte Carlo samplings (one  
556 million random points) of the individual forcing PDFs were then used to combine terms to yield net ERFs  
557 and the uncertainties (95% likelihood range) for the sum of all terms and for only non-CO<sub>2</sub> terms (**Figure**  
558 **7**). The forcing terms are generally assumed to be independent (uncorrelated) with the notable exception  
559 of the NO<sub>x</sub> component terms which have strong paired correlations as shown in Appendix Figure D.1.  
560 Only the short-term O<sub>3</sub> and CH<sub>4</sub> terms were included in L09 and a 100% correlation was assumed, in part,  
561 because the assumption of uncorrelated effects was deemed less acceptable. A subsequent study showed  
562 that these terms are indeed strongly correlated ( $R^2 = 0.79$ ) (Holmes et al., 2011), similar to the present  
563 results in Appendix Figure D.1. The Holmes et al. (2011) study further concluded that the assumption of  
564 100% correlation in this case would lead to an underestimate of uncertainty in the NO<sub>x</sub> RF. Another  
565 correlation of forcing terms not considered here may be the dependence of the soot direct effect and  
566 contrail properties on the soot number index since ice nucleation at the time of contrail formation depends  
567 on the soot number index (e.g., Kärcher, 2018).

## 568 **6. Emission equivalency metrics**

569 Using the best estimate ERFs, we calculate updated aviation-specific Global Warming Potential (GWP)  
570 and Global Temperature change Potential (GTP) values, presented for 20-, 50-, and 100-year time  
571 horizons in **Table 5**. These metrics assign so-called ‘CO<sub>2</sub>-emission equivalences’ for non-CO<sub>2</sub> emissions  
572 via ratios of time-integrated ERF and changes in future temperatures, respectively. The choice of metric  
573 depends upon the particular underlying application (Fuglestedt et al., 2010) such that there is no  
574 uniquely ‘correct’ metric or time horizon, and alternative metrics are available. GWP and GTP are the  
575 most commonly applied metrics and the values calculated here allow a comparison with previous  
576 estimations (e.g., Lee et al., 2010; Lund et al. 2017). In calculating the GWPs and GTPs, the CO<sub>2</sub> IRF  
577 from Joos et al. (2013) is used and the climate response IRF from Boucher and Reddy (2008) for the  
578 GTPs (see Appendix F for further details about the metrics calculations).

579 GWPs and GTPs for contrail cirrus and for water vapor reported here are similar to, albeit slightly smaller  
580 than, corresponding results previously reported, while soot and sulfate numbers are larger in magnitude  
581 (positive and negative) than previous estimates (Fuglestedt et al. 2010; Lund et al. 2017). The  
582 Fuglestedt et al. (2010) estimates for soot are based on RF due to soot emissions from all sources, not  
583 just aviation, which yields a lower radiative efficiency (i.e., forcing per unit emission) than in the present  
584 study. Also given in **Table 5** are CO<sub>2</sub>-equivalent aviation emissions, along with ratios of total CO<sub>2</sub>-  
585 equivalent emissions to CO<sub>2</sub> emissions. Such ratios are sometimes used as ‘multipliers’ to illustrate the  
586 additional climate impact from aviation non-CO<sub>2</sub> terms over those from CO<sub>2</sub> emissions alone. Here,  
587 estimated multipliers for 2018 range from 1.0 to 4.0 depending on the choice of time horizon and  
588 emission metric. This is broadly consistent with what has been reported and used previously (Lee et al.,  
589 2010). The broad range emphasizes the challenges associated with developing comparisons of emission  
590 equivalences for short- and long-lived climate forcers within a common framework and how such  
591 considerations strongly depend on the chosen perspective.



592 One of the significant uncertainties in calculating GWPs and GTPs is the treatment of climate-carbon (C-  
 593 cycle) feedbacks in the modeling framework. The efficiency of carbon sinks reduces with increasing  
 594 warming (Ciais et al., 2013) and this climate feedback is implicitly included in the Absolute GWP of CO<sub>2</sub>  
 595 through the IRF used (Joos et al., 2013). However, Myhre et al. (2013) highlighted that this introduces an  
 596 inconsistency since the numerators for the GWP and GTP do not include such a climate carbon feedback.  
 597 One of the studies that have proposed ways of addressing this inconsistency is Gasser et al. (2017). They  
 598 show that when the C-cycle feedback is consistently accounted for, the non-CO<sub>2</sub> emission metrics  
 599 increase, but less so than initially suggested by Myhre et al. (2013). They also find that removing the C-  
 600 cycle feedback from both numerator and denominator give similar metric values as including it in both  
 601 places. Using the CO<sub>2</sub> IRF without the C-cycle feedback provided by Gasser et al. (2017), we calculate a  
 602 second set of aviation emission metrics (Table F.1), showing that the changes to the GWP100 and  
 603 GTP100 values from those given in Table 5 are rather small.

604 In response to the challenges related to comparing short-lived and long-lived forcing components, a  
 605 number of new ‘flow-based’ methods have been introduced representing both short-lived and long-lived  
 606 climate forcings explicitly as ‘warming-equivalent’ emissions that have approximately the same impact on  
 607 the global average surface temperature over multi-decade to century timescales (Lauder et al., 2012; Allen  
 608 et al., 2016; 2018; Cain et al., 2019; Collins et al., 2019). A simple version of these methods, known as  
 609 GWP\*, defines the average annual rate of CO<sub>2</sub>-warming-equivalent emissions ( $E_{CO_2e}^*$ ) over a period of  $\Delta t$   
 610 years arising from a particular component of RF or ERF by (Cain et al., 2019):

$$611 \quad E_{CO_2e}^* = [(1 - \alpha)H/AGWP_H] \Delta F / \Delta t + [\alpha/AGWP_H] \bar{F}, \quad (1)$$

612 where  $\Delta F$  is the ERF change and  $\bar{F}$  the average ERF arising from that component over that period,  
 613  $AGWP_H$  is the Absolute GWP of CO<sub>2</sub> (Wm<sup>-2</sup> kg<sup>-1</sup> year) over time-horizon  $H$  and  $\alpha$  is a small coefficient  
 614 depending on the previous history of that RF component. This equation gives the rate of CO<sub>2</sub> emission  
 615 that would, alone, create the same rate of global temperature increase as the combined effect of aviation  
 616 climate forcings. For historically small and/or rapidly changing RF components,  $\alpha$  may be neglected, and  
 617 hence to a good approximation, total CO<sub>2</sub>-warming-equivalent emissions over this period ( $\Delta t E_{CO_2e}^*$ ) are  
 618 approximated by an increase in forcing,  $\Delta F$ , multiplied by  $H/AGWP_H$  (see Appendix A.6), which is about  
 619 1000 GtCO<sub>2</sub> per W/m<sup>2</sup> for  $H$  in the range 20 to 100 years (Myhre et al, 2013; IPCC, 2018, Figure SPM.1,  
 620 caption). This result follows from the definition of AGWP: since all GWP calculations assume a  
 621 linearization, the  $AGWP_H$  is equivalent to the forcing change resulting from the emission of  $H$  tonnes of  
 622 CO<sub>2</sub> spread over  $H$  years (Shine et al, 2005), so  $AGWP_H/H$  is the forcing change per tonne of CO<sub>2</sub>. Under  
 623 the historical profile of increasing global annual aviation-related emissions and associated ERFs, CO<sub>2</sub>-  
 624 warming-equivalent emissions based on GWP\* indicate that aviation emissions are currently warming the  
 625 climate around three times faster than that associated with aviation CO<sub>2</sub> emissions alone (**Table 5**).

626 It is important to note that, unlike the conventional GWP and GTP metrics given in **Table 5**, the ratio  
 627 between total CO<sub>2</sub>-warming-equivalent emissions from all forcing agents and those from CO<sub>2</sub> alone will  
 628 change substantially if future aviation emissions deviate from their current growth trajectory (calculated  
 629 here over the period 2000–2018). If annual global aviation emissions were to stabilize, this ratio declines  
 630 towards unity, as  $\Delta F / \Delta t$  would decline to zero. This does not indicate, however, that the non-CO<sub>2</sub> effects  
 631 do not have a warming affect. This human-induced warming still represents a mitigation potential.  
 632 Warming-equivalent emissions capture the fact that constant emission of short-lived climate forcings  
 633 maintain an approximately constant level of warming, whilst constant emissions of long-lived climate  
 634 forcings, such as CO<sub>2</sub>, continue to accumulate in the atmosphere resulting in a constantly increasing level  
 635 of associated warming. Hence warming-equivalent emissions show that the widely-used assumption of a  
 636 constant ‘multiplier’, assuming that net warming due to aviation is a constant ratio of warming due to  
 637 aviation CO<sub>2</sub> emissions alone, only applies in a situation in which aviation emissions are rising  
 638 exponentially such that the rate of change of non-CO<sub>2</sub> RF is approximately proportional to the rate of CO<sub>2</sub>  
 639 emissions (assuming non-CO<sub>2</sub> RF is proportional to CO<sub>2</sub> emissions, and noting that the rate of change any

640 quantity is proportional to that quantity only when both are growing exponentially). In contrast, under a  
641 future hypothetical trajectory of decreasing aviation emissions, this GWP\* based multiplier could fall  
642 below unity, as a steadily falling rate of emission of (positive) short-lived climate forcers has the same  
643 effect on global temperature as active removal of CO<sub>2</sub> from the atmosphere. The GWP\* based ‘multiplier’  
644 calculated here (which depends on the ratio of the increase in net aviation warming to the increase in  
645 warming due to aviation CO<sub>2</sub> emissions alone over the recent past), should not be applied to future  
646 scenarios that deviate substantially from the current trend of increasing aviation-related emissions. The  
647 broad range of values for a ‘multiplier’ presented here is an illustration of the limitations of using a  
648 constant multiplier in the assessment of climate impacts of aviation, and a reminder that the choice of  
649 metric for such a multiplier involves subjective choices.

## 650 7. Aviation CO<sub>2</sub> vs non-CO<sub>2</sub> forcings

651 Since IPCC (1999), the comparison of aviation CO<sub>2</sub> RF with the non-CO<sub>2</sub> RFs has been a major scientific  
652 topic, as well as a discussion point amongst policy makers and civil society (ICAO, 2019). Aviation as a  
653 sector is not unique in having significant non-CO<sub>2</sub> forcings; the same is true of agriculture with significant  
654 CH<sub>4</sub> and N<sub>2</sub>O emissions, or maritime shipping with net-negative current-day RF despite CO<sub>2</sub> emissions of  
655 a similar magnitude to those from aviation (Fuglesvedt et al., 2009). However, unlike direct emissions of  
656 the greenhouse gases N<sub>2</sub>O and CH<sub>4</sub> from the agricultural sector, aviation non-CO<sub>2</sub> forcings are not  
657 covered by the former Kyoto Protocol. It is unclear whether future developments of the Paris Agreement  
658 or ICAO negotiations to mitigate climate change, in general, will include short-lived indirect greenhouse  
659 gases like NO<sub>x</sub> and CO, aerosol-cloud effects, or other aviation non-CO<sub>2</sub> effects. Aviation is not  
660 mentioned explicitly in the text of the Paris Agreement, but according to its Article 4, total global  
661 greenhouse-gas emissions need to be reduced rapidly to achieve a balance between anthropogenic  
662 emissions by sources and removals by sinks of greenhouse gases in the second half of this century.

663 The IPCC concludes: “*Reaching and sustaining net-zero global anthropogenic CO<sub>2</sub> emissions and*  
664 *declining net non-CO<sub>2</sub> radiative forcing would halt anthropogenic global warming on multi-decadal time*  
665 *scales.*” (IPCC, 2018, bullet A2.2, SPM). Crucially, both conditions would need to be met to halt global  
666 warming. Hence, to halt aviation’s contribution to global warming, the aviation sector would need to  
667 achieve net-zero CO<sub>2</sub> emissions and declining non-CO<sub>2</sub> radiative forcing (unless balanced by net negative  
668 emissions from another sector): neither condition is sufficient alone. Some combination of reductions in  
669 CO<sub>2</sub> emissions and non-CO<sub>2</sub> forcings might halt further warming temporarily, but only for a few years: it  
670 would not be possible to offset continued warming from CO<sub>2</sub> by varying non-CO<sub>2</sub> radiative forcing, or  
671 *vice versa*, over multi-decade timescales.

672 That aviation’s non-CO<sub>2</sub> forcings are not included in global climate policy has resulted in studies as to  
673 whether they could be incorporated into existing policies, such as the European Emissions Trading  
674 Scheme, using an appropriate overall emissions ‘multiplier’; however, scientific uncertainty has so far  
675 precluded this (Faber et al., 2008). In addition, as noted above, the multiplier is highly dependent on the  
676 future emissions scenario (Section 6). Alternatively, proposals have been made to reduce aviation’s non-  
677 CO<sub>2</sub> forcings by, for example, avoiding contrail formation by re-routing aircraft (Matthes et al., 2017), or  
678 optimizing flight times to avoid the more positive (warming) fractional forcings (e.g., by avoiding night  
679 flights, Stuber et al., 2006). There is a developing body of literature on this topic (e.g., Newinger and  
680 Burkhardt, 2012; Yin et al., 2018). Similarly, studies have assessed whether changes in cruise altitudes  
681 could mitigate NO<sub>x</sub> impacts (e.g. Frömming et al., 2012). The potential impacts of changes in technology  
682 have also been examined to reduce the non-CO<sub>2</sub> forcings such as lowering the emission index for NO<sub>x</sub>  
683 (Freeman et al., 2018) or soot particle number emissions (Moore et al., 2017) to reduce net NO<sub>x</sub> and  
684 contrail cirrus forcings, respectively (Burkhardt et al., 2018).

685 Avoidance of contrail formation through re-routing can incur a fuel penalty and therefore additional CO<sub>2</sub>  
686 emissions during a flight, and changes in combustor technology to minimize NO<sub>x</sub> generally increases

1 July 2020 Revised

687 marginal fuel burn and CO<sub>2</sub> emission. Both methods invoke the usage of climate metrics such as those  
688 calculated and presented in Section 6 to evaluate whether there is a net climate benefit or disbenefit over  
689 a defined period. In examining such mitigation scenarios involving tradeoffs (e.g. Teoh et al., 2020), the  
690 perceived success or otherwise of the outcome will be a function of the user's choice of metric and time  
691 horizon. A limitation noted for the GWP is that it has an 'artificial memory' over longer time horizons,  
692 since the integrated-RF nature of the metric accumulates 'signal' over time that the climate system has  
693 'forgotten' (Fuglestedt et al., 2010). The GTP, being an 'end point' metric that captures the temperature  
694 response, overcomes this limitation of the GWP but is not yet in usage within current climate policy.

695 Changes to aviation operations or technology that result in a reduction of a non-CO<sub>2</sub> forcing with the  
696 added consequence of increased CO<sub>2</sub> emissions can result in net reductions of forcing on short timescales  
697 while increasing the net forcing on longer timescales (e.g., Freeman et al., 2018). In a case study of  
698 contrail avoidance through routing changes, Teoh et al. (2019) found that the resultant small increase in  
699 CO<sub>2</sub> emissions still reduces the net forcing over a timescale of 100 years. In such 'tradeoff cases' the  
700 balance between non-CO<sub>2</sub> and CO<sub>2</sub> forcings have to be weighted carefully, since CO<sub>2</sub> accumulates in the  
701 atmosphere and a fraction has millennial timescales (Archer and Brovkin, 2008; IPCC, 2007). Prior to the  
702 COVID-19 pandemic, global aviation traffic and emissions were projected to grow to 2050 (Fleming and  
703 Lepinay, 2019). As the COVID-19 pandemic diminishes, aviation traffic is likely to recover to meet  
704 projected rates on varying timescales (IATA, 2020), with continued growth further increasing CO<sub>2</sub>  
705 emissions. Thus, reducing CO<sub>2</sub> aviation emissions will remain a continued focus in reducing future  
706 anthropogenic climate change, along with aviation non-CO<sub>2</sub> forcings. The latter increase the current-day  
707 impact on global average temperatures by a factor of around 3 (using GWP\*) above that due to CO<sub>2</sub>  
708 alone.

#### 709 **Author Contributions**

710 **D. S. Lee, D. W. Fahey**

711 Role: Investigation, Methodology, Writing–review & editing, Data curation; Formal analysis, Project  
712 administration, Supervision

713 **A. Skowron**

714 Role: Investigation, Methodology, Writing–review & editing, Data curation, Formal analysis;  
715 Software

716 **M. R. Allen, U. Burkhardt, Q. Chen, S. J. Doherty, S. Freeman, P.M. Forster, J. Fuglestedt, A.  
717 Gettelman, R. R. De León, L. L. Lim, M. T. Lund, R. J. Millar, B. Owen, J. E. Penner, G. Pitari,  
718 M. J. Prather, R. Sausen, L. J. Wilcox**

719 Role: Writing–review & editing, Investigation, Methodology, Writing–original draft, Data curation;  
720 Formal analysis;

#### 721 **Declaration of competing interest**

722 The authors declare that they have no known competing financial interests or personal relationships that  
723 could have appeared to influence the work reported in this paper.

#### 724 **Acknowledgements**

725 We gratefully acknowledge discussions with many colleagues during the preparation of this paper, in  
726 particular Andreas Bier and Bernd Kärcher. We acknowledge help with graphical displays from Beth  
727 Tully (Figure 1) and Chelsea R. Thompson (Figures 5, 6 and 7).

#### 728 **Funding**

1 July 2020 Revised

729 DSL, AS, RRdL, LL, BO acknowledge support from the UK Department for Transport. PMF  
730 acknowledges support of the European Union's Horizon 2020 Research and Innovation Programme under  
731 grant agreement number 820829 (CONSTRAIN) by the UK National Environment Research Council  
732 (NERC) SMURPHS project (NE/N006038/1). MRA acknowledges support from the EU H2020 grant  
733 agreement number 821205 (FORCeS) and the Oxford Martin Programme on Climate Pollutants. MTL  
734 and JSF acknowledges support from the Norwegian Research Council (RCN) grant number 300718  
735 (AVIATE), for which DSL and RS have a collaboration agreement. JEP acknowledges support from the  
736 National Science Foundation (NSF 1540954).

### 737 **Data Availability**

738 Supplementary data to this article is a spreadsheet that can be found online at: <https://doi.org/xxxxx>.

739

### 740 **References**

- 741 Airbus, Global Market Forecast 2017–2036 (Airbus, France 2017).
- 742 Allen, M. R. J. S. Fuglestedt, K. P. Shine, A. Reisinger, R. T. Pierrehumbert, and P. M. Forster, New use  
743 of global warming potentials to compare cumulative and short-lived climate pollutants. *Nature Climate*  
744 *Change* 6 (8), 773–776, <https://doi.org/10.1038/nclimate2998> (2016).
- 745 Allen, M. R. K. P. Shine, J. S. Fuglestedt, R. J. Millar, M. Cain, D. J. Frame, A. H. Macey, A solution to  
746 the misrepresentations of CO<sub>2</sub>-equivalent emissions of short-lived climate pollutants under ambitious  
747 mitigation. *npj Climate and Atmospheric Science* 1:16; <https://doi.org/10.1038/s41612-018-0026-8>  
748 (2018).
- 749 Agarwal, A., R. L. Speth, T. M. Fritz, S. D. Jacob, T. Rindlisbacher, R. Iovinelli, B. Owen, R. C. Miake-  
750 Lye, J. S. Sabnis, S. R. H. Barrett, SCOPE11 method for estimating aircraft black carbon mass and  
751 particle number emissions. *Environmental Science and Technology* 53, 1364–1373,  
752 <https://doi.org/10.1021/acs.est.8b04060>, (2019).
- 753 Alfsen, K. H. and T. Berntsen, T., An Efficient and Accurate Carbon Cycle Model for Use in Simple  
754 Climate Models. CICERO, Oslo, Norway, <https://core.ac.uk/reader/52082516>
- 755 Archer, D. and V. Brovkin, The millennial atmospheric lifetime of anthropogenic CO<sub>2</sub>. *Climatic Change*  
756 90, 283–297, <https://doi.org/10.1007/s10584-008-9413-1> (2008).
- 757 Balkanski, Y., G. Myhre, M. Gauss, G. Rädcl, E. J. Highwood, K. P. Shine, Direct radiative effect of  
758 aerosols emitted by transport: from road, shipping and aviation. *Atmospheric Chemistry and Physics*  
759 10(10), 4477–4489, <https://doi.org/10.5194/acp-10-4477-2010> (2010).
- 760 Barrett, S., M. Prather, J. Penner, H. Selkirk, S. Balasubramanian, A. Doppelheuer, G. Fleming, M. Gupta,  
761 R. Halthore, J. Hileman, M. Jacobson, S. Kuhn, S. Lukachko, R. Miake-Lye, A. Petzold, C. Roof, M.  
762 Schaefer, U. Schumann, I. Waitz, R. Wayson R., Guidance on the use of AEDT gridded aircraft emissions  
763 in atmospheric models. Massachusetts Institute for Technology, Laboratory for Aviation and the  
764 Environment, LAE-2010-008-N. (2010)  
765 <http://citeseerx.ist.psu.edu/viewdoc/download?doi=10.1.1.719.2090&rep=rep1&type=pdf>
- 766 Bellouin, N., J. Quaas, E. Gryspeerdt, S. Kinne, P. Stier, D. Watson-Parris, O. Boucher, K.S. Carslaw, M.  
767 Christensen, A.-L. Daniau, J.-L. Dufresne, G. Feingold, Bounding global aerosol radiative forcing of  
768 climate change. *Reviews of Geophysics* 58, e2019RG000660, <https://doi.org/10.1029/2019RG000660>  
769 (2019).
- 770 Bickel, M., M. Ponater, L. Bock, U. Burkhardt, S Reineke, Estimating the effective radiative forcing of  
771 contrail cirrus, *Journal of Climate*, 33, 1991–2005, <https://doi.org/10.1175/JCLI-D-19-0467.1> (2020).

1 July 2020 Revised

- 772 Bier, A., U. Burkhardt, L. Bock, Synoptic control of contrail cirrus life cycles and their modification due  
773 to reduced soot number emissions. *Journal of Geophysical Research Atmospheres* 122 (21), 11,584-  
774 11,603 <https://doi.org/10.1002/2017JD027011> (2017).
- 775 Bier, A. and A. U. Burkhardt, Variability in contrail ice nucleation and its dependence on soot number  
776 emissions. *Journal of Geophysical Research Atmospheres* 124, 3384–3400,  
777 <https://doi.org/10.1029/2018JD029155> (2019).
- 778 Bock, L. and U. Burkhardt, Reassessing properties and radiative forcing of contrail cirrus using a climate  
779 model. *Journal of Geophysical Research Atmospheres* 121, 9717–9736,  
780 <https://doi.org/10.1002/2016JD025112> (2016).
- 781 Boeing, Orders and Deliveries for January 2018, <http://www.boeing.com/commercial/#/orders-deliveries>  
782 (2018).
- 783 Boucher, O. and M. S. Reddy, Climate trade-off between black carbon and carbon dioxide emissions.  
784 *Energy Policy* 36, 193–200, <https://doi.org/10.1016/j.enpol.2007.08.039> (2008).
- 785 Brasseur, G. P., M. Gupta, B. E. Anderson, S. Balasubramanian, S. Barrett, D. Duda, G. Fleming, P. M.  
786 Forster, J. Fuglestedt, et al., Impact of Aviation on Climate: FAA’s Aviation Climate Change Research  
787 Initiative (ACCRI) Phase II. *Bulletin of the American Meteorological Society* 97, 561–583,  
788 <https://doi.org/10.1175/BAMS-D-13-00089.1> (2016).
- 789 Burkhardt, U., B. Kärcher, U. Schumann, Global Modelling of the contrail and contrail cirrus climate  
790 impact. *Bulletin of the American Meteorological Society* 91, 479-484,  
791 <https://doi.org/10.1175/2009BAMS2656.1> (2010).
- 792 Burkhardt, U. and B. Kärcher, Global radiative forcing from contrail cirrus. *Nature Climate Change* 1,  
793 54–58, <https://doi.org/10.1038/nclimate1068> (2011).
- 794 Burkhardt, U., L. Bock, A. Bier, Mitigating the contrail cirrus climate impact by reducing aircraft soot  
795 number emissions. *npj Climate and Atmospheric Science* 1:37, [https://doi.org/10.1038/s41612-018-0046-](https://doi.org/10.1038/s41612-018-0046-4)  
796 4 (2018).
- 797 Cain, M., J. Lynch, M. R. Allen, J. S. Fuglestedt, D. J. Frame, A. H. Macey, Improved calculation of  
798 warming-equivalent emissions for short-lived climate pollutants. *npj Climate and Atmospheric Science*,  
799 2:29, <https://doi.org/10.1038/s41612-019-0086-4> (2019).
- 800 Carlin, B., Q. Fu, U. Lohmann, G. Mace, K. Sassen, J. Comstock, High-cloud horizontal inhomogeneity  
801 and solar albedo bias. *Journal of Climate* 15, 2321–2339, [https://doi.org/10.1175/1520-](https://doi.org/10.1175/1520-0442(2002)015<2321:HCHIAS>2.0.CO;2)  
802 0442(2002)015<2321:HCHIAS>2.0.CO;2 (2002).
- 803 Chen, C.-C., A. Gettelman, C. Craig, P. Minnis, D. P. Duda, Global contrail coverage simulated by  
804 CAM5 with the inventory of 2006 global aircraft emissions. *Journal of Advances in Modeling Earth*  
805 *Systems* 4, 04003. <https://doi.org/10.1029/2011MS000105> (2012).
- 806 Chen, C.-C. and A. Gettelman, Simulated radiative forcing from contrails and contrail cirrus. *Atmospheric*  
807 *Chemistry and Physics*, 13, 12525–12536, <https://doi.org/10.5194/acp-13-12525-2013> (2013).
- 808 Ciais, P., Sabine, C., Bala, G., Bopp, L., Brovkin, V., Canadell, J., Chhabra, A., DeFries, R., Galloway, J.,  
809 Heimann, M., Jones, C., Le Quéré, C., Myneni, R. B., Piao, S., and Thornton, P. Carbon and Other  
810 Biogeochemical Cycles, in: Climate Change 2013: The Physical Science Basis. Contribution of Working  
811 Group I to the Fifth Assessment Report of the Intergovernmental Panel on Climate Change, edited by:  
812 Stocker, T. F., Qin, D., Plattner, G.-K., Tignor, M., Allen, S. K., Boschung, J., Nauels, A., Xia, Y., Bex,  
813 V., and Midgley, P. M., Cambridge University Press, Cambridge, UK and New York, NY, USA (2013)

1 July 2020 Revised

- 814 Clarke, L., J. Edmonds, H. Jacoby, H. Pitcher, J. Reilly, R. Richels, “Scenarios of Greenhouse Gas  
815 Emissions and Atmospheric Concentrations”. Sub-report 2.1A of Synthesis and Assessment Product 2.1  
816 by the U.S. Climate Change Science Program and the Subcommittee on Global Change Research  
817 (Department of Energy, Office of Biological & Environmental Research, Washington, 7 DC. 2007) pp.  
818 54, [https://globalchange.mit.edu/sites/default/files/CCSP\\_SAP2-1a-FullReport.pdf](https://globalchange.mit.edu/sites/default/files/CCSP_SAP2-1a-FullReport.pdf).
- 819 Collins, W. J., D. J. Frame, J. S. Fuglestedt, K. P. Shine, Stable climate metrics for emissions of short  
820 and long-lived species – combining steps and pulses. *Environmental Research Letters* 15(2), 024018,  
821 <https://doi.org/10.1088/1748-9326/ab6039> (2019).
- 822 Creutzig, F., P. Jöcjem, O. Y. Edelenbosch, L. Mattauach, D. P. van Vuuren, D. McCollum, J. Minx,  
823 Transport: a roadblock to climate change mitigation? *Science* 350, 911–912,  
824 <https://doi.org/10.1126/science.aac8033> (2015).
- 825 Dalsøren, S. B., C. L. Myhre, G. Myhre, A. J. Gomez-Pelaez, O. A. Søvde, I. S. A. Isaksen, R. F. Weiss,  
826 C. M. Harth, Atmospheric methane evolution the last 40 years. *Atmospheric Chemistry and Physics* 16,  
827 3099–3126, <https://doi.org/10.5194/acp-16-3099-2016> (2016).
- 828 DeMott, P. J., Y. Chen, S. M. Kreidenweis, D. C. Rogers, D. E. Sherman, Ice formation by black carbon  
829 particles. *Geophysical Research Letters* 26, 2429–2432, <https://doi.org/10.1029/1999GL900580> (1999).
- 830 Derwent, R. G., W. J. Collins, C. E. Johnson, D. S. Stevenson, Transient behaviour of tropospheric ozone  
831 precursors in a global 3-D CTM and their indirect greenhouse effects. *Climatic Change* 49, 463–487,  
832 <https://doi.org/10.1023/A:1010648913655> (2001).
- 833 Dstan 91-91 “Turbine fuel, kerosene type, Jat A-1. Ministry of Defence, Defence Standard 91-91”, Issue  
834 7, Amendment 3. Defence Equipment and Support (UK Defence Standardization, Glasgow, UK, 2015).
- 835 Ebbinghaus, A. and P. Wiesen, Aircraft fuels and their effects upon engine emissions. *Air and Space*  
836 *Europe* 3, 101-103, [https://doi.org/10.1016/S1290-0958\(01\)90026-7](https://doi.org/10.1016/S1290-0958(01)90026-7) (2001).
- 837 Etminan, M., G. Myhre, E. J. Highwood, K. P. Shine, Radiative forcing of carbon dioxide, methane, and  
838 nitrous oxide: A significant revision of the methane radiative forcing. *Geophysical Research Letters* 43,  
839 12,614–12,623 <https://doi.org/10.1002/2016GL071930> (2016).
- 840 Faber, J., D. Greenwood, D. S. Lee, M. Mann, P. M. de Leon, D. Nelissen, B. Owen, M. Ralph, J. Tilston,  
841 A. van Velzen, G. van de Vreede, “Lower NO<sub>x</sub> at higher altitudes: policies to reduce the climate impact of  
842 aviation NO<sub>x</sub> emissions”. (CE-Delft, 08.7536.32, Delft, The Netherlands, 2008).
- 843 Fleming, G. and U. Ziegler, Environmental trends in aviation to 2050. In ‘ICAO Environmental Report,  
844 2016’, International Civil Aviation Organization, Montreal. (2016) [https://www.icao.int/environmental-](https://www.icao.int/environmental-protection/Documents/EnvironmentalReports/2019/ENVReport2019_pg17-23.pdf)  
845 [protection/Documents/EnvironmentalReports/2019/ENVReport2019\\_pg17-23.pdf](https://www.icao.int/environmental-protection/Documents/EnvironmentalReports/2019/ENVReport2019_pg17-23.pdf)
- 846 Fleming, G. and I. de Lepinay, “Environmental trends in aviation to 2050”, in ICAO Environmental  
847 Report, 2019 Destination Green the Next Chapter, (ICAO Montreal, 2019),  
848 [https://www.icao.int/environmental-](https://www.icao.int/environmental-protection/Documents/EnvironmentalReports/2019/ENVReport2019_pg17-23.pdf)  
849 [protection/Documents/EnvironmentalReports/2019/ENVReport2019\\_pg17-23.pdf](https://www.icao.int/environmental-protection/Documents/EnvironmentalReports/2019/ENVReport2019_pg17-23.pdf) (2019)
- 850 Forster, P.M.d.F. and K. P. Shine, Radiative forcing and temperature trends from stratospheric ozone  
851 changes. *Journal of Geophysical Research* 102, 10841–10855, <https://doi.org/10.1029/96JD03510>  
852 (1997).
- 853 Forster, C., A. Stohl, P. James, V. Thouret, The residence times of aircraft emissions in the stratosphere  
854 using a mean emission inventory and emissions along actual flight tracks. *Journal of Geophysical*  
855 *Research Atmospheres* 108, 8524, <https://doi.org/10.1029/2002JD002515> (2003).

1 July 2020 Revised

- 856 Freeman, S., D. S. Lee, L. L. Lim, A. Skowron, R. R. De León, Trading off aircraft fuel burn and NO<sub>x</sub>  
857 emissions for optimal climate policy. *Environmental Science and Technology* 52, 2498–2505,  
858 <https://doi.org/10.1021/acs.est.7b05719> (2018).
- 859 Friedlingstein, P., P. Cox, R. Betts, L. Bopp, W. von Bloh, V. Brovkin, P. Cadule, S. Doney, M. Eby, I.  
860 Fung, G. Bala, J. John, C. Jones, F. Joos, T. Kato, M. Kawamiya, W. Knorr, K. Lindsay, H. D. Matthews,  
861 T. Raddatz, P. Rayner, C. Reick, E. Roeckner, K.-G. Schnitzler, R. Schnur, K. Strassmann, A. J. Weaver,  
862 C. Yoshikawa and N. Zeng, Climate-carbon cycle feedback analysis: Results from the C<sup>4</sup>MIP model  
863 intercomparison, *Journal of Climate* 19, 3337–3353, <https://doi.org/10.1175/JCLI3800.1> (2006)
- 864 Frömming, C., M. Ponater, K. Dahlmann, V. Grewe, D. S. Lee, R. Sausen, Aviation-induced radiative  
865 forcing and surface temperature change in dependency of the emission altitude. *Journal of Geophysical*  
866 *Research Atmospheres* 117, 9717–9736, <https://doi.org/10.1029/2012JD018204> (2012).
- 867 Fuglestad, J. S. and T. Berntsen, “A simple model for scenario studies of changes in climate, Version  
868 1.0”, (CICERO, Oslo, Norway, 1999) pp. 59, <https://cicero.oslo.no/no/publications/internal/326>.
- 869 Fuglestad, J. S., T. K. Berntsen, I. S. A. Isaksen, H. T. Mao, X. Z. Liang, W. C. Wang, Climatic forcing  
870 of nitrogen oxides through changes in tropospheric ozone and methane; global 3D model studies.  
871 *Atmospheric Environment* 33, 961–977 (1999).
- 872 Fuglestad, J., T. Berntsen, G. Myhre, K. Rypdal, R. B. Skeie Climate forcing from the transport sectors.  
873 *Proceedings of the National Academy of Sciences U.S.A.* 105(2), 454-458,  
874 <https://doi.org/10.1073/pnas.0702958104> (2008).
- 875 Fuglestad, J. S., T. Berntsen, V. Eyring, I. Isaksen, D. S. Lee, R. Sausen, Shipping emissions: from  
876 cooling to warming of climate—and reducing impacts on health. *Environmental Science and Technology*  
877 43, 9057–9062, <https://doi.org/10.1021/es901944r> (2009).
- 878 Fuglestad, J. S., K. P. Shine, T. Berntsen, J. Cook, D. S. Lee, A. Stenke, R. B. Skeie, G. J. M. Velders,  
879 I. A. Waitz, Transport impacts on atmosphere and climate: Metrics. *Atmospheric Environment* 44, 4648–  
880 4677, <https://doi.org/10.1016/j.atmosenv.2009.04.044> (2010).
- 881 Fuglestad, J., J. Rogelj, R. J. Millar, M. Allen, O. Boucher, M. Cain, P. M. Forster, E. Kriegler, D.  
882 Shindell, Implications of possible interpretations of ‘greenhouse gas balance’ in the Paris Agreement.  
883 *Philosophical Transactions of the Royal Society A* 376: 20160445.  
884 <http://dx.doi.org/10.1098/rsta.2016.0445> (2018).
- 885 Gauss, M., I. S. A. Isaksen, S. Wong, W. C. Wang, Impact of H<sub>2</sub>O emissions from cryoplanes and  
886 kerosene aircraft on the atmosphere, *Journal of Geophysical Research Atmospheres* 108 (D10), 4304,  
887 <https://doi.org/10.1029/2002JD002623> (2003).
- 888 Gettelman, A. and C. Chen, The climate impact of aviation aerosols. *Geophysical Research Letters* 40,  
889 2785–2789, <https://doi.org/10.1002/grl.50520> (2013).
- 890 Gounou, A. and R. J. Hogan, A sensitivity study of the effect of horizontal photon transport on the  
891 radiative forcing of contrails. *Journal of the Atmospheric Sciences* 64, 1706–1716,  
892 <https://doi.org/10.1175/JAS3915.1> (2007).
- 893 Gottschaldt, K., C. Voigt, P. Jöckel, M. Righi, R. Deckert, S. Dietmüller, Global sensitivity of aviation  
894 NO<sub>x</sub> effects to the HNO<sub>3</sub>-forming channel of the HO<sub>2</sub> + NO reaction. *Atmospheric Chemistry and Physics*  
895 13, 3003–3025, <https://doi.org/10.5194/acp-13-3003-2013> (2013).
- 896 Grewe, V., and A. Stenke, AirClim: an efficient tool for climate evaluation of aircraft technology.  
897 *Atmospheric Chemistry and Physics* 8, 4621–4639, <https://doi.org/10.5194/acp-8-4621-2008> (2008).

1 July 2020 Revised

- 898 Hansen, J., M. Sato, R. Ruedy, Radiative forcing and climate response. *Journal of Geophysical Research*  
899 *Atmospheres* 102 (D6), 6831–6864, <https://doi.org/10.1029/96JD03436> (1997).
- 900 Hansen, J., and L. Nazarenko Soot climate forcing via snow and ice albedos. *Proceedings of the National*  
901 *Academy of Sciences U.S.A.* 101, 423–428, <https://doi.org/10.1073/pnas.2237157100> (2004).
- 902 Hansen, J., M. Sato, R. Ruedy, L. Nazarenko, A. Lacis, G. A. Schmidt, G. Russell, I. Aleinov, M. Bauer,  
903 S. Bauer, N. Bell, B. Cairns, V. Canuto, M. Chandler, Y. Cheng, A. Del Genio, G. Faluvegi, E. Fleming,  
904 A. Friend, T. Hall, C. Jackman, M. Kelley, N. Kiang, D. Koch, J. Lean, J. Lerner, K. Lo, S. Menon, R.  
905 Miller, P. Minnis, T. Novakov, V. Oinas, Ja. Perlwitz, Ju. Perlwitz, D. Rind, A. Romanou, D. Shindell, P.  
906 Stone, S. Sun, N. Tausnev, D. Thresher, B. Wielicki, T. Wong, M. Yao, S. Zhang, Efficacy of climate  
907 forcings. *Journal of Geophysical Research Atmospheres* 110, D18104.  
908 <https://doi.org/10.1029/2005JD005776> (2005).
- 909 Hari, T. K., Z. Yaakob, N. Binitha, Aviation biofuel from renewable resources: routes, opportunities and  
910 challenges. *Renewable and Sustainable Energy Reviews* 42, 1234–1244  
911 <https://doi.org/10.1016/j.rser.2014.10.095> (2015).
- 912 Hasselmann K., S. Hasselmann, R. Giering, V. Ocana, H. von Storch, Sensitivity study of optimal CO<sub>2</sub>  
913 emission paths using a Simplified Structural Integrated Assessment Model (SIAM). *Climatic Change* 37,  
914 345–386, <https://doi.org/10.1023/A:1005339625015> (1997).
- 915 Hendricks, J., B. Kärcher, U. Lohmann, Effects of ice nuclei on cirrus clouds in a global climate model.  
916 *Journal of Geophysical Research Atmospheres* 116, 2156–2202, <https://doi.org/10.1029/2010JD015302>  
917 (2011).
- 918 Hodnebrog, Ø., T. K. Berntsen, O. Dessens, M. Gauss, V. Grewe, I. S. A. Isaksen, B. Koffi, G. Myhre, D.  
919 Olivié, M. J. Prather, J. A. Pyle, F. Stordal, S. Szopa, Q. Tang P. van Velthoven, J. E. Williams, K.  
920 Ødemark, Future impact of non-land based traffic emissions on atmospheric ozone and OH – an  
921 optimistic scenario and a possible mitigation strategy. *Atmospheric Chemistry and Physics* 11, 11,293–  
922 11,317, <https://doi.org/10.5194/acp-11-11293-2011> (2011).
- 923 Hodnebrog, Ø., T. K. Berntsen, O. Dessens, M. Gauss, V. Grewe, I. S. A. Isaksen, B. Koffi, G. Myhre, D.  
924 Olivié, M. J. Prather, F. Stordal, S. Szopa, Q. Tang, P. van Velthoven, J. E. Williams, Future impact of  
925 traffic emissions on atmospheric ozone and OH based on two scenarios. *Atmospheric Chemistry and*  
926 *Physics* 12, 12,211–12,225, <https://doi.org/10.5194/acp-12-12211-2012> (2012).
- 927 Holmes, C. D., Q. Tang, M. J. Prather, Uncertainties in climate assessment for the case of aviation  
928 NO. *Proceedings of the National Academy of Science U.S.A.* 108(27), 10997–11002,  
929 <https://doi.org/10.1073/pnas.1101458108> (2011).
- 930 Holmes, C. D., M. J. Prather, O. A. Søvde, G. Myhre, Future methane, hydroxyl, and their uncertainties:  
931 key climate and emission parameters for future predictions. *Atmospheric Chemistry and Physics* 13, 285–  
932 302, <https://doi.org/10.5194/acp-13-285-2013> (2013).
- 933 Hoor, P., J. Borken-Kleefeld, D. Caro, O. Dessens, O. Endresen, M. Gauss, V. Grewe, D. Hauglustaine, I.  
934 S. A. Isaksen, P. Jöckel, J. Lelieveld, G. Myhre, E. Meijer, D. Olivié, M. Prather, C. Schnadt-Poberaj, K.  
935 P. Shine, J. Staehelin, Q. Tang, J. van Aardenne, P. van Velthoven, R. Sausen, The impact of traffic  
936 emissions on atmospheric ozone and OH: results from QUANTIFY. *Atmospheric Chemistry and Physics*  
937 9, 3113–3136, <https://doi.org/10.5194/acp-9-3113-2009> (2009).
- 938 Hoose, C. and O. Möhler, Heterogeneous ice nucleation on atmospheric aerosols: a review of results from  
939 laboratory experiments. *Atmospheric Chemistry and Physics* 12, 9817–9854, <https://doi.org/10.5194/acp-12-9817-2012> (2012).



1 July 2020 Revised

- 941 Hough, A. M., The development of a two-dimensional global tropospheric model – 1. The model  
942 transport. *Atmospheric Environment* 23, 1235–1261, [https://doi.org/10.1016/0004-6981\(89\)90150-9](https://doi.org/10.1016/0004-6981(89)90150-9)  
943 (1989).
- 944 Hough, A. M., Development of a two-dimensional global tropospheric model: model chemistry. *Journal*  
945 *of Geophysical Research Atmospheres* 96, 7325–7362, <https://doi.org/10.1029/90JD01327> (1991).
- 946 Irvine, E. A., B. J. Hoskins, K. P. Shine, A Lagrangian analysis of ice-supersaturated air over the North  
947 Atlantic. *Journal of Geophysical Research Atmospheres* 119, 90–100,  
948 <https://doi.org/10.1002/2013JD020251> (2013).
- 949 IATA, Economic Performance of the Airline Industry.  
950 [https://www.iata.org/contentassets/f88f0ceb28b64b7e9b46de44b917b98f/iata-economic-performance-of-](https://www.iata.org/contentassets/f88f0ceb28b64b7e9b46de44b917b98f/iata-economic-performance-of-the-industry-end-year-2018-report.pdf)  
951 [the-industry-end-year-2018-report.pdf](https://www.iata.org/contentassets/f88f0ceb28b64b7e9b46de44b917b98f/iata-economic-performance-of-the-industry-end-year-2018-report.pdf) (2019).
- 952 IATA, Outlook for air travel in the next 5 years, [https://www.iata.org/en/iata-](https://www.iata.org/en/iata-repository/publications/economic-reports/covid-19-outlook-for-air-travel-in-the-next-5-years/)  
953 [repository/publications/economic-reports/covid-19-outlook-for-air-travel-in-the-next-5-years/](https://www.iata.org/en/iata-repository/publications/economic-reports/covid-19-outlook-for-air-travel-in-the-next-5-years/) (2020)
- 954 ICAO (2018) ICAO Carbon Emissions Calculator Methodology, version 11, June 2018,  
955 ([https://www.icao.int/environmental-](https://www.icao.int/environmental-protection/CarbonOffset/Documents/Methodology%20ICAO%20Carbon%20Calculator_v11-2018.pdf)  
956 [protection/CarbonOffset/Documents/Methodology%20ICAO%20Carbon%20Calculator\\_v11-2018.pdf](https://www.icao.int/environmental-protection/CarbonOffset/Documents/Methodology%20ICAO%20Carbon%20Calculator_v11-2018.pdf))  
957 accessed 19-05-2020.
- 958 ICAO, ‘Destination Green the Next Chapter’, ICAO Environmental Report, Montreal,  
959 [https://www.icao.int/environmental-protection/Documents/ICAO-ENV-Report2019-F1-WEB%20\(1\).pdf](https://www.icao.int/environmental-protection/Documents/ICAO-ENV-Report2019-F1-WEB%20(1).pdf)  
960 (2019).
- 961 IEA, International Energy Agency. International Energy Agency Oil Information, 1960-2017. [data  
962 collection]. 12th Edition. UK Data Service. SN: 5187, <http://doi.org/10.5257/iea/oil/2019-1> (2019).
- 963 IPCC (1999), “*Aviation and the Global Atmosphere*”, Intergovernmental Panel on Climate Change  
964 Special Report, J. E. Penner, D. H. Lister, D. J. Griggs, D. J. Dokken, M. McFarland, Eds. (Cambridge  
965 University Press, Cambridge, UK, 1999) [https://www.ipcc.ch/report/aviation-and-the-global-atmosphere-](https://www.ipcc.ch/report/aviation-and-the-global-atmosphere-2/)  
966 [2/](https://www.ipcc.ch/report/aviation-and-the-global-atmosphere-2/).
- 967 IPCC (2001) “Climate Change 2001: The Scientific Basis. Contribution of Working Group I to the Third  
968 Assessment Report of the Intergovernmental Panel on Climate Change”. J.T. Houghton, Y. Ding, D.J.  
969 Griggs, M. Noguer, P.J. van der Linden, X. Dai, K. Maskell and C.A. Johnson (eds). Cambridge  
970 University Press, UK. [https://www.ipcc.ch/site/assets/uploads/2018/07/WG1\\_TAR\\_FM.pdf](https://www.ipcc.ch/site/assets/uploads/2018/07/WG1_TAR_FM.pdf)
- 971 IPCC (2007), “Climate change 2007. “Mitigation of climate change”, in: Contribution of Working Group  
972 III to the Fourth Assessment Report of the Intergovernmental Panel on Climate Change”, B. Metz, O. R.  
973 Davidson, P. R. Bosch, R. Dave, L. A. Meyer, eds (Cambridge University Press, UK)  
974 <https://www.ipcc.ch/report/ar4/wg3/>
- 975 IPCC (2013) “Climate Change 2013: The Physical Science Basis, Contribution of Working Group I to the  
976 Fifth Assessment Report of the Intergovernmental Panel on Climate Change”, T. F. Stocker, D. Qin, G. -  
977 K. Plattner, M. Tignor, S. K. Allen, J. Boschung, A. Nauels, Y. Xia, V. Bex, P. M. Midgley, Eds.  
978 (Cambridge University Press, Cambridge, United Kingdom and New York, NY, USA, 2013).  
979 <https://www.ipcc.ch/report/ar5/wg1/>
- 980 IPCC (2018) “Global Warming of 1.5°C. An IPCC Special Report on the impacts of global warming of  
981 1.5°C above pre-industrial levels and related global greenhouse gas emission pathways, in the context of  
982 strengthening the global response to the threat of climate change, sustainable development, and efforts to  
983 eradicate poverty”, Masson-Delmotte, V., P. Zhai, H.-O. Pörtner, D. Roberts, J. Skea, P.R. Shukla, A.  
984 Pirani, W. Moufouma-Okia, C. Péan, R. Pidcock, S. Connors, J.B.R. Matthews, Y. Chen, X. Zhou, M.I.

1 July 2020 Revised

- 985 Gomis, E. Lonnoy, T. Maycock, M. Tignor, and T. Waterfield (eds), (2018).  
986 <https://www.ipcc.ch/sr15/download/>
- 987 Joos, F., M. Bruno, R. Fink, T. F. Stocker, U. Siegenthaler, C. LeQuéré, J. L. Sarmiento, J.L., An efficient  
988 and accurate representation of complex oceanic and biospheric models for anthropogenic carbon uptake.  
989 *Tellus* 48B, 397e417, <https://doi.org/10.1034/j.1600-0889.1996.t01-2-00006.x> (1996)
- 990 Joos, F., R. Roth, J. S. Fuglestedt, G. P. Peters, I. G. Enting, W. von Bloh, V. Brovkin, E. J. Burke, M.  
991 Eby, N. R. Edwards, T. Friedrich, T. L. Frolicher, P. R. Halloran, P. B. Holden, C. Jones, T. Kleinen, F. T.  
992 Mackenzie, K. Matsumoto, M. Meinshausen, G.-K. Plattner, A. Reisinger, J. Segschneider, G. Shaffer,  
993 M. Steinacher, K. Strassmann, K. Tanaka, A. Timmermann, A. J. Weaver, Carbon dioxide and climate  
994 impulse response functions for the computation of greenhouse gas metrics: a multi-model analysis.  
995 *Atmospheric Chemistry and Physics* 13, 2793–2825, <https://doi.org/10.5194/acp-13-2793-2013> (2013).
- 996 Kapadia, Z. Z., D. V. Spracklen, S. R. Arnold, D. J. Borman, G. W. Mann, K. J. Pringle, S. A. Monks, C.  
997 L. Reddington, F. Benduhn, A. Rap, C. E. Scott, E. W. Butt, M. Yoshioka, Impacts of aviation fuel sulfur  
998 content on climate and human health. *Atmospheric Chemistry and Physics* 16, 10521–10541,  
999 <https://doi.org/10.5194/acp-16-10521-2016> (2016).
- 1000 Kärcher, B., U. Burkhardt, A. Bier, L. Bock, I. J. Ford, The microphysical pathway to contrail formation.  
1001 *Journal of Geophysical Research Atmospheres* 120, 7893–7927, <https://doi.org/10.1002/2015JD023491>  
1002 (2015).
- 1003 Kärcher, B. Formation and radiative forcing of contrail cirrus. *Nature Communications* 9:1824,  
1004 <https://doi.org/10.1038/s41467-018-04068-0> (2018).
- 1005 Khodayari, A., D. J. Wuebbles, S. Olsen, J. S. Fuglestedt, T. Berntsen, M. T. Lund, I. Waitz, P. Wolfe,  
1006 P. M. Forster, M. Meinshausen, D. S. Lee, L. L. Lim, Intercomparison of the capabilities of simplified  
1007 climate models to project the effects of aviation CO<sub>2</sub> on climate. *Atmospheric Environment* 75, 321–328,  
1008 <https://doi.org/10.1016/j.atmosenv.2013.03.055> (2013).
- 1009 Khodayari, A., S. C. Olsen, D. J. Wuebbles, Evaluation of aviation NO<sub>x</sub>-induced radiative forcings for  
1010 2005 and 2050. *Atmospheric Environment* 91, 95–103, <https://doi.org/10.1016/j.atmosenv.2014.03.044>  
1011 (2014a).
- 1012 Khodayari, A., S. Tilmes, S. C. Olsen, D. B. Phoenix, D. J. Wuebbles, J.-F. Lamarque, C.-C. Chen,  
1013 Aviation 2006 NO<sub>x</sub>-induced effects on atmospheric ozone and HO<sub>x</sub> in Community Earth System Model  
1014 (CESM). *Atmospheric Chemistry and Physics* 14, 9925–9939, <https://doi.org/10.5194/acp-14-9925-2014>  
1015 (2014b).
- 1016 Köhler, M. O., G. Rädcl, O. Dessens, K. P. Shine, H. L. Rogers, O. Wild, J. A. Pyle, Impact of  
1017 perturbation of nitrogen oxide emissions from global aviation *Journal of Geophysical Research*  
1018 *Atmospheres* 113, D11305, <https://doi.org/10.1029/2007JD009140> (2008).
- 1019 Köhler, M. O., G. Rädcl, K. P. Shine, H. L. Rogers, J. A. Pyle, Latitudinal variation of the effect of  
1020 aviation NO<sub>x</sub> emissions on atmospheric ozone and methane and related climate metrics. *Atmospheric*  
1021 *Environment* 64, 1–9, <https://doi.org/10.1016/j.atmosenv.2012.09.013> (2013).
- 1022 Lamarque, J.-F., T. C. Bond, V. Eyring, C. Granier, A. Heil, Z. Klimont, D. Lee, C. Liou, A. Mieville,  
1023 B. Owen, M. G. Schultz, D. Shindell, S. J. Smith, E. Stehfest, J. van Aardenne, O. R. Cooper, M.  
1024 Kainuma, N. Mahowald, J. R. McConnell, V. Naik, K. Riahi, D. P. van Vuuren, Historical (1850–2000)  
1025 gridded anthropogenic and biomass burning emissions of reactive gases and aerosols: methodology and  
1026 application. *Atmospheric Chemistry and Physics* 10, 7017–7039, [https://doi.org/10.5194/acp-10-7017-](https://doi.org/10.5194/acp-10-7017-2010)  
1027 2010 (2010).

1 July 2020 Revised

- 1028 Lamquin, N., C. J. Stubenrauch, K. Gierens, U. Burkhardt, H. Smit, A global climatology of upper  
1029 tropospheric ice supersaturation occurrence inferred from the Atmospheric Infrared Sounder calibrated by  
1030 MOZAIC. *Atmospheric Chemistry and Physics* 12, 381–405, <https://doi.org/10.5194/acp-12-381-2012>  
1031 (2012).
- 1032 Lauder, A. R., I. G. Enting, J. O. Carter, N. Clisby, A. L. Cowie, B. K. Henry, M. R. Raupach, Offsetting  
1033 methane emissions — An alternative to emission equivalence metrics. *International Journal of*  
1034 *Greenhouse Gas Control* 12, 419–429, <https://doi.org/10.1016/j.ijggc.2012.11.028> (2012).
- 1035 Lee, D. S., D. Fahey, P. M. Forster, P. J. Newton, R. C. N. Wit, L. L. Lim, B. Owen, R. Sausen, Aviation  
1036 and global climate change in the 21st century. *Atmospheric Environment* 43, 3520–3537  
1037 <https://doi.org/10.1016/j.atmosenv.2009.04.024> (2009).
- 1038 Lee, D. S., G. Pitari, V. Grewe, K. Gierens, J. E. Penner, A. Petzold, M. Prather, U. Schumann, A. Bais,  
1039 T. Berntsen, D. Iachetti, L. L. Lim, R. Sausen, Transport impacts on atmosphere and climate: Aviation.  
1040 *Atmospheric Environment* 44, 4678–4734, <https://doi.org/10.1016/j.atmosenv.2009.06.005> (2010).
- 1041 Le Quéré, C. and 76 others, Global carbon budget 2018. *Earth System Science Data* 10, 2141–2194,  
1042 <https://doi.org/10.5194/essd-10-2141-2018> (2018).
- 1043 Le Quéré, C., R. B. Jackson, M. W. Jones, A. J. P. Smith, S. Abernethy, R. M. Andrew, A. J. De-Goll, D.  
1044 R. Willis, Y. Shan, J. G. Canadell, P. Friedlingstein, F. Creutzig and G. P. Peters, Temporary reduction in  
1045 daily global CO<sub>2</sub> emissions during the COVID-19 forced confinement, *Nature Climate Change*,  
1046 <https://doi.org/10.1038/s41558-020-0797-x> (2020).
- 1047 Lim, L. L., D. S. Lee, B. Owen, A. Skowron, S. Matthes, U. Burkhardt, S. Dietmuller, G. Pitari, G. Di  
1048 Genova, D. Iachetti, I. Isaksen, O. A. Søvde, REACT4C: Simplified mitigation study. TAC-4  
1049 Proceedings, June 22nd to 25th, 2015, Bad Kohlgrub, 181-185,  
1050 [https://www.pa.op.dlr.de/tac/2015/Proceedings\\_of\\_TAC4\\_conference\\_final.pdf](https://www.pa.op.dlr.de/tac/2015/Proceedings_of_TAC4_conference_final.pdf) (2015).
- 1051 Liou, K. N., Y. Takano, Q. Yue, P. Yang, On the radiative forcing of contrail cirrus contaminated by  
1052 black carbon. *Geophysical Research Letters* 40, 778–784, <https://doi.org/10.1002/GRL.50110> (2013).
- 1053 Lund, M. T., B. Aamaas, T. Berntsen, L. Bock, U. Burkhardt, J. S. Fuglestedt, K. P. Shine, Emission  
1054 metrics for quantifying regional climate impacts of aviation. *Earth System Dynamics* 8, 547–563,  
1055 <https://doi.org/10.5194/esd-8-547-2017> (2017).
- 1056 Mahrt, F., K. Kilchhofer, C. Marcolli, P. Grönquist, R. O. David, M. Rösch, U. Lohmann, Z. A. Kanji,  
1057 The impact of cloud processing on the ice nucleation abilities of soot particles at cirrus temperatures.  
1058 *Journal of Geophysical Research* 125, e2019JD030922, <https://doi.org/10.1029/2019JD030922> (2020).
- 1059 Maier-Reimer, E. and K. Hasselmann, Transport and storage of CO<sub>2</sub> in the ocean—An inorganic ocean-  
1060 circulation carbon cycle model. *Climate Dynamics* 2, 63–90, <https://doi.org/10.1007/BF01054491> (1987).
- 1061 Matthes, M., V. Grewe, K. Dahlmann, C. Frömming, E. Irvine, L. Lim, F. Linke, B. Lührs, B. Owen, K.  
1062 Shine, S. Stromatas, H. Yamashita, F. Yin, A concept for multi-criteria environmental assessment of  
1063 aircraft trajectories. *Aerospace* 4 42, <https://doi.org/10.3390/aerospace4030042> (2017).
- 1064 Markowicz, K. M. and M. L. Witek, Simulations of contrail optical properties and radiative forcing for  
1065 various crystal shapes. *Journal of Applied Meteorology and Climatology* 50, 1740–1755,  
1066 <https://doi.org/10.1175/2011JAMC2618.1> (2011).
- 1067 Marquart, S., R. Sausen, M. Ponater, V. Grewe, Estimate of the climate impact of the cryoplanes,  
1068 *Aerospace Science and Technology*, 5, 73-84, [https://doi.org/10.1016/S1270-9638\(00\)01084-1](https://doi.org/10.1016/S1270-9638(00)01084-1) (2001).
- 1069 Mastrandrea, M. D., K. J. Mach, G. K. Plattner, O. Edenhofer, T. F. Stocker, C. B. Field, K. L. Ebi, P. R.  
1070 Matschoss, The IPCC AR5 guidance note on consistent treatment of uncertainties: a common approach

1 July 2020 Revised

- 1071 across the working groups. *Climatic Change* 108, 675–691, <https://doi.org/10.1007/s10584-011-0178-6>  
1072 (2011).
- 1073 Meinshausen, M., S. J. Smith, K. Calvin, J. S. Daniel, M. L. T. Kainuma, J. -F. Lamarque, K. Matsumoto,  
1074 S. A. Montzka, S. C. B. Raper, K. Riahi, A. Thomson, G. J. M. Velders, D. P. P. van Vuuren, The RCP  
1075 greenhouse gas concentrations and their extensions from 1765 to 2300. *Climatic Change* 109, 213–241,  
1076 <https://doi.org/10.1007/s10584-011-0156-z> (2011).
- 1077 Millar, R. J., Z. R. Nicholls, P. Friedlingstein, M. R. Allen, A modified impulse-response representation  
1078 of the global near-surface air temperature and atmospheric concentration response to carbon dioxide  
1079 emissions. *Atmospheric Chemistry and Physics*. 17, 7213–7228, [https://doi.org/10.5194/acp-17-7213-](https://doi.org/10.5194/acp-17-7213-2017)  
1080 2017 (2017).
- 1081 Miller, M., P. Brook and C. Eyers, Reduction of Sulphur limits in aviation fuel standards (SULPHUR).  
1082 EASA research project EASA.2008/C11, European Aviation Safety Agency. (2010)  
1083 [https://www.easa.europa.eu/sites/default/files/dfu/2009-SULPHUR-](https://www.easa.europa.eu/sites/default/files/dfu/2009-SULPHUR-Reduction%20of%20sulphur%20limits%20in%20aviation%20fuel%20standards-Final%20Report.pdf)  
1084 [Reduction%20of%20sulphur%20limits%20in%20aviation%20fuel%20standards-Final%20Report.pdf](https://www.easa.europa.eu/sites/default/files/dfu/2009-SULPHUR-Reduction%20of%20sulphur%20limits%20in%20aviation%20fuel%20standards-Final%20Report.pdf)
- 1085 Minnis, P., S. T. Bedka, D. P. Duda, K. M. Bedka, T. Chee, J. K. Ayers, R. Palikonda, D. A.  
1086 Spangenberg, K. V. Khlopenkov, R. Boeke, Linear contrail and contrail cirrus properties determined from  
1087 satellite data. *Geophysical Research Letters*, 40, 3220–3226, <https://doi.org/10.1002/grl.50569> (2013).
- 1088 Möhler, O., S. Büttner, C. Linke, M. Schnaiter, H. Saathof, O. Stetzer, R. Wagner, M. Krämer, A.  
1089 Mangold, V. Ebert, U. Schurath, Effect of sulfuric acid coating on heterogenous ice nucleation by soot  
1090 aerosol particles. *Journal of Geophysical Research* 110 (D11), <https://doi.org/10.1029/2004JD005169>  
1091 (2005).
- 1092 Montzka, S. A., C. M. Spivakovsky, J. H. Butler, J. W. Elkins, L. T. Lock, D. J. Mondeel, New  
1093 observational constraints for atmospheric hydroxyl on global and hemispherical scales. *Science* 288, 500–  
1094 503, <https://doi.org/10.1126/science.288.5465.500> (2000).
- 1095 Moore, R. H., K. L. Thornhill, B. Weinzierl, D. Sauer, E. D'Ascoli, J. Kim, et al., Biofuel blending  
1096 reduces particle emissions from aircraft engines at cruise conditions. *Nature*, 543, 411–415,  
1097 <https://doi.org/10.1038/nature21420> (2017)
- 1098 Myhre, G., J. S. Nilsen, L. Gulstad, K. P. Shine, B. Rognerud, I. S. A. Isaksen, Radiative forcing due to  
1099 stratospheric water vapor from CH<sub>4</sub> oxidation. *Geophysical Research Letters* 34, L01807,  
1100 <https://doi.org/10.1029/2006GL027472> (2007).
- 1101 Myhre, G., M. Kvalevåg, G. Rädcl, J. Cook, K. P. Shine, H. Clark, F. Karcher, K. Markowicz, A. Kardas,  
1102 P. Wolkenberg, Y. Balkanski, M. Ponater, P. Forster, A. Rap, R. R. de Leon, Intercomparison of  
1103 radiative forcing calculations of stratospheric water vapour and contrails. *Meteorologische Zeitschrift* 18,  
1104 585–596, <https://doi.org/10.1127/0941-2948/2009/0411> (2009).
- 1105 Myhre, G., K. P. Shine, G. Rädcl, M. Gauss, I. S. A. Isaksen, Q. Tang, M. J. Prather, J. E. Williams, P.  
1106 van Velthoven, O. Dessens, B. Koffi, S. Szopa, P. Hoor, V. Grewe, J. Borken-Kleefeld, T. K. Berntsen, J.  
1107 S. Fuglestvedt, Radiative forcing due to changes in ozone and methane caused by the transport sector.  
1108 *Atmospheric Environment* 45, 387–394, <https://doi.org/10.1016/j.atmosenv.2010.10.001> (2011).
- 1109 Myhre, G., D. Shindell, F. -M Breon, W. Collins, J. Fuglestvedt, J. Huang, D. Koch, J. -F. Lamarque, D.  
1110 Lee., B. Mendoza, T. Nakajima, A. Robock, G. Stephens, T. Takemura, H. Zhang, “Anthropogenic and  
1111 Natural Radiative Forcing” in *Climate Change 2013: the Physical Science Basis, Contribution of*  
1112 *Working Group I to the Fifth Assessment Report of the Intergovernmental Panel on Climate Change,*  
1113 (Cambridge University Press, 2013). <https://www.ipcc.ch/report/ar5/wg1/>

1 July 2020 Revised

- 1114 Newinger, C. and U. Burkhardt, Sensitivity of contrail cirrus radiative forcing to air traffic scheduling.  
1115 *Journal of Geophysical Research Atmospheres* 117, D10205, <https://doi.org/10.1029/2011JD016736>  
1116 (2012).
- 1117 OECD, Green growth and the future of aviation. Paper prepared for the 27th Round Table on Sustainable  
1118 Development held at OECD Headquarters 23-24 January 2012 (OECD 2012). [https://www.oecd.org/sd-](https://www.oecd.org/sd-roundtable/papersandpublications/49482790.pdf)  
1119 [roundtable/papersandpublications/49482790.pdf](https://www.oecd.org/sd-roundtable/papersandpublications/49482790.pdf)
- 1120 Olivié, D. J. L., D. Cariolle, H. Teyssèdre, D. Salas, A. Voltaire, H. Clark, D. Saint-Martin, M. Michou,  
1121 F. Karcher, Y. Balkanski, M. Gauss, O. Dessens, B. Koffi, R. Sausen, Modeling the climate impact of  
1122 road transport, maritime shipping and aviation over the period 1860–2100 with an AOGCM. *Atmospheric*  
1123 *Chemistry and Physics* 12, 1449–1480, <https://doi.org/10.5194/acp-12-1449-2012> (2012).
- 1124 Olsen, S. C., G. P. Brasseur, D. J. Wuebbles, S. R. H. Barrett, H. Dang, S. D. Eastham, M. Z. Jacobson,  
1125 A. Khodayari, H. Selkirk, A. Sokolov, N. Unger, Comparison of model estimates of the effects of  
1126 aviation emissions on atmospheric ozone and methane. *Geophysical Research Letters* 40, 6004–6009,  
1127 <https://doi.org/10.1002/2013GL057660> (2013).
- 1128 Penner, J.E., Y. Chen, M. Wang, and X. Liu, Possible influence of anthropogenic aerosols on cirrus  
1129 clouds and anthropogenic forcing. *Atmospheric Chemistry and Physics*, 9, 879–96,  
1130 <https://doi.org/10.5194/acp-9-879-2009> (2009).
- 1131 Penner, J. E., C. Zhou, A. Garnier, D. L. Mitchell, Anthropogenic aerosol indirect effects in cirrus clouds.  
1132 *Journal of Geophysical Research Atmospheres*, 123, 11,652–11,677,  
1133 <https://doi.org/10.1029/2018JD029204> (2018).
- 1134 Petzold, A., M. Gysel, X. Vancassel, R. Hitzenberger, H. Puxbaum, S. Vrochticky, E. Weingartner, U.  
1135 Baltensperger, P. Mirabel, On the effects of organic matter and sulphur-containing compounds on the  
1136 CCN activation of combustion particles. *Atmospheric Chemistry and Physics* 5, 3187–3203,  
1137 <https://doi.org/10.5194/acp-5-3187-2005> (2005).
- 1138 Pitari, G., D. Iachetti, G. Genova, N. De Luca, O. A. Søvde, Ø. Hodnebrog, D. S. Lee, L. L. Lim, Impact  
1139 of coupled NO<sub>x</sub>/aerosol aircraft emissions on ozone photochemistry and radiative forcing. *Atmosphere* 6,  
1140 751–782, <https://doi.org/10.3390/atmos6060751> (2015).
- 1141 Pitari, G., I. Cionni, G. Di Genova, O. A. Søvde, L. Lim, Radiative forcing from aircraft emissions of  
1142 NO<sub>x</sub>: model calculations with CH<sub>4</sub> surface flux boundary condition. *Meteorologische Zeitschrift* 26(6),  
1143 663-687, <https://doi.org/10.1127/metz/2016/0776> (2017).
- 1144 Pomroy, H. R. and J. A. Illingworth, Ice cloud inhomogeneity: Quantifying bias in emissivity from radar  
1145 observations. *Geophysical Research Letters* 27, 2101–2104, <https://doi.org/10.1029/1999GL011149>  
1146 (2000).
- 1147 Ponater, M., S. Marquart, R. Sausen, U. Schumann, On contrail climate sensitivity. *Geophysical Research*  
1148 *Letters* 32, L10706, <https://doi.org/10.1029/2005GL022580> (2005).
- 1149 Ponater, M., S. Pechtl, R. Sausen, U. Schumann, G. Hüttig, Potential of the cryoplane technology to  
1150 reduce aircraft climate impact: a state-of-the-art assessment. *Atmospheric Environment* 40, 6928-6944,  
1151 <https://doi.org/10.1016/j.atmosenv.2006.06.036> (2006).
- 1152 Ponater, M., M. Bickel, L. Bock, and U. Burkhardt, Towards determining the efficacy of contrail cirrus.  
1153 In Matthes, S. and A. Blum, Making Aviation Environmentally Sustainable, 3rd ECATS Conference,  
1154 Book of Abstracts, Volume 1. ISBN 978-1-910029-58-9. 51-44 (2020). ([http://www.ecats-](http://www.ecats-network.eu/uploads/2020/06/ECATS_Main_BookOfAbstracts_Vol1_final.pdf)  
1155 [network.eu/uploads/2020/06/ECATS\\_Main\\_BookOfAbstracts\\_Vol1\\_final.pdf](http://www.ecats-network.eu/uploads/2020/06/ECATS_Main_BookOfAbstracts_Vol1_final.pdf))

1 July 2020 Revised

- 1156 Prather, M. J., Lifetimes and eigenstates in atmospheric chemistry. *Geophysical Research Letters* 21,  
1157 801–804, <https://doi.org/10.1029/94GL00840> (1994).
- 1158 Prather, M., D. Ehhalt, F. Dentener, R. Derwent, E. Dlugokencky E, “Atmospheric chemistry and  
1159 greenhouse gases”, in *Climate Change 2001: The Scientific Basis, Contribution of Working Group I to*  
1160 *the Third Assessment Report of the Intergovernmental Panel on Climate Change*, J. T. Houghton ed.  
1161 (Cambridge University Press, Cambridge, United Kingdom and New York, NY, USA, 2001) pp. 239–  
1162 287. <https://www.ipcc.ch/site/assets/uploads/2018/03/TAR-04.pdf>
- 1163 Prather, M. J., C. D. Holmes, J. Hsu, Reactive greenhouse gas scenarios: Systematic exploration of  
1164 uncertainties and the role of atmospheric chemistry, *Geophysical Research Letters*, 39, L09803,  
1165 <https://doi.org/10.1029/2012GL051440> (2012).
- 1166 Rap, A., P. M. Forster, J. M. Haywood, A. Jones, O. Boucher, Estimating the climate impact of linear  
1167 contrails using the UK Met Office climate model. *Geophysical Research Letters* 37, L20703,  
1168 <https://doi.org/10.1029/2010GL045161> (2010).
- 1169 Revelle, R. and H. E. Suess, Carbon dioxide exchange between atmosphere and ocean and the question of  
1170 an increase of atmospheric CO<sub>2</sub> during the past decades, *Tellus*, 9, 18–27, [https://doi.org/10.1111/j.2153-](https://doi.org/10.1111/j.2153-3490.1957.tb01849.x)  
1171 [3490.1957.tb01849.x](https://doi.org/10.1111/j.2153-3490.1957.tb01849.x) (1957).
- 1172 Richardson, T. B., P.M. Forster, C. J. Smith, A. C. Maycock, T. Wood, T. Andrews, O. Boucher, G.  
1173 Faluvegi, D. Fläschner, Ø. Hodnegrog, M. Kasoar, A. Kirkevåg, J.-F. Lamarque, J. Mülmenstädt, G.  
1174 Myhre, D. Olivíe, R. W. Portmann, B. H. Samset, D. Shawki, D. Shindell, P. Stier, T. Takemura, A.  
1175 Voulgarakis, D. Watson-Parris, Efficacy of climate forcings in PDRMIP models. *Journal of Geophysical*  
1176 *Research: Atmospheres* 124, <https://doi.org/10.1029/2019JD030581>
- 1177 Righi, M., J. Hendricks, R. Sausen, The global impact of the transport sectors on atmospheric aerosol:  
1178 simulations for year 2000 emissions. *Atmospheric Chemistry and Physics* 13, 9939–9970,  
1179 <https://doi.org/10.5194/acp-13-9939-2013> (2013).
- 1180 Sander, S. P., R. R. Friedl, A. R. Ravishankara, D. M. Golden, C. E. Kolb, M. J. Kurylo, M. J. Molina, G.  
1181 K. Moortgat, B. J. Finlayson-Pitts, “Chemical Kinetics and Photochemical Data for Use in Atmospheric  
1182 Studies”, (JPL Publ. 06-2, No. 15, 2006). [https://jpldataeval.jpl.nasa.gov/pdf/JPL\\_02-25\\_rev02.pdf](https://jpldataeval.jpl.nasa.gov/pdf/JPL_02-25_rev02.pdf)
- 1183 Sausen R. and U. Schumann, Estimates of the climate response to aircraft CO<sub>2</sub> and NO<sub>x</sub> emissions  
1184 scenarios. *Climatic Change* 44, 27–58 (2000).
- 1185 Sausen, R. I. Isaksen, V. Grewe, D. Hauglustaine, D. S. Lee, G. Myhre, M. O. Köhler, G. Pitari, U.  
1186 Schumann, F. Stordal, C. Zerefos, Aviation radiative forcing in 2000: An update on IPCC (1999).  
1187 *Meteorologische Zeitschrift* 14, 555–561, <https://doi.org/10.1127/0941-2948/2005/0049> (2005).
- 1188 Schumann, U., J. E. Penner, Y. Chen, C. Zhou, K. Graf, Dehydration effects from contrails in a coupled  
1189 contrail-climate model. *Atmospheric Chemistry and Physics* 15, 11179–11199,  
1190 <https://doi.org/10.5194/acp-15-11179-2015> (2015).
- 1191 Schumann, U., R. Baumann, D. Baumgardner, S. T. Bedka, D. P. Duda, V. Freudenthaler, J.-F. Gayet, A.  
1192 J. Heymsfield, P. Minnis, M. Quante, E. Raschke, H. Schlager, M. Vázquez-Navarro, C. Voigt, Z. Wang,  
1193 Properties of individual contrails: a compilation of observations and some comparisons. *Atmospheric*  
1194 *Chemistry and Physics* 17, 403–438, <https://doi.org/10.5194/acp-17-403-2017> (2017a).
- 1195 Schumann, U., C. Kiemle, H. Schlager, R. Weigel, S. Bormann, F. D’Amato, M. Krämer, R. Matthey, A.  
1196 Protat, C. Voigt, C. M. Volk, Long-lived contrails and convective cirrus above the tropical tropopause.  
1197 *Atmospheric Chemistry and Physics* 17, 2311–2346, <https://doi.org/10.5194/acp-17-2311-2017> (2017b).

1 July 2020 Revised

- 1198 Shine, K. P., J.S. Fuglestedt, K. Hailemariam, N. Stuber, Alternatives to the global warming potential  
1199 for comparing climate impacts of emissions of greenhouse gases. *Climatic Change* 68, 281–302,  
1200 <https://doi.org/10.1007/s10584-005-1146-9> (2005).
- 1201
- 1202 Skeie, R. B., J. Fuglestedt, T. Berntsen, G. P. Peters, R. Andrew, M. Allen, S. Kallbekken, Perspective  
1203 has a strong effect on the calculation of historical contributions to global warming. *Environmental*  
1204 *Research Letters* 12, 024022, <https://doi.org/10.1088/1748-9326/aa5b0a> (2017).
- 1205 Skowron, A., D. S. Lee, J. Hurley, “Aviation NO<sub>x</sub> Global Warming Potential”, in 2nd International  
1206 Conference on Transport, Atmosphere and Climate, 25-28 June 2009, Aachen/Maastricht,  
1207 Germany/Netherlands, <https://www.pa.op.dlr.de/tac/2009/proceedings/FB2010-10.pdf> (2009).
- 1208 Skowron, A., D. S. Lee, R. R. de León, The assessment of the impact of aviation NO<sub>x</sub> on ozone and other  
1209 radiative forcing responses—The importance of representing cruise altitudes accurately. *Atmospheric*  
1210 *Environment* 74, 159–168, <https://doi.org/10.1016/j.atmosenv.2013.03.034> (2013).
- 1211 Skowron, A., D. S. Lee, R. R. de León, Variation of radiative forcings and global warming potentials  
1212 from regional aviation NO<sub>x</sub> emissions. *Atmospheric Environment* 104, 69–78,  
1213 <https://doi.org/10.1016/j.atmosenv.2014.12.043> (2015).
- 1214 Søvde, O. A., S. Matthes, A. Skowron, D. Iachetti, L. Lim, B. Owen, Ø. Hodnebrog, G. Di Genova, G.  
1215 Pitari, D. S. Lee, G. Myhre, I. S. A. Isaksen, Aircraft emission mitigation by changing route altitude: A  
1216 multi-model estimate of aircraft NO<sub>x</sub> emission impact on O<sub>3</sub> photochemistry. *Atmospheric Environment*  
1217 95, 468–479, <https://doi.org/10.1016/j.atmosenv.2014.06.049> (2014).
- 1218 Smith, C. J., R. J. Kramer, G. Myhre, P. M. Forster, B. J. Soden, T. Andrews, O. Boucher, G. Faluvegi,  
1219 D. Fläschner, Ø. Hodnebrog, M. Kasoar, V. Kharin, A. Kirkevåg, J.-F. Lamarque, J. Mülmenstädt, D.  
1220 Olivié, T. Richardson, B. H. Samset, D. Shindell, P. Stier, T. Takemura, A. Voulgarakis, D. Watson-  
1221 Parris, Understanding rapid adjustments to diverse forcing agents. *Geophysical Research Letters* 45,  
1222 doi:10.1029/2018GL079826 (2018)
- 1223 Stevenson, D. S., C. E. Johnson, W. J. Collins, R. G. Derwent, K. P. Shine, J. M. Edwards, Evolution of  
1224 tropospheric ozone radiative forcing. *Geophysical Research Letters* 25, 3819–3822,  
1225 <https://doi.org/10.1029/1998GL900037> (1998).
- 1226 Stevenson, D. S., R. M. Doherty, M. G. Sanderson, W. J. Collins, C. E. Johnson, R. G. Derwent,  
1227 Radiative forcing from aircraft NO<sub>x</sub> emissions: mechanisms and seasonal dependence *Journal of*  
1228 *Geophysical Research Atmospheres* 109, D17307, <https://doi.org/10.1029/2004JD004759> (2004).
- 1229 Stordal, F., M. Gauss, G. Myhre, E. Mancini, D. A. Hauglustaine, M. O. Köhler, T. Berntsen, E. J. G.  
1230 Stordal, D. Iachetti, G. Pitari, I. S. A. Isaksen, TRADEOFFs in climate effects through aircraft routing:  
1231 forcing due to radiatively active gases. *Atmospheric Chemistry and Physics Discussions* 6, 10733–10771  
1232 (2006).
- 1233 Stuber, N., M. Ponater, R. Sausen, Why radiative forcing might fail as a predictor of climate change.  
1234 *Climate Dynamics* 24, 497–510 doi:10.1007/s00382-004-0497-7 (2005).
- 1235 Stuber, N., P. Forster, G. Rädcl, K. Shine, The importance of the diurnal and annual cycle of air traffic for  
1236 contrail radiative forcing. *Nature* 441, 864–867, <https://doi.org/10.1038/nature04877> (2006).
- 1237 Teoh, R., M. E. J. Stettler, A. Majumdar, U. Schumann, B. Graves, A. M. Boies, A methodology to relate  
1238 black carbon particle number and mass emissions. *Journal of Aerosol Science* 132, 44–59,  
1239 <https://doi.org/10.1016/j.jaerosci.2019.03.00> (2019).

1 July 2020 Revised

- 1240 Teoh, R., Schumann, U., Majumdar, A., Stettler, M. E. J., Mitigating the climate forcing of aircraft  
1241 contrails by small-scale diversions and technology adoption. *Environmental Science and Technology*, 54  
1242 2941–2950, doi: 10.1021/acs.est.9b05608.
- 1243 Tesche, M., P. Achtert, P. Glantz, K. J. Noone, Aviation effects on already-existing cirrus clouds. *Nature*  
1244 *Communications* 7, 12016, <https://doi.org/10.1038/ncomms12016> (2016).
- 1245 UKDS (2016) [http://stats.ukdataservice.ac.uk/index.aspx?r=349678&DataSetCode=IEA\\_COAL\\_BA](http://stats.ukdataservice.ac.uk/index.aspx?r=349678&DataSetCode=IEA_COAL_BA),  
1246 2016.
- 1247 UNFCCC, <https://unfccc.int/nationally-determined-contributions-ndcs>
- 1248 Unger, N., T. C. Bond, J. S. Wang, D. M. Koch, S. Menon, D. T. Shindell, S. Bauer, Attribution of  
1249 climate forcing to economic sectors. *Proceedings of the National Academy of Sciences U.S.A.* 107, 3382–  
1250 3387, <https://doi.org/10.1073/pnas.0906548107> (2010).
- 1251 Unger, N., Global climate impact of civil aviation for standard and desulfurized jet fuel. *Geophysical*  
1252 *Research Letters* 38, 1–6, <https://doi.org/10.1029/2011GL049289> (2011).
- 1253 Unger, N., Y. Zhao, H. Dang, Mid-21st century chemical forcing of climate by the civil aviation sector.  
1254 *Geophysical Research Letters* 40, 641–645, <https://doi.org/10.1002/grl.50161> (2013).
- 1255 Unterstrasser, S., Large-eddy simulation study of contrail microphysics and geometry during the vortex  
1256 phase and consequences on contrail-to-cirrus transition. *Journal of Geophysical Research Atmospheres*  
1257 119, 7537–7555, <https://doi.org/10.1002/2013JD021418> (2014).
- 1258 Voulgarakis, A., V. Naik, J.-F. Lamarque, D. T. Shindell, P. J. Young, M. J. Prather, O. Wild, R. D. Field,  
1259 D. Bergmann, P. Cameron-Smith, I. Cionni, W. J. Collins, S. B. Dalsøren, R. M. Doherty, V. Eyring, G.  
1260 Faluvegi, G. A. Folberth, L. W. Horowitz, B. Josse, I. A. McKenzie, T. Nagashima, D. A. Plummer, M.  
1261 Righi, S. T. Rumbold, D. S. Stevenson, S. A. Strode, K. Sudo, S. Szopa, G. Zeng, Analysis of present-day  
1262 and future OH and methane lifetime in the ACCMIP simulations. *Atmospheric Chemistry and Physics* 13,  
1263 2563–2587, <https://doi.org/10.5194/acp-13-2563-2013> (2013).
- 1264 Wilcox, L., K. P. Shine, B. J. Hoskins, Radiative forcing due to aviation water vapour emissions.  
1265 *Atmospheric Environment* 63, 1–13, <https://doi.org/10.1016/j.atmosenv.2012.08.072> (2012).
- 1266 Wild, O., M. J. Prather, H. Akimoto, Indirect long-term global radiative cooling from NO<sub>x</sub> emissions.  
1267 *Geophysical Research Letters* 28, 1719–1722, <https://doi.org/10.1029/2000GL012573> (2001).
- 1268 Xie B., H. Zhang, Z. Wang, S. Zhao, Q. Fu, A modelling study of effective radiative forcing and climate  
1269 response due to tropospheric ozone. *Advances in Atmospheric Sciences* 33, 819–828 doi: 10.1007/s00376-  
1270 016-5193-0
- 1271 Yin, F., V. Grewe, C. Frömming, H. Yamashita, Impact on flight trajectory characteristics when avoiding  
1272 the formation of persistent contrails for transatlantic routes. *Transportation Research Part D: Transport*  
1273 *and Environment* 65, 466–484, <https://doi.org/10.1016/j.trd.2018.09.017> (2018).
- 1274 Zhou, C. and J. E. Penner, Aircraft soot indirect effect on large-scale cirrus clouds: Is the indirect forcing  
1275 by aircraft soot positive or negative? *Journal of Geophysical Research Atmospheres* 119, 11,303–11,320,  
1276 <https://doi.org/10.1002/2014JD021914> (2014).
- 1277



1 July 2020 Revised

1278 **Table 1.** Emission indices used in ERF and RF calculations

Emission	Emission index	Reference	Notes
CO <sub>2</sub>	3.16 kg/kg fuel	ICAO (2018)	
NO <sub>x</sub>	15.14 g/kg fuel	Fleming and Ziegler (2016)	2018, 2011
	14.12 g/kg fuel	Barrett et al. (2010)	2005
Water vapor	1.231 kg/kg fuel	Barrett et al. (2010)	
Soot	0.03 g/kg fuel	Barrett et al. (2010)	
	$2 \times 10^{14}$ particles/kg fuel <sup>a</sup>		
Sulphur (SO <sub>2</sub> )	1.2 g/kg fuel	Miller et al. (2010)	Assumed S content of 600 ppm

1279 <sup>a</sup> Assumes mean particle size in the range of 11–79 nm diameter.

1280

1 July 2020 Revised

1281

1282

1283

**Table 2.** Best estimates and high/low limits of the 90% likelihood ranges for aviation ERF components derived in this study

ERF (mW m <sup>-2</sup> )	2018 <sup>a</sup>	2011 <sup>a</sup>	2005 <sup>a</sup>	Sensitivity to emissions	ERF/RF
Contrail cirrus	57.4 (17, 98)	44.1 (13, 75)	34.8 (10, 59)	9.36 x 10 <sup>-10</sup> mW m <sup>-2</sup> km <sup>-1</sup>	0.42
CO <sub>2</sub>	34.3 (28, 40)	29.0 (24, 34)	25.0 (21, 29)		1.0
Short-term O <sub>3</sub> increase	49.3 (32, 76)	37.3 (24, 58)	33.0 (21, 51)	34.4 ± 9.9 mW m <sup>-2</sup> (Tg (N) yr <sup>-1</sup> ) <sup>-1</sup>	1.37
Long-term O <sub>3</sub> decrease	-10.6 (-20, -7.4)	-7.9 (-15, -5.5)	-6.7 (-13, -4.7)	-9.3 ± 3.4 mW m <sup>-2</sup> (Tg (N) yr <sup>-1</sup> ) <sup>-1</sup>	1.18
CH <sub>4</sub> decrease	-21.2 (-40, -15)	-15.8 (-30, -11)	-13.4 (-25, -9.4)	-18.7 ± 6.9 mW m <sup>-2</sup> (Tg (N) yr <sup>-1</sup> ) <sup>-1</sup>	1.18
Stratospheric water vapor decrease	-3.2 (-6.0 -2.2)	-2.4 (-4.4, -1.7)	-2.0 (-3.8, -1.4)	-2.8 ± 1.0 mW m <sup>-2</sup> (Tg (N) yr <sup>-1</sup> ) <sup>-1</sup>	1.18
Net NO <sub>x</sub>	17.5 (0.6, 29)	13.6 (0.9, 22)	12.9 (1.9, 20)	5.5 ± 8.1 mW m <sup>-2</sup> (Tg (N) yr <sup>-1</sup> ) <sup>-1</sup>	
Stratospheric H <sub>2</sub> O increase	2.0 (0.8, 3.2)	1.5 (0.6, 2.4)	1.4 (0.6, 2.3)	0.0052 ± 0.0026 mW m <sup>-2</sup> (Tg (H <sub>2</sub> O) yr <sup>-1</sup> ) <sup>-1</sup>	---
Soot (aerosol-radiation)	0.94 (0.1, 4.0)	0.71 (0.1, 3.0)	0.67 (0.1, 2.8)	100.7 ± 165.5 mW m <sup>-2</sup> (Tg (BC) yr <sup>-1</sup> ) <sup>-1</sup>	---
Sulfate (aerosol-radiation)	-7.4 (-19, -2.6)	-5.6 (-14, -1.9)	-5.3 (-13, -1.8)	-19.9 ± 16.0 mW m <sup>-2</sup> (Tg (SO <sub>2</sub> ) yr <sup>-1</sup> ) <sup>-1</sup>	---
Sulfate and soot (aerosol-cloud)	----	----	----	----	---
Net ERF (only non-CO <sub>2</sub> terms)	66.6 (21, 111)	51.4 (16, 85)	41.9 (14, 69)	----	---
Net aviation ERF	100.9 (55, 145)	80.4 (45, 114)	66.9 (38, 95)	----	---
Net anthropogenic ERF in 2011	----	2290 (1130, 3330) <sup>b</sup>	----	----	---

1284

1285

1286

1287

<sup>a</sup> The uncertainty distributions for all forcing terms are lognormal except for CO<sub>2</sub> and contrail cirrus (normal) and Net NO<sub>x</sub> (discrete pdf).

<sup>b</sup> Boucher et al., 2013. IPCC also separately estimated the contrail cirrus term for 2011 as 50 (20, 150) mW m<sup>-2</sup>.

1 July 2020 Revised

1288 **Table 3.** Best estimates and low/high limits of the 95% likelihood ranges for aviation RF components  
 1289 derived in this study <sup>a</sup>

RF (mW m <sup>-2</sup> )	2018 <sup>b</sup>	2011 <sup>b</sup>	2005 <sup>b</sup>	L09 2005 values	Sensitivity to emissions (this work)
Contrail cirrus	111.4 (33, 189)	85.6 (25, 146)	67.5 (20, 115)	(11.8 <sup>c</sup> )	1.82 x 10 <sup>-9</sup> mW m <sup>-2</sup> km <sup>-1</sup>
CO <sub>2</sub>	34.3 (31, 38)	29.0 (26, 32)	25.0 (23, 27)	28.0	
Short-term O <sub>3</sub> increase	36.0 (23, 56)	27.3 (17, 42)	24.0 (15, 37)	26.3	25.1 ± 7.3 mW m <sup>-2</sup> (Tg (N) yr <sup>-1</sup> ) <sup>-1</sup>
Long-term O <sub>3</sub> decrease	-9.0 (-17, -6.3)	-6.7 (-13, -4.7)	-5.7 (-11, -4.0)	----	-7.9 ± 2.9 mW m <sup>-2</sup> (Tg (N) yr <sup>-1</sup> ) <sup>-1</sup>
CH <sub>4</sub> decrease	-17.9 (-34, -13)	-13.4 (-25, -9.3)	-11.4 (-21, -7.9)	-12.5	-15.8 ± 5.9 mW m <sup>-2</sup> (Tg (N) yr <sup>-1</sup> ) <sup>-1</sup>
Stratospheric water vapor decrease	-2.7 (-5.0 -1.9)	-2.0 (-3.8, -1.4)	-1.7 (-3.2, -1.2)	----	-2.4 ± 0.9 mW m <sup>-2</sup> (Tg (N) yr <sup>-1</sup> ) <sup>-1</sup>
Net NO <sub>x</sub>	8.2 (-4.8, 16)	6.5 (-3.3, 12)	6.6 (1.9, 12)	13.8 <sup>d</sup>	1.0 ± 6.6 mW m <sup>-2</sup> (Tg (N) yr <sup>-1</sup> ) <sup>-1</sup>
Stratospheric H <sub>2</sub> O increase	2.0 (0.8, 3.2)	1.5 (0.6, 2.4)	1.4 (0.6, 2.3)	2.8	0.0052 ± 0.0026 mW m <sup>-2</sup> (Tg (H <sub>2</sub> O) yr <sup>-1</sup> ) <sup>-1</sup>
Soot (aerosol-radiation)	0.94 (0.1, 4.0)	0.71 (0.1, 3.0)	0.67 (0.1, 2.8)	3.4	100.7 ± 165.5 mW m <sup>-2</sup> (Tg (BC) yr <sup>-1</sup> ) <sup>-1</sup>
Sulfate (aerosol-radiation)	-7.4 (-19, -2.6)	-5.6 (-14, -1.9)	-5.3 (-13, -1.8)	-4.8	-19.9 ± 16.0 mW m <sup>-2</sup> (Tg (SO <sub>2</sub> ) yr <sup>-1</sup> ) <sup>-1</sup>
Sulfate and soot (aerosol-cloud)	----	----	----	----	----
Net RF (only non-CO <sub>2</sub> terms)	114.8 (35, 194)	88.4 (27, 149)	70.3 (22, 119)	----	----
Net aviation RF	149.1 (70, 229)	117.4 (56, 179)	95.2 (47, 144)	78.0	----

1290 <sup>a</sup> ERF values are shown in **Table 2**.

1291 <sup>b</sup> The uncertainty distributions for all forcing terms are lognormal except for CO<sub>2</sub> and contrail cirrus (normal) and Net  
 1292 NO<sub>x</sub> (discrete pdf).

1293 <sup>c</sup> Linear contrails only; excludes the increase in cirrus cloudiness due to aged spreading contrails.

1294 <sup>d</sup> Excludes updated CH<sub>4</sub> RF evaluation of Etminan et al. (2016) and equilibrium-to-transient correction.

1295

1 July 2020 Revised

1296 **Table 4a.** Confidence levels for the ERF estimates in **Figure 3**

Terms	Evidence	Agreement	Conf. level	Basis for uncertainty estimates	Understanding change since L09
<b>Contrail cirrus formation in high-humidity regions</b>	Limited	Medium	Low*	Robust evidence for the phenomenon. Large remaining uncertainties in magnitude in part due to incomplete representation of key processes	The inclusion of contrail cirrus processes in global climate models.
<b>Carbon dioxide (CO<sub>2</sub>) emissions</b>	Robust	Medium	High**	Trends in aviation CO <sub>2</sub> emissions and differences between simplified C-cycle models	Better assessment of uncertainties from multiple models
<b>Short-term ozone increase</b>					
Short-term ozone increase	Medium	Medium	Medium*	Observed trends of tropospheric ozone and laboratory studies of chemical kinetics, reliance on a large number of model results for aviation emissions	Elevated owing to many more studies
<b>Long-term ozone decrease</b>					
Long-term ozone decrease	Limited	Medium	Low*	Reliance on chemical modelling studies	Not provided previously
<b>Methane decrease</b>					
Methane decrease	Medium	Medium	Medium*	Observed trends of tropospheric methane and laboratory studies of chemical kinetics, reliance on a large number of model results for aviation emissions	Elevated owing to many more studies
<b>Stratospheric water vapour decrease</b>					
Stratospheric water vapour decrease	Limited	Medium	Low*	Reliance on chemical modelling studies	Not provided previously
<b>Net NO<sub>x</sub></b>					
Net NO <sub>x</sub>	Medium	Limited	Low*	Associated uncertainties with combining above effects	Elevated owing to more studies but lowered in total owing to additional terms and methodological constraints
<b>Water vapor emissions in the stratosphere</b>					
Water vapor emissions in the stratosphere	Medium	Medium	Medium	Limited studies of perturbation of water vapor budget of UT/LS	Elevated owing to more studies
<b>Aerosol-radiation interactions</b>					
From soot emissions	Limited	Medium	Low	Limited studies and uncertain emission index	More studies
From sulfur emissions	Limited	Medium	Low	Limited studies and uncertain emission index	More studies
<b>Aerosol-cloud interactions</b>					
From sulfur emissions	Limited	Low	Very low	None available; few studies, probably a negative ERF	Not provided previously
From soot emissions	Limited	Low	Very low	None available; few studies, varying in sign and magnitude of ERF constrained by poor understanding of processes	Not provided previously

1297 \* This term has the additional uncertainty of the derivation of an effective radiative forcing from a radiative forcing.

1298 \*\* This term differs from 'Very High' level in IPCC (2013) because additional uncertainties are introduced by the  
1299 assessment of marginal aviation CO<sub>2</sub> emissions and their resultant concentrations in the atmosphere from simplified  
1300 carbon cycle models.

1301

1302

1303

1 July 2020 Revised

1304 **Table 4b.** Basis for confidence levels in **Table 4a**<sup>a</sup>

<b>Medium</b> <i>High agreement</i> <i>Limited evidence</i>	<b>High</b> <i>High agreement</i> <i>Medium evidence</i>	<b>Very High</b> <i>High agreement</i> <i>Robust evidence</i>
<b>Low</b> <i>Medium agreement</i> <i>Limited evidence</i>	<b>Medium</b> <i>Medium agreement</i> <i>Medium evidence</i>	<b>High</b> <i>Medium agreement</i> <i>Robust evidence</i>
<b>Very Low</b> <i>Low agreement</i> <i>Limited evidence</i>	<b>Low</b> <i>Low agreement</i> <i>Medium evidence</i>	<b>Medium</b> <i>Low agreement</i> <i>Robust evidence</i>

1305 <sup>a</sup> The basis for the confidence level is given as a combination of evidence  
 1306 (limited, medium, robust) and agreement (low, medium and high) based  
 1307 on guidance given by Mastrandrea et al. (2011).

1308

1 July 2020 Revised

1309 **Table 5.** Emission metrics and corresponding CO<sub>2</sub>-equivalent emissions for the ERF components of 2018  
 1310 aviation emissions and cloudiness

1311 **Metrics**

ERF term	GWP <sub>20</sub>	GWP <sub>50</sub>	GWP <sub>100</sub>	GTP <sub>20</sub>	GTP <sub>50</sub>	GTP <sub>100</sub>
CO <sub>2</sub>	1	1	1	1	1	1
Contrail cirrus (Tg CO <sub>2</sub> basis)	2.32	1.09	0.63	0.67	0.11	0.09
Contrail cirrus (km basis)	39	18	11	11	1.8	1.5
Net NO <sub>x</sub>	619	205	114	-222	-69	13
Aerosol-radiation						
Soot emissions	4288	2018	1166	1245	195	161
SO <sub>2</sub> emissions	-832	-392	-226	-241	-38	-31
Water vapor emissions	0.22	0.10	0.06	0.07	0.01	0.008

1312

1313 **CO<sub>2</sub>-eq emissions (Tg CO<sub>2</sub> yr<sup>-1</sup>) for 2018**

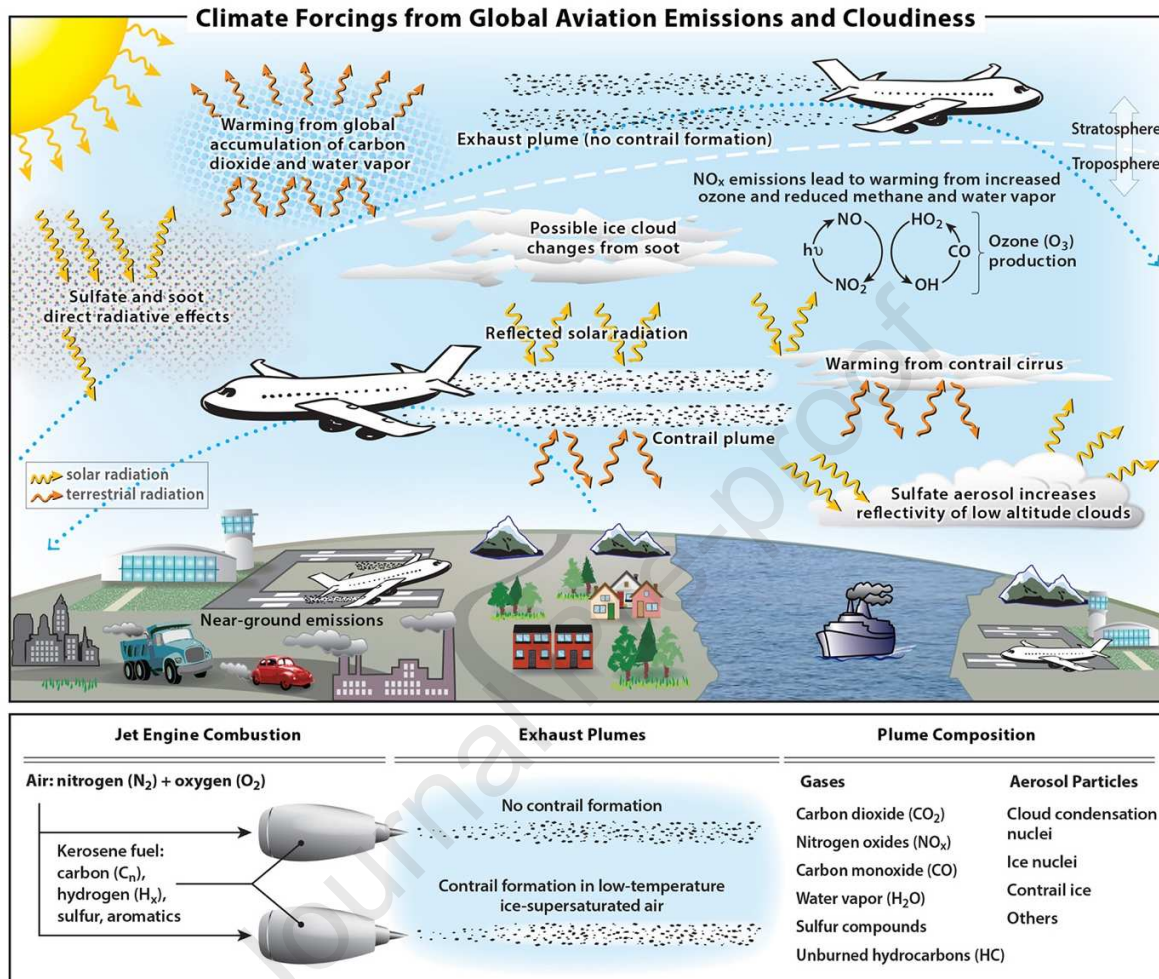
ERF term	GWP <sub>20</sub>	GWP <sub>50</sub>	GWP <sub>100</sub>	GTP <sub>20</sub>	GTP <sub>50</sub>	GTP <sub>100</sub>	GWP* <sub>100</sub> (E* <sub>CO2e</sub> )
CO <sub>2</sub>	1034	1034	1034	1034	1034	1034	1034
Contrail cirrus (Tg CO <sub>2</sub> basis)	2399	1129	652	695	109	90	1834
Contrail cirrus (km basis)	2395	1127	651	694	109	90	1834
Net NO <sub>x</sub>	887	293	163	-318	-99	19	339
Aerosol-radiation							
Soot emissions	40	19	11	12	2	2	20
SO <sub>2</sub> emissions	-310	-146	-84	-90	-14	-12	-158
Water vapor emissions	83	39	23	27	4	3	42
Total CO <sub>2</sub> -eq (using km basis)	4128	2366	1797	1358	1035	1135	3111
Total CO <sub>2</sub> -eq / CO <sub>2</sub>	4.0	2.3	1.7	1.3	1.0	1.1	3.0

1314

1 July 2020 Revised

1315

1316

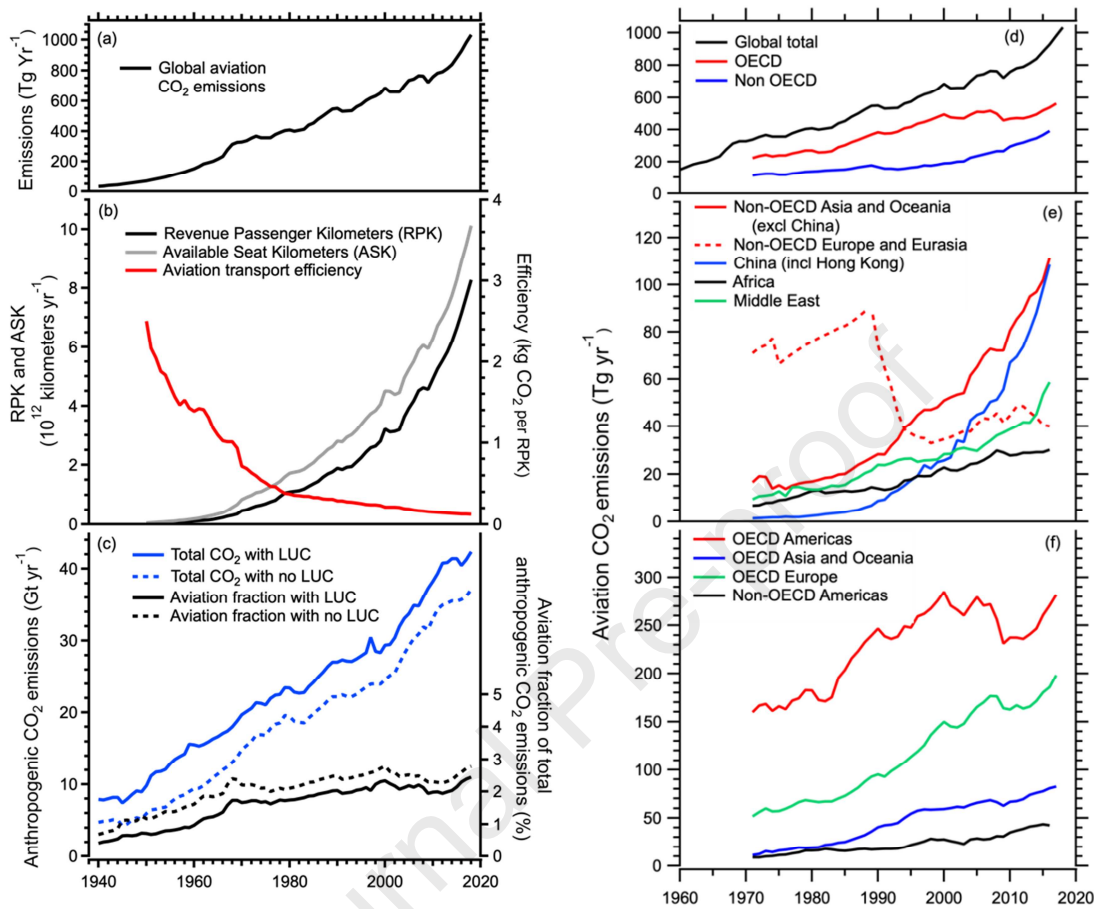


1317 **Figure 1.** Schematic overview of the processes by which aviation emissions and increased cirrus  
 1318 cloudiness affect the climate system. Net positive RF (warming) contributions arise from CO<sub>2</sub>, water  
 1319 vapor, NO<sub>x</sub>, and soot emissions, and from contrail cirrus (consisting of linear contrails and the cirrus  
 1320 cloudiness arising from them). Negative RF (cooling) contributions arise from sulfate aerosol production.  
 1321 Net warming from NO<sub>x</sub> emissions is a sum over warming (short-term ozone increase) and cooling  
 1322 (decreases in methane and stratospheric water vapor, and a long-term decrease in ozone) terms. Net  
 1323 warming from contrail cirrus is a sum over the day/night cycle. These contributions involve a large number  
 1324 of chemical, microphysical, transport and, radiative processes in the global atmosphere. The quantitative  
 1325 ERF values associated with these processes are shown in **Figure 3** for 2018.

1326

1 July 2020 Revised

1327



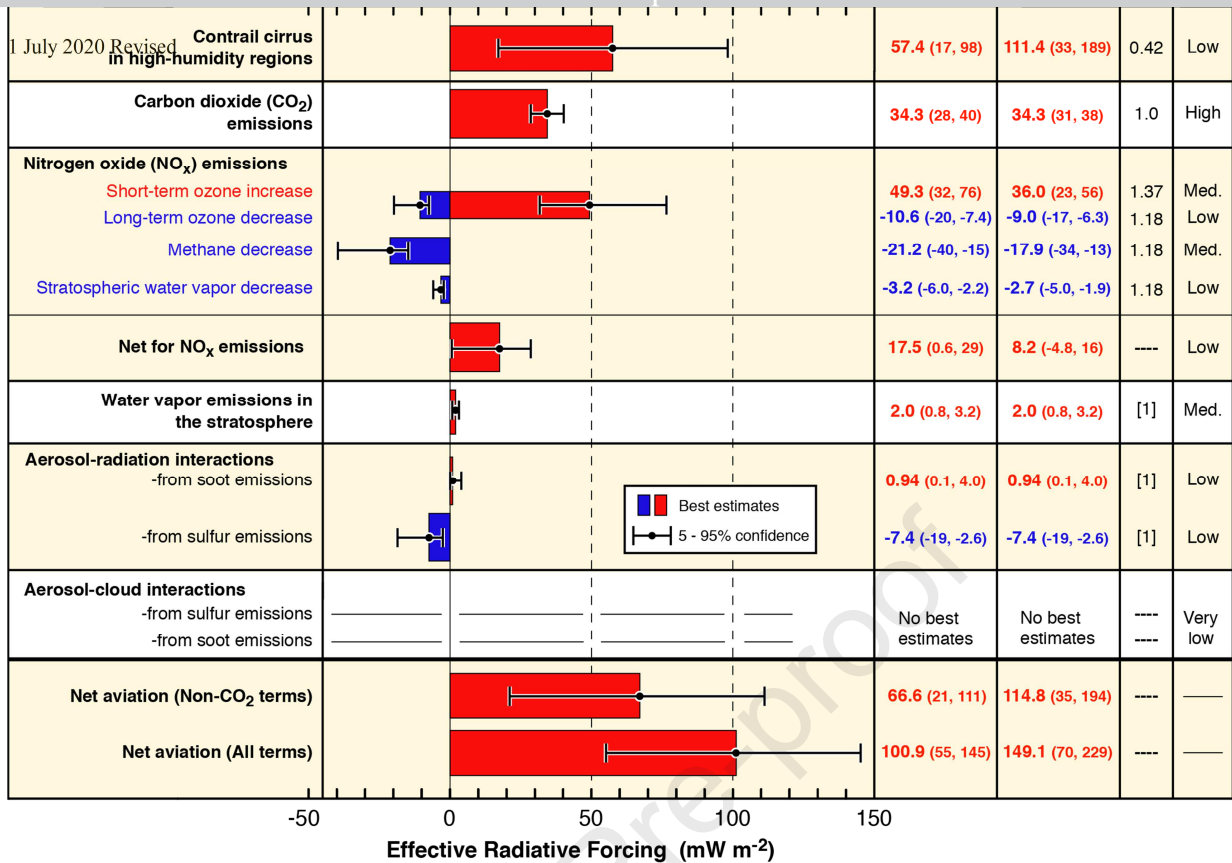
1328

1329 **Figure 2.** Data related to the growth of aviation traffic and CO<sub>2</sub> emissions from 1940 to 2018. Panel (a):  
 1330 Global aviation CO<sub>2</sub> emissions. Underlying fuel usage data for 1940 to 1970 are derived from Sausen and  
 1331 Schumann (2000) and for 1970–2016 from International Energy Agency (UKDS, 2016) data, which  
 1332 include international bunker fuels. For 2017/18, the values are scaled from information from the  
 1333 International Air Transport Association (see Appendix A). The average annual increase of global  
 1334 emissions from 1960 to 2018 is 15 Tg CO<sub>2</sub> yr<sup>-1</sup> and the corresponding decadal average growth rates are 8.0,  
 1335 2.2, 3.0, 2.3 and 1.1% yr<sup>-1</sup>, yielding an overall average of 3.3% yr<sup>-1</sup>. Panel (b): Global aviation traffic in  
 1336 RPK and ASK from Airlines.org (<http://airlines.org/dataset/world-airlines-traffic-and-capacity/>), and the  
 1337 transport efficiency of global aviation in kg CO<sub>2</sub> per RPK. The passenger load factor defined as RPK/ASK  
 1338 increased from about 60% in 1960 to 82% in 2018. Panel (c): Total anthropogenic CO<sub>2</sub> emissions and the  
 1339 aviation fractions of this total with and without the inclusion of CO<sub>2</sub> emissions from land use change  
 1340 (LUC) from the Global Carbon Budget 2018 (Le Quéré et al., 2018). Panel (d)–(f): Additional aviation  
 1341 emissions data by region and year. The yearly sums of OECD and non-OECD values in (d) equal the  
 1342 respective global total values. The regional values in (e) and (f) also sum to equal the yearly global total  
 1343 values. Note different vertical scales. (<http://www.oecd.org/about/membersandpartners/>) (UKDS, 2016)  
 1344 (Country listings in SD Spreadsheet).

1345

1346





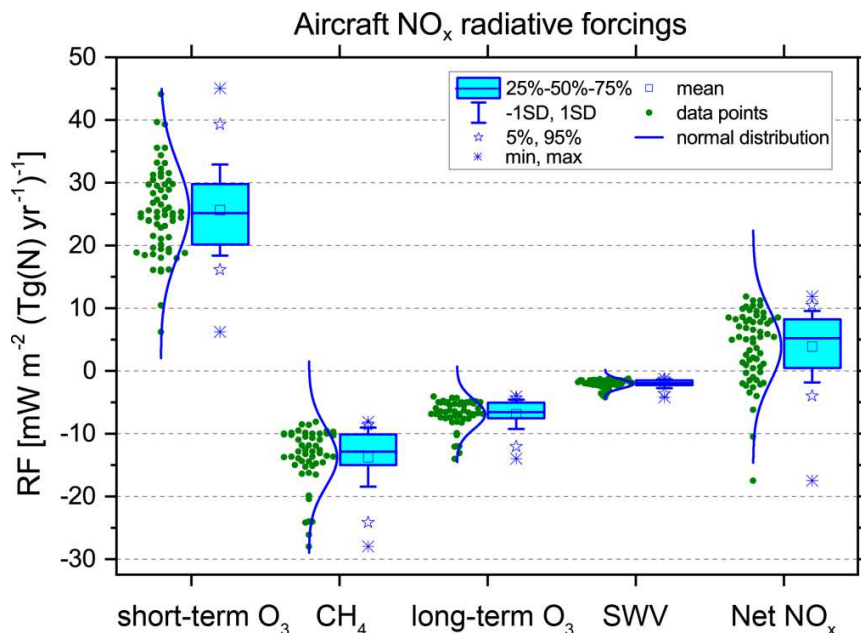
1347

1348

1349 **Figure 3.** Best-estimates for climate forcing terms from global aviation from 1940 to 2018. The bars and  
 1350 whiskers show ERF best estimates and the 5–95% confidence intervals, respectively. Red bars indicate  
 1351 warming terms and blue bars indicate cooling terms. Numerical ERF and RF values are given in the  
 1352 columns with 5–95% confidence intervals along with ERF/RF ratios and confidence levels. ERF and RF  
 1353 values are shown for other years in **Tables 2 and 3, Figure 6** and the SD spreadsheet. RF values are  
 1354 multiplied by the respective ERF/RF ratio to yield ERF values. ERF/RF values designated as [1] indicate  
 1355 that no estimate is available yet. The basis for confidence levels is presented in **Table 4**.

1356

1357

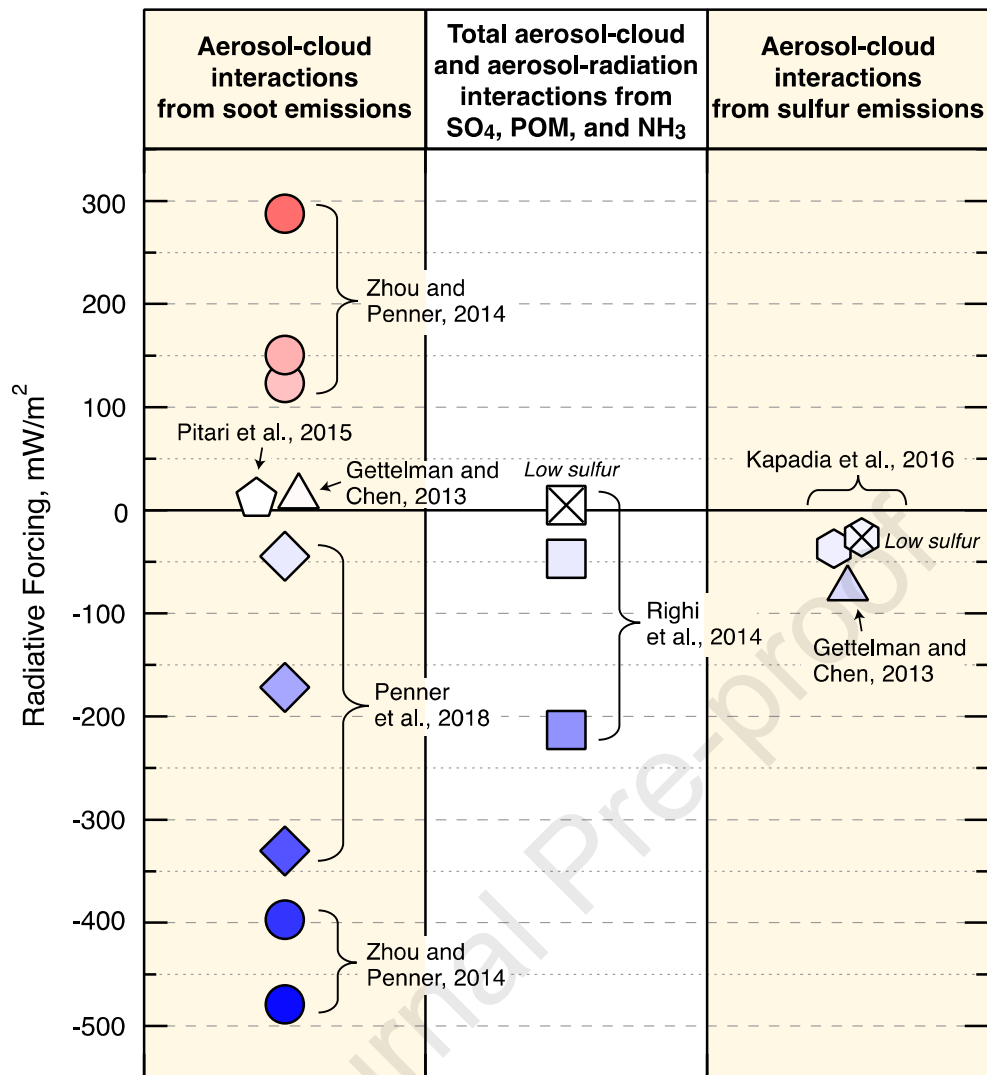


1 July 2020 Revised

1358 **Figure 4.** Results from an ensemble of 18 models from 20 studies for aviation NO<sub>x</sub> impacts: short-term O<sub>3</sub>  
1359 increases; CH<sub>4</sub> reductions, CH<sub>4</sub>-induced long-term reductions of O<sub>3</sub>, CH<sub>4</sub>-induced reductions of  
1360 stratospheric water vapor (SWV) and Net NO<sub>x</sub>. Each data point represents a value of RF per unit emission  
1361 (mW m<sup>-2</sup> (Tg N yr<sup>-1</sup>)<sup>-1</sup>) as normalized from a published study (see SD). CH<sub>4</sub>-induced O<sub>3</sub> and SWV are  
1362 calculated using standardized methodology (see text for details). Note that the displayed values do not  
1363 include correction factors to account for the non-steady-state CH<sub>4</sub> responses to NO<sub>x</sub> emissions and the new  
1364 CH<sub>4</sub> RF parameterization. These adjustments are applied in forming the best estimates as discussed in  
1365 Appendix D.

1366

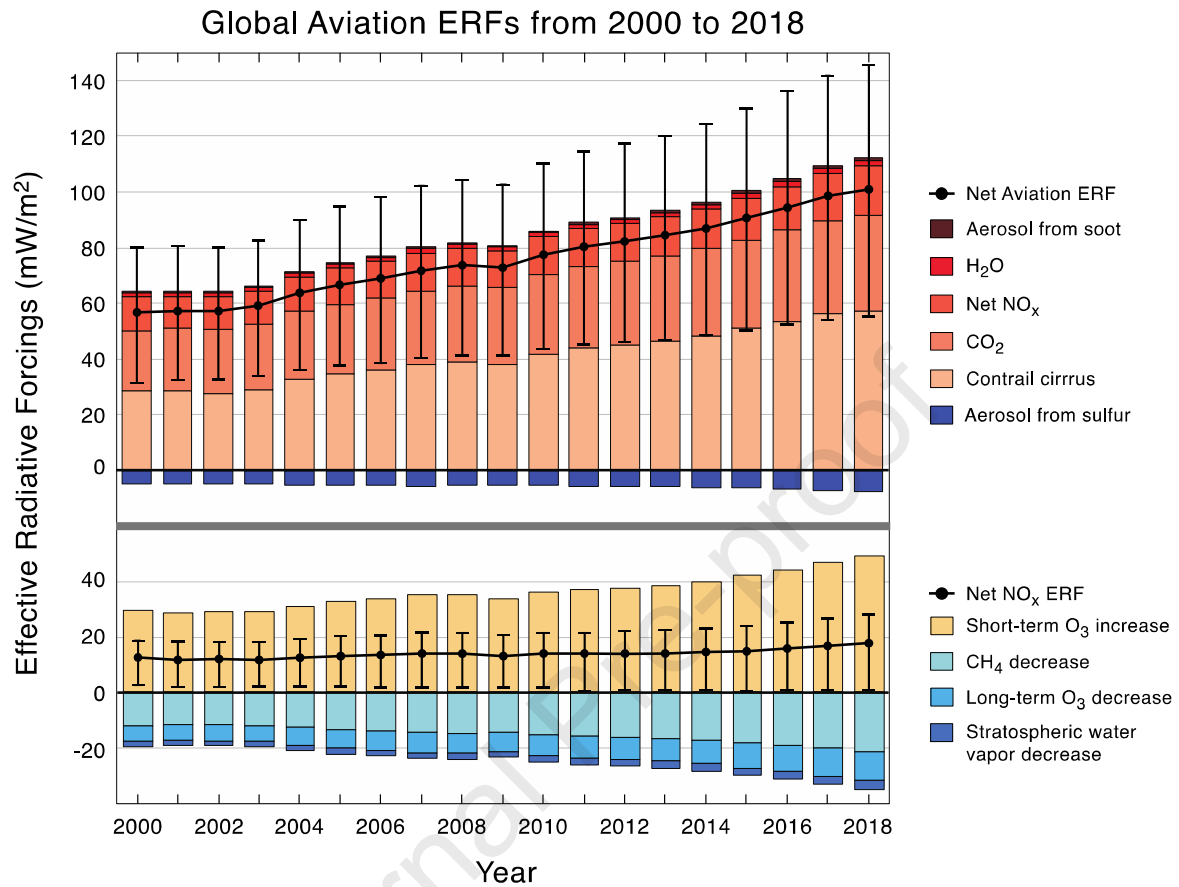
Journal Pre-proof



1367

1368 **Figure 5.** Summary of RF estimates for aerosol-cloud interactions for aviation aerosol as calculated in the  
 1369 SD spreadsheet for a variety of published results normalized to 2018 air traffic and 600 ppm fuel sulfur.  
 1370 The results are shown for soot; total particulate organic matter (POM), sulfate and ammonia (NH<sub>3</sub>); and  
 1371 sulfate aerosol from the indicated studies. The color shading gradient in the symbols indicates increasing  
 1372 positive or negative magnitudes. No best estimate was derived in the present study for any aerosol-cloud  
 1373 effect due to the large uncertainties. In previous studies, the estimates for the soot aerosol-cloud effect are  
 1374 associated with particularly large uncertainty in magnitude and uncertainty in the sign of the effect (Penner  
 1375 et al., 2009; Zhou and Penner, 2014; Penner et al., 2018). As part of the present study, an author (JEP) re-  
 1376 evaluated these earlier studies and it concluded that the Penner et al. (2018) results supersede the earlier  
 1377 Penner et al. (2009) and Zhou and Penner (2014) results because of assumptions regarding updraft  
 1378 velocities during cloud formation. In addition, a bounding sensitivity case in which all aviation soot acts as  
 1379 an IN in Penner et al. (2018) is not included here.

1 July 2020 Revised

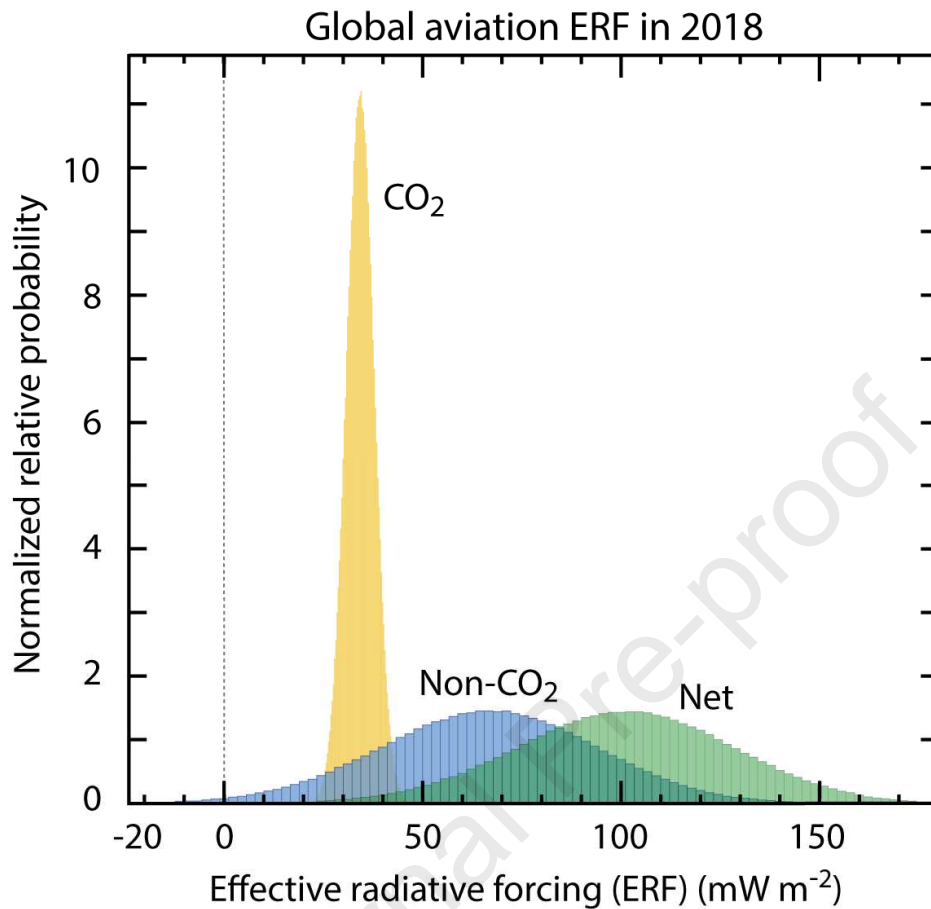


1380

1381 **Figure 6.** Timeseries of calculated ERF values and confidence intervals for annual aviation forcing terms  
 1382 from 2000 to 2018. The top panel shows all ERF terms and the bottom panel shows only the NO<sub>x</sub> terms  
 1383 and net NO<sub>x</sub> ERF. All values are available in the SD spreadsheet, in Tables 2 and 3, and in **Figure 3** for  
 1384 2018 values. The net values are not arithmetic sums of the annual values because the net ERF, as shown in  
 1385 **Figure 3** for 2018, requires a Monte Carlo analysis that properly includes uncertainty distributions and  
 1386 correlations (see text).

1387

1 July 2020 Revised



1388

1389 **Figure 7.** Probability distribution functions (PDFs) for aviation ERFs in 2018 based on the results in  
1390 **Figure 3** and **Table 2**. PDFs are shown separately for CO<sub>2</sub>, the sum of non-CO<sub>2</sub> terms, and the net  
1391 aviation ERF. Since the area of each distribution is normalized to the same value, relative probabilities can  
1392 be intercompared. Uncertainties are expressed by a distribution about the best-estimate value that is normal  
1393 for CO<sub>2</sub> and contrail cirrus, and lognormal for all other components. A one-million-point Monte Carlo  
1394 simulation run was used to calculate all PDFs.

1395

1396 **Appendices**1397 **A. Trends in aviation CO<sub>2</sub> emissions**

1398 Global aviation CO<sub>2</sub> emissions for 1940–1970 were taken from Sausen and Schumann (2000) and for the  
 1399 years 1971–2016 were calculated from International Energy Agency (IEA) data on usage of JET-A and  
 1400 aviation gasoline, largely from annual ‘Oil Information’ digests (e.g., [https://webstore.iea.org/oil-](https://webstore.iea.org/oil-information-2019)  
 1401 [information-2019](https://webstore.iea.org/oil-information-2019)). The regional data are from the same source but accessed online from the IEA Oil  
 1402 Information (1960–2017) held at the UK Data Service (IEA, 2019). Note that these data are proprietary  
 1403 and must be purchased from IEA. Data were unavailable for 2017 and 2018, so incremental annual  
 1404 percentage increases in global aviation fuel usage and, therefore CO<sub>2</sub> emissions, for those years were taken  
 1405 from reports of the International Air Transport Association (IATA, 2019). Some uncertainties exist from  
 1406 the annual fuel estimations and to a much smaller extent, the emission factors. The IEA does not give  
 1407 uncertainties for annual kerosene fuel sales or usage. Sausen and Schumann (2000), from which the 1940  
 1408 to 1970 data are based here, estimated that the uncertainty in cumulative fuel consumption from 1940 to  
 1409 1995 (their dataset) is 20%. There is a known discrepancy of IEA estimates of aviation fuel usage being  
 1410 greater by about 10% than that derived from bottom-up global civil aviation inventories. Actual fuel usage  
 1411 is likely to be somewhere between the two estimates: aviation emissions inventories are known to be  
 1412 incomplete, with only scheduled traffic being available from some air traffic regions, and fuel usage  
 1413 potentially being underestimated from flight routing and cruise altitudes; IEA data on the other hand  
 1414 includes military aviation fuel (not included in civil aviation inventories) and a small fraction of kerosene  
 1415 not used in aviation, but sold for that purpose (L09). The CO<sub>2</sub> emission factors for aviation fuel on the  
 1416 other hand are well determined, and the uncertainty is likely within 1%.

1417 **B. Aviation CO<sub>2</sub> radiative forcings**1418 **Calculation of CO<sub>2</sub> concentrations from emissions—LinClim SCM**

1419 The response of CO<sub>2</sub> concentrations,  $C(t)$ , to a CO<sub>2</sub> aviation emissions rate,  $E(t)$ , is modelled using the  
 1420 method described in Hasselmann et al., (1997) and is expressed as:

$$1421 \quad \Delta C(t) = \int_{t_0}^t G_C(t-t')E(t')dt' \quad (B.1)$$

1422 where

$$1423 \quad G_C(t) = \sum_{j=0}^5 \alpha_j e^{-t/\tau_j} \quad (B.2)$$

1424 and  $\tau_j$  is the e-folding time of mode  $j$  and the equilibrium response of mode  $j$  to a unit emissions of  $\alpha_j \tau_j$ .

1425 The mode parameters used in this study are presented in Sausen and Schumann (2000) and approximate  
 1426 the carbon-cycle model in Meier-Reimer and Hasselmann (1987). The applicability of these parameters in  
 1427 the context of aviation response was tested in a model intercomparison exercise (Khodayari et al., 2013).  
 1428 For the time horizon of 50-60 years into the future, these were found to compare well with other more  
 1429 sophisticated carbon-cycle models such as MAGICC 6.0, which is widely used in the IPCC Fourth  
 1430 Assessment Report (IPCC, 2007). Beyond this horizon, aviation CO<sub>2</sub> concentrations begin to have an  
 1431 impact on the ocean and biosphere uptake of CO<sub>2</sub> and the non-linearities of the system must be accounted  
 1432 for.

1433 **Calculation of CO<sub>2</sub> concentrations from emissions—CICERO-2 SCM**

1434 The CICERO-2 SCM (Fuglestad and Berntsen, 1999; Skeie et al., 2017) uses interconnected process-  
 1435 specific IRFs with explicit treatment of air-sea and air-biosphere exchange of CO<sub>2</sub> (Joos et al., 1996;  
 1436 Alfsen and Berntsen, 1999) that forms a nonlinear carbon cycle. The ocean and biosphere IRFs in

1 July 2020 Revised

1437 CICERO-2 express how the CO<sub>2</sub> impulse decays within each reservoir. The CO<sub>2</sub> partial pressure in each  
 1438 reservoir is calculated as a function of the carbon in that reservoir, and the CO<sub>2</sub> partial pressure in each  
 1439 reservoir is related to the CO<sub>2</sub> partial pressure in the atmosphere by explicitly solving for the  
 1440 atmosphere/ocean/biosphere CO<sub>2</sub> mass transfer. Therefore, the CICERO-2 carbon cycle takes into account  
 1441 the nonlinearity in ocean chemistry and biosphere uptake at high CO<sub>2</sub> partial pressures since it represents  
 1442 the atmospheric change in CO<sub>2</sub> as a function of total background.

#### 1443 **Calculation of CO<sub>2</sub> concentrations from emissions—FaIR SCM**

1444 The FaIR SCM is described by Millar et al. (2017) and summarized as follows. FaIR is a modified version  
 1445 of the IPCC AR5 four time-constant impulse response function (IRF) model, which represents the  
 1446 evolution of atmospheric CO<sub>2</sub> by partitioning emissions of anthropogenic CO<sub>2</sub> between four reservoirs of  
 1447 an atmospheric CO<sub>2</sub> concentrations change, following a pulse emission (see Myhre et al., 2013 for more  
 1448 details). In more comprehensive models, ocean uptake efficiency declines with accumulated CO<sub>2</sub> in ocean  
 1449 sinks (Revelle and Suess, 1957) and uptake of carbon into both terrestrial and marine sinks are reduced by  
 1450 warming (Friedlingstein et al., 2006). FAIR captures some of these dynamics within the simple IRF  
 1451 structure, mimicking the behaviour of Earth System Models/Earth System Models of Intermediate  
 1452 Complexity in response to finite-amplitude CO<sub>2</sub> injections; this is achieved by introducing a state-  
 1453 dependent carbon uptake with a single scaling factor,  $\alpha$ , to all four of the time constants in the carbon cycle  
 1454 of the IPCC AR5 impulse response model used for the calculation of CO<sub>2</sub>-equivalence metrics. This  
 1455 approach is described in more detail by Millar et al. (2017).

#### 1456 **C. Radiative forcing, efficacy and effective radiative forcing (ERF)**

1457 Radiative forcing (RF) has been introduced as a predictor for the expected equilibrium global mean of the  
 1458 (near) surface temperature change  $\Delta T_s$  that results from the introduction of climate forcers, such as  
 1459 additional atmospheric CO<sub>2</sub> or a change in the solar irradiation (e.g., IPCC, 2007):

$$1460 \quad \Delta T_s = \lambda \text{ RF} \quad (\text{C.1})$$

1461 where  $\lambda$  is the climate sensitivity parameter ( $\text{K} (\text{W m}^{-2})^{-1}$ ). Several definitions of RF exist. According to  
 1462 the simplest one, the instantaneous RF is the change in the total irradiation (incoming short-wave solar  
 1463 radiation minus the outgoing long-wave terrestrial radiation) at the top of the atmosphere over the  
 1464 industrial era. However, for most of the climate forcers a better definition (with respect to the linearity of  
 1465 Eq. (C.1)) is the stratosphere-adjusted RF at the tropopause. Here, after the introduction of the new climate  
 1466 forcer, the temperature of the stratosphere is allowed to reach a new radiative equilibrium, while all other  
 1467 atmospheric state variables are kept constant. The stratosphere-adjusted RF at the tropopause was used in  
 1468 many of the earlier IPCC reports (IPCC, 1999) and in earlier assessments of aviation climate impacts  
 1469 (Sausen et al., 2005; L09).

1470 While Eq. (C.1) is a fairly good approximation for many nearly spatially homogeneously distributed  
 1471 climate forcers, such as global increases of CO<sub>2</sub> or CH<sub>4</sub>, Eq. (C.1) fails to some extent for many forcers  
 1472 that are heterogeneously distributed either horizontally or vertically; such is the case for aviation-induced  
 1473 ozone perturbations and contrail cirrus (e.g., Hansen et al., 1997, 2005; Forster and Shine, 1997; Stuber et  
 1474 al., 2005). To overcome this problem Hansen and Nazarenko (2004) introduced the efficacy,  $r_i$ , into Eq.  
 1475 (C.1):

$$1476 \quad \Delta T_s = r_i \lambda_{\text{CO}_2} \text{ RF} = \lambda_i \text{ RF} \text{ with } \lambda_i = r_i \lambda_{\text{CO}_2} \quad (\text{C.2})$$

1477 Here  $\lambda_{\text{CO}_2}$  is the climate sensitivity parameter for a CO<sub>2</sub> perturbation. While  $\lambda$  in (C.1) is considered a  
 1478 universal constant, which can only be determined by climate models and hence is model dependent,  $\lambda_i$   
 1479 depends on the type of forcing, as does  $r_i$ . (While  $r_{\text{CO}_2}$  is 1 by definition,  $r_{\text{linear contrails}}$  is  $<1$  (Ponater, et al.,  
 1480 2005; Rap et al., 2010)). Eq. (C.2) can also be expressed differently:

$$1481 \quad T_s = \lambda_{\text{CO}_2} \text{ RF}_i^* \text{ with } \text{RF}_i^* = r_i \text{ RF} \quad (\text{C.3})$$

1482 Here  $RF_i^*$  is the forcing modified by the efficacy, which yields a better approximation for the surface  
 1483 temperature change than RF. However, the calculation of the  $RF_i^*$  is computationally much more  
 1484 expensive than the calculation of RF, as it requires the determination of the equilibrium temperature  
 1485 change,  $\Delta T_s$ , with a comprehensive climate model.

1486 As an alternative, the effective radiative forcing (ERF) has been introduced as a more practical indicator of  
 1487 the eventual global mean temperature response (IPCC, 2013). While  $RF_i^*$  assumes equilibrium climate  
 1488 change, ERF only includes all 'fast' atmospheric responses to a given climate forcer. For example, rapid  
 1489 adjustments in cloud cover, such as from aerosols, or in properties that respond to changes in water vapor,  
 1490 can either increase or decrease the initial RF. In contrast, the instantaneous, stratosphere-adjusted, and  
 1491 effective RFs for well-mixed greenhouse gases are nearly equal. In practice, ERF is determined with a  
 1492 comprehensive climate model, which calculates a new equilibrium radiative imbalance, while the sea  
 1493 surface temperature and/or the global surface temperature is kept constant. As a consequence, an ERF  
 1494 value is expected to be somewhere between RF and  $RF_i^*$  values and closer to  $RF_i^*$  values.

#### 1495 **D. Aviation $NO_x$ radiative forcings**

##### 1496 **Impacts of $NO_x$ emissions on ozone, methane and stratospheric water vapor**

1497 *Model studies.* In this ensemble analysis of the climate forcing from aviation  $NO_x$  emissions, the results of  
 1498 20 studies published since the IPCC (1999) aviation report were considered: IPCC (1999), Sausen et al.  
 1499 (2005), Stordal et al. (2006), Köhler et al. (2008), Hoor et al. (2009), Myhre et al. (2011), Frömming et al.  
 1500 (2012), Olivié et al. (2012), Gottschaldt et al. (2013), Köhler et al. (2013), Olsen et al. (2013), Skowron  
 1501 et al. (2013), Khodayari et al. (2014a), Khodayari et al. (2014b), Søvde et al. (2014), Skowron et al. (2015),  
 1502 Pitari et al. (2015), Kapadia et al. (2016), Pitari et al. (2016), Lund et al. (2017). Three studies that reported  
 1503 results from a 100-year integration of a pulse  $NO_x$  emission (Wild et al. 2001, Derwent et al. 2001,  
 1504 Stevenson et al. 2004) were not included in this analysis, nor has as Unger et al. (2010) which uses a  
 1505 different methodology to the aforementioned.

1506 This model ensemble represents various methodologies in calculating and treating the long-term effects; in  
 1507 order to avoid gaps and additional uncertainties, standardized RFs for reductions in  $CH_4$ -induced  $O_3$  and  
 1508 SWV were adopted, except for one study that calculates the 'real' long-term effects from their 50-yr  
 1509 integrations (Pitari et al., 2016):

- 1510 • All analyzed short-term  $O_3$  RFs account for a stratospheric adjustment: Assuming that it reduces the  
 1511 instantaneous RF by ~20% (Myhre et al., 2013, Stevenson et al., 1998), a factor of 0.8 was applied to  
 1512 any  $O_3$  RF that is an instantaneous RF (e.g., in the cases of Khodayari et al. (2014a,b) and Olsen et al.  
 1513 (2013)).
- 1514 • Reductions in  $CH_4$ -induced  $O_3$  and SWV are defined as 50% (Myhre et al., 2013) and 15% (Myhre et  
 1515 al., 2007) of reported  $CH_4$  RFs, respectively. This is applicable for studies that either originally did not  
 1516 provide  $CH_4$ -induced  $O_3$  and SWV estimates (e.g., IPCC, 1999, Sausen et al., 2005, Olsen et al., 2013)  
 1517 or derived these RFs using another assumptions (e.g., Stordal et al., 2006, Köhler et al., 2008, Hoor et  
 1518 al., 2009, Gottschaldt et al., 2013, Köhler et al., 2013, Skowron et al., 2013, Khodayari et al., 2014a).

1519 Further assumptions regarding data treatment are:

- 1520 • Frömming et al. (2012), Olivié et al. (2012), Khodayari et al. (2014b) and Kapadia et al. (2016)  
 1521 provide the short-term  $O_3$  RFs only and p-TOMCAT in Stordal et al. (2006) calculates just the long-  
 1522 term effects; thus, these numbers are included in the respective  $NO_x$  variable analysis but do not  
 1523 contribute to the net  $NO_x$  estimate.
- 1524 • Whenever the same estimate appears repetitively in subsequent studies, it is treated as a single entry:  
 1525 this is the case for CAM4 short-term  $O_3$  RF that appears in Khodayari et al. (2014a; b) and Olsen et al.



1 July 2020 Revised

1526 (2013), CAM5 short-term O<sub>3</sub> RF that can be found in Khodayari et al. (2014a; b) and NASA ModelE2  
1527 short-term O<sub>3</sub> and CH<sub>4</sub> RFs presented by Unger et al. (2013) and Olsen et al. (2013).

1528 In addition, the ERF estimates for the CH<sub>4</sub> term include shortwave RF (Etminan et al., 2016). The  
1529 inclusion of shortwave forcing in the simplified expression increases CH<sub>4</sub> RF from aviation NO<sub>x</sub> emissions  
1530 by 23% (based on MOZART-3 CTM runs driven for all the aircraft emission inventories represented in the  
1531 model ensemble) (**Table D.1**).

1532 **Ensemble values.** This ensemble analysis covers a period of almost two decades; however, none of the RF  
1533 per unit of emitted N estimates show any trends over time of publication and the spread in RF per unit of  
1534 emitted N values has not changed. The short-term O<sub>3</sub> RF varies from 6.2 to 45.1 mW m<sup>-2</sup> (Tg (N) yr<sup>-1</sup>)<sup>-1</sup>,  
1535 where these values come from the NASA ModelE2 (Olsen et al., 2013) and p-TOMCAT (Hoor et al.,  
1536 2009) models, respectively. The long-term CH<sub>4</sub> RF varies from -27.9 to -8.1 mW m<sup>-2</sup> (Tg (N) yr<sup>-1</sup>)<sup>-1</sup>, from  
1537 the p-TOMCAT (Köhler et al., 2008) and MOZART3 (Skowron et al., 2015) models, respectively. The  
1538 spread of other CH<sub>4</sub>-induced long-term effects follows that of CH<sub>4</sub>. The net-NO<sub>x</sub> RF varies from -17.5 to  
1539 11.9 mW m<sup>-2</sup> (Tg (N) yr<sup>-1</sup>)<sup>-1</sup> from ECHAM/MESSy (Gottschaldt et al., 2013) and CAM4 (Khodayari et al.,  
1540 2014a), respectively. The results from the mid-1990s CTMs are within the envelope of RFs generated  
1541 more recently (**Figure 3**). The numbers from IPCC (1999) and related studies, Sausen et al. (2005) and  
1542 L09, where the non-CO<sub>2</sub> effects were originally calibrated to the results from IPCC (1999), do not alter the  
1543 best NO<sub>x</sub> RF values and their uncertainties (**Table D.2**).

1544 **Correlations.** The correlations between the NO<sub>x</sub> RF components are shown in **Figure D.1**. In addition to  
1545 the significant negative correlations between the short-term and the long-term aviation RF components,  
1546 correlations between the net-NO<sub>x</sub> effect and its components are also apparent, especially for the short-term  
1547 O<sub>3</sub> and net-NO<sub>x</sub> components; however, their strength is around half. The high correlations (p=1, R<sup>2</sup>=1)  
1548 across the long-term effects is expected since CH<sub>4</sub>-induced O<sub>3</sub> and SWV are all derived based on CH<sub>4</sub> RFs.  
1549 In units of mW m<sup>-2</sup> (Tg(N) yr<sup>-1</sup>)<sup>-1</sup>, 49% of this ensemble short-term O<sub>3</sub> RF is concentrated between 20 and  
1550 35, 43% of CH<sub>4</sub> RFs is found between -14 and -10, 41% of CH<sub>4</sub>-induced O<sub>3</sub> RFs is between -7 and -5 and  
1551 45% of SWV RFs vary from -2.5 to -1.5. Of the normalized net-NO<sub>x</sub> RFs resulting from this ensemble,  
1552 44% are observed between 5 and 10 mW m<sup>-2</sup> (Tg(N) yr<sup>-1</sup>)<sup>-1</sup>.

1553 **Transient vs. equilibrium.** In calculating the CH<sub>4</sub> RF response to aviation NO<sub>x</sub> emissions, the lack of steady-  
1554 state conditions is an important consideration. Since methane (CH<sub>4</sub>) has a lifetime of the order 8–12 years  
1555 (largely model-dependent) any NO<sub>x</sub> perturbation takes on the order ~40 years to come within 2% of the  
1556 steady state solution. Moreover, the timescale of removal of CH<sub>4</sub> from the atmosphere is made longer  
1557 through a positive chemical feedback (Prather et al. 1994). In order to overcome the necessity to run a  
1558 global chemical transport model (CTM) with full chemistry for such long integrations, a parameterization  
1559 to account for this perturbation was originally developed by Fuglested et al. (1999) and has been widely  
1560 adopted since then. However, with the significant annual increases in aviation NO<sub>x</sub> emissions over the last  
1561 several decades (**Figure D.2a**) the CH<sub>4</sub> response does not reach its steady-state value in any given year of  
1562 emissions, so the steady-state solution generally overstates the CH<sub>4</sub> response in a particular year from  
1563 historical time-evolving emissions. Similar considerations apply to other sectors with substantial NO<sub>x</sub>  
1564 emissions such as shipping (Myhre et al., 2011). If steady-state conditions are utilized, there is a  
1565 conceptual and quantitative mismatch when comparing the NO<sub>x</sub> RF from aviation with other RF terms,  
1566 since RF represents a particular condition at a point in time, not the steady-state conditions. To remedy this  
1567 mismatch, Myhre et al. (2011) suggested that a factor accounting for the non-steady-state condition of CH<sub>4</sub>  
1568 be introduced, thereby modifying the CH<sub>4</sub> impact for a given year of interest, and further suggested that for  
1569 the aviation RF in the year 2000 the CH<sub>4</sub> term be reduced by approximately 35% for aircraft emissions  
1570 using a simplified estimation derived from Grewe and Stenke (2008).

1571 Here, we present an updated methodology to calculate the non-steady-state aviation-NO<sub>x</sub>-induced CH<sub>4</sub>  
1572 perturbation for the specific year of 2018. The method relies on transient and steady-state runs of the

1 July 2020 Revised

1573 TROPOS 2D CTM. The results of the steady-state runs using constant emissions for a given year are  
1574 compared with those of transient runs using background historical surface emissions from anthropogenic  
1575 activities and the corresponding aviation  $\text{NO}_x$  emissions. The latter requires full implementation of time-  
1576 varying  $\text{CH}_4$  emissions into the model simulation, a requirement that is not a standard set-up for many of  
1577 the CTM/GCMs currently in use where  $\text{CH}_4$  conditions are defined from observations as fixed  
1578 concentrations with relaxation terms introduced to accommodate perturbations to these concentrations. The  
1579 use of CTM runs explicitly accounts for changing background atmospheric conditions over the integration  
1580 period as well as the change in emission rate dependence of the  $\text{O}_3$  and  $\text{CH}_4$  responses.

1581 *Method.* In order to compare these two methods, two types of experiments were performed:

- 1582 • Transient experiment: a long-term simulation with anthropogenic (surface and aviation) emissions  
1583 evolving over time covering the period 1950–2050, using historical data up to 2000 and the RCP-4.5  
1584 scenario after 2000 (**Figure D.2a**),
- 1585 • Steady-state experiment: a 100-year simulation with constant anthropogenic (surface and aviation)  
1586 emissions representing the year 2000, 2018 or 2050 (**Figure D.2a**); the steady-state  $\text{CH}_4$  response starts  
1587 to be observed 60–70 years into the run.

1588 Each of these experiments was run twice, with and without aviation emissions, and the difference between  
1589 these two results defined as the aircraft response (e.g., **Figure D.2d-f**). The initial concentrations of  $\text{CH}_4$   
1590 were set using the observations from NOAA surface stations (Montzka et al., 2000) for 1950 and 2000; for  
1591 the year 2050 the  $\text{CH}_4$  concentrations are taken from projections of the MAGICC model (Meinshausen et  
1592 al., 2011). The background anthropogenic emissions of  $\text{CO}$ ,  $\text{CH}_4$ ,  $\text{NO}_x$ ,  $\text{N}_2\text{O}$ , and non-methane volatile  
1593 organic carbon (NMVOC) compounds, as well as aircraft  $\text{NO}_x$  emissions, evolve during the period 1950-  
1594 2050 (Lamarque et al., 2010; Clarke et al., 2007) (**Figure D.2a**). The natural emissions from soils and  
1595 oceans were kept constant and represent the year 2000 (Prather et al., 2001).

1596 The TROPOS CTM is a latitudinally-averaged, two-dimensional Eulerian global tropospheric chemistry  
1597 model extensively evaluated by Hough (1989; 1991). The model's domain extends from pole-to-pole (24  
1598 latitudinal grid cells) and from the surface to an altitude of 24 km (12 vertical layers). TROPOS is driven  
1599 by chemistry, emissions, transport, removal processes and upper boundary conditions. There are 56  
1600 chemical species in the chemical mechanism of the model, which consists of 91 thermal reactions, 27  
1601 photolytic reactions and 7 more reactions, which include night-time  $\text{NO}_3$  chemistry. The reaction rates and  
1602 cross sections were updated to the evaluation of Sander et al. (2006) (see Skowron et. al, 2009). There are  
1603 no fixed concentrations within the model domain other than the upper boundary conditions, which are  
1604 specified for long-lived species and for gases that have stratospheric sources. This 2D CTM has the  
1605 disadvantage of zonal symmetry but has the advantage of an adequate chemical scheme and computational  
1606 efficiency, such that long-term integrations can be reasonably performed. Owing to the aforementioned  
1607 reasons, the  $\text{O}_3$  response in TROPOS is overestimated by a factor of  $\sim 2$  by comparison with a range of up-  
1608 to-date 3D models. As a consequence, the  $\text{CH}_4$  results in **Figures. D.2d-f** were reduced accordingly. This  
1609 modification of the original TROPOS responses does not affect the core result of this study, which is the  
1610 *relative* difference of  $\text{CH}_4$  responses between transient and equilibrium methods.

1611 *Results.* **Figure D.2b** shows the evolution of the global  $\text{CH}_4$  burden over the period 1950–2050 in the  
1612 transient TROPOS simulation. There is a steady growth in the atmospheric  $\text{CH}_4$  burden, with a small  
1613 decline over the period 1997–2007 in response to the decrease in  $\text{CH}_4$  emissions over the period 1990–  
1614 2000. The steady-state simulations for the year 2000 and 2050 agree well (within 1%) with transient  $\text{CH}_4$   
1615 responses for the respective years. A similar agreement is observed for modelled transient and steady-state  
1616  $\text{CH}_4$  lifetimes in **Figure D.2c**. Most of the  $\text{CH}_4$  loss in the atmosphere is driven by OH and the oxidative  
1617 capacity of the atmosphere changes over time (thus  $\text{CH}_4$  lifetime as well), influenced by emissions of  $\text{CO}$ ,  
1618  $\text{NO}_x$ , NMVOC or  $\text{CH}_4$ .

1 July 2020 Revised

1619 **Figure D.2c** shows the evolution of global CH<sub>4</sub> lifetime (LT) over the period 1950–2050: there is a  
1620 decrease in the CH<sub>4</sub> lifetime between 1950 and 2000 (until around 2007), whilst under the RCP-4.5  
1621 scenario the opposite is observed, with the CH<sub>4</sub> lifetime increasing by 3.5% by the end of 2050 compared  
1622 with 2000. The TROPOS CH<sub>4</sub> lifetimes agree relatively well with other studies (e.g., Holmes et al., 2013;  
1623 Voulgarakis et al.; 2013, Dalsøren et al., 2016) not only in terms of absolute numbers but also the rate of  
1624 changes; a detailed comparison is presented in **Table D.3**. The perturbation lifetime of CH<sub>4</sub> in TROPOS is  
1625 37% longer than its global lifetime and the sensitivity coefficient  $s = \partial \ln(\text{LT}) / \partial \ln(\text{CH}_4)$  is 0.27, placing  
1626 these estimates in the middle of model ranges (e.g., Prather 2001, Holmes et al. 2011). These terms were  
1627 calculated using a 5% increase of CH<sub>4</sub> global levels for the year 2000. There is no need to apply the  
1628 feedback factor (1.37) to the TROPOS CH<sub>4</sub> estimates as it is already included in the observed responses;  
1629 TROPOS does not have a fixed boundary conditions, so CH<sub>4</sub> and OH can *freely* interact.

1630 Aircraft NO<sub>x</sub> emissions, via the chemical coupling to OH and HO<sub>2</sub>, enhance OH, which reduces the global  
1631 CH<sub>4</sub> lifetime. **Figure D.2d** shows the evolution of the CH<sub>4</sub> lifetime reduction in the transient 1950–2050  
1632 simulation and in steady-state runs for conditions representing the years 2000 and 2050. In the transient  
1633 run, there is a steady decrease of global CH<sub>4</sub> lifetime as a consequence of a constant increase of aviation  
1634 NO<sub>x</sub> emissions during the period 1950–2050. The agreement in 2000 and 2050 between the transient and  
1635 steady-state CH<sub>4</sub> lifetime reductions is within 6% (on a global scale) (see **Table D.3**). These relatively  
1636 small differences in CH<sub>4</sub> lifetime lead to much more pronounced differences in the associated global CH<sub>4</sub>  
1637 burdens as shown in **Figure D.2e**. In contrast to the lifetime results, the CH<sub>4</sub> burden response in the  
1638 transient run lags behind the steady-state CH<sub>4</sub> response with differences of 27% in the year 2000 and 20%  
1639 in the year 2050. Similarly, the calculations for 2018 emissions yield a multiplicative correction factor of  
1640 0.79 (**Figure D.2f**), which has been incorporated into the ERF values of CH<sub>4</sub>, long-term O<sub>3</sub> and SWV  
1641 shown in **Figure 5**.

1642 The CH<sub>4</sub> results contrast with O<sub>3</sub> changes from aircraft NO<sub>x</sub> emissions, which agree within 3% between  
1643 transient and steady-state experiments with aircraft O<sub>3</sub> burdens of 10.3 and 10.6 Tg (O<sub>3</sub>), respectively, in  
1644 the year 2000. These TROPOS O<sub>3</sub> magnitudes are at the upper limit of model ranges, as present-day  
1645 aircraft O<sub>3</sub> perturbations found in the literature vary from 3 to 11 Tg (O<sub>3</sub>) (e.g., Hoor et al., 2009; Holmes  
1646 et al., 2011; Khodayari et al., 2014a). The aircraft O<sub>3</sub> burden increases by 41% in 2050, reaching 17.2 and  
1647 18.0 Tg(O<sub>3</sub>) for transient and steady-state experiments, respectively. This agrees with other studies (e.g.,  
1648 Olsen et al., 2013) that report a multi-model average increase of 44% in O<sub>3</sub> burden from future aircraft  
1649 NO<sub>x</sub> emissions under the RCP-4.5 scenario.

1650 The present approach is in general agreement with that presented by Grewe and Stenke (G&S) (2008),  
1651 which accounts for CH<sub>4</sub> concentrations not being in steady-state with OH changes in the year of  
1652 simulation. The present CTM results further demonstrate the importance of explicitly calculating CH<sub>4</sub>  
1653 changes in response to time-dependent aviation NO<sub>x</sub> emissions rather than assuming constant emissions.  
1654 The difference between transient and steady-state CH<sub>4</sub> for the year 2000 found with TROPOS is smaller  
1655 than that resulting from the G&S approach (Myhre et al., 2011) (27% and 35%, respectively). **Table D.4**  
1656 presents a further comparison of CH<sub>4</sub> correction factors derived in this study. The systematic differences  
1657 are likely due to the G&S values being based on a simplified chemistry/climate model (AirClim) and the  
1658 present TROPOS simulations having a different experimental setup (all our emissions (surface + aircraft)  
1659 are time-varying) and a full chemical reaction scheme with explicit calculations performed on time-  
1660 varying emissions. Indeed, if TROPOS is run with constant background emissions representing the year  
1661 2000 in a similar manner using G&S methodology, the difference between transient and steady-state CH<sub>4</sub>  
1662 for the year 2000 increases from 27% to 31%. This change shows that background emissions modify the  
1663 CH<sub>4</sub> correction factor and further emphasizes the need to have surface and aircraft emissions that  
1664 simultaneously follow historical pathways. In other studies using the G&S methodology, CH<sub>4</sub> correction  
1665 factors vary from 0.74 to 1.15 depending on the investigated year (2025 or 2050) and aircraft emission

1 July 2020 Revised

1666 scenario (SRES A1B, B1 and B1 ACARE) (the factor can be larger than 1 if the aircraft emissions are  
1667 assumed to decrease in the preceding years) (Hodnebrog et al., 2011; 2012).

1668 Uncertainties in the CH<sub>4</sub> correction factor are associated mainly with inter-model differences and the  
1669 applied emission scenarios; the correction factor is sensitive, within ~10%, to inter-model differences  
1670 (based on two models, TROPOS and AirClim) and it can vary by another  $\pm 10\%$  depending on emission  
1671 scenario (based on a range of RCP projections up to 2050). Given that the uncertainties of the CH<sub>4</sub>  
1672 correction factor on the net-NO<sub>x</sub> RF are rather small, especially when compared with overall uncertainties,  
1673 we do not include in the estimated uncertainty of the net-NO<sub>x</sub> RF value a separate uncertainty due to the  
1674 correction factor.

## 1675 E. Contrail cirrus

1676 The global contrail cirrus RF is calculated by homogenizing existing estimates through the use of specific  
1677 scaling factors. The factors relate to the choice of air traffic inventory and its basis year; the use of the full  
1678 3D flight distance; the use of hourly air traffic data; the feedback of natural clouds; and correcting for  
1679 weaknesses in the radiative transfer calculations. The corrections and scaling actions are:

- 1680 • The estimate of Chen and Gettelman (2013) was corrected by redoing the CAM simulation using a  
1681 lower ice crystal radius of 7  $\mu\text{m}$  and a larger contrail cross-sectional area of 0.09 km<sup>2</sup> for the  
1682 initialization of contrails at an age of about 15–20 minutes, in agreement with observations (Schumann  
1683 et al., 2017b). The resulting change in cirrus cloudiness including the adjustment in cloudiness due to  
1684 the presence of contrail cirrus leads to a radiative forcing of 57 mW m<sup>-2</sup>.
- 1685 • A scaling S<sub>1</sub> of 1.4 is applied for estimates based on the AERO2k inventory for the year 2002 instead  
1686 of the AEDT inventory for the year 2006 (Bock and Burkhardt, 2016);
- 1687 • A scaling S<sub>2</sub> of 1.14 is applied to estimates that are based on track distance instead of slant distance  
1688 (Bock and Burkhardt, 2016). The ‘slant’ air traffic distance is the full flight distance and not the ground  
1689 projected ‘track’ distance.
- 1690 • A scaling S<sub>3</sub> of 0.87 is applied to estimates that used monthly instead of hourly resolved air traffic  
1691 data. This scaling is based on an estimate for the impact of the temporal resolution of the air traffic data  
1692 of -25% to -30% within CAM (Chen et al., 2012) and one of no significant change in ECHAM4-  
1693 CCMod.
- 1694 • A scaling S<sub>4</sub> of 1.15 is applied to account for the underestimation of RF in radiative transfer  
1695 calculations that use frequency bands instead of line by line calculations (Myhre et al. 2009).

1696 The study details and scaling results are shown in **Table E.1**. Weighting each estimate equally, the best  
1697 estimate of global contrail cirrus RF is approximately 66 mW m<sup>-2</sup>. As noted in the main text, the Chen and  
1698 Gettelman (2013) calculation is interpreted as being closer to an ERF than an RF, so was excluded from  
1699 this averaging. This mean RF estimate does not include the RF due to contrails forming within natural  
1700 cirrus. Uncertainty due to scalings S<sub>3</sub>–S<sub>4</sub> is included in the uncertainty discussion below, whereas  
1701 uncertainty in scalings S<sub>1</sub>–S<sub>2</sub>, namely updating the ECHAM4-CCMod estimates using sensitivities from  
1702 ECHAM5-CCMod, is neglected.

1703 The statistical uncertainty of global contrail cirrus RF cannot be estimated from the small number of  
1704 available studies. Uncertainties affecting our contrail cirrus estimates are, on the one hand, due to (A)  
1705 uncertainties in the radiative response to the presence of contrail cirrus and, on the other hand, (B)  
1706 uncertainties in the upper tropospheric water budget and the contrail cirrus scheme. In most cases, we can  
1707 only infer very rough estimates for the uncertainties related to specific processes.

1708 (A) Uncertainties associated with the radiative response to contrail cirrus are:

1 July 2020 Revised

- 1709 A1. Uncertainty related to the model's radiative transfer scheme of approximately 35% (Myhre et al.,  
1710 2009).
- 1711 A2. Uncertainty in the inhomogeneity of ice clouds within a grid box of a climate model (Carlin et al.,  
1712 2002; Pomroy and Illingworth, 2000), the vertical cloud overlap, and the use of plane parallel geometry  
1713 as compared to full 3D radiative transfer (Gounou and Hogan, 2007), which together amount to  
1714 approximately 35%.
- 1715 A3. Uncertainty estimating radiative transfer in a global climate model in the presence of very small ice  
1716 crystals within young contrails, which may amount to about 10% (Bock and Burkhardt, 2016). The  
1717 uncertainty is dependent on the contrail cirrus ice water content.
- 1718 A4. Uncertainty due to the ice crystal habit is approximately 20% according to Markowicz and Witek  
1719 (2011).
- 1720 A5. Uncertainty in the radiative transfer due to soot cores within the contrail cirrus ice crystals is  
1721 thought to be large, as the change in the shortwave (SW) albedo is large (Liou et al., 2013). The soot  
1722 impact on contrail cirrus RF has not yet been quantified.
- 1723 Overall, uncertainty in the radiative response to contrail cirrus (excluding A3) is estimated to be about  
1724 55%, assuming independence of different uncertainties and excluding the impact of ice crystal soot cores.  
1725 The uncertainty A3 is included in the uncertainty estimate under (B) because A3 and B2 are dependent  
1726 uncertainties.
- 1727 (B) Uncertainty in contrail cirrus RF associated with the upper-tropospheric water budget and the contrail  
1728 cirrus scheme are:
- 1729 B1. Uncertainty in contrail cirrus RF associated with the uncertainty in upper-tropospheric ice  
1730 supersaturation. This results from a lack of knowledge in ambient conditions due to the low vertical  
1731 resolution of satellite instruments (Lamquin et al., 2012) and to the ability of models to reproduce the  
1732 observed statistics of ice supersaturation. This contributes about 20% to uncertainty.
- 1733 B2. There is uncertainty related to ice crystal number densities within young contrails. Ice nucleation  
1734 within the plume can vary drastically depending on the water supersaturation reached within the plume  
1735 and on the soot emissions (Kärcher et al., 2015; 2018). This dependency on the atmospheric state leads  
1736 to a reduction in the number of nucleated ice crystals in particular in the tropics and at lower flight  
1737 levels (Bier and Burkhardt, 2019) leading to a large uncertainty in the impact of tropical and subtropical  
1738 air traffic. Depending on the atmospheric state and ice crystal numbers, a varying fraction of ice crystals  
1739 can be lost in the contrail vortex phase (Unterstrasser, 2014). We assume an uncertainty in average  
1740 contrail ice crystal numbers after the vortex phase of about 50% leading to an uncertainty in contrail  
1741 cirrus RF of about 20%. This estimate of the sensitivity of contrail cirrus RF to ice crystal numbers in  
1742 newly formed contrails is based on simulations with ECHAM5-CCMod (Burkhardt et al., 2018).
- 1743 B3. The uncertainty in the lifetime of contrail cirrus, affecting the day-/night-time contrail cover, has  
1744 only a small impact on the estimated contrail cirrus RF (Chen and Gettelman, 2013; Newinger and  
1745 Burkhardt, 2012). We estimate the associated uncertainty to be 5–10%.
- 1746 B4. From the sensitivity of the contrail cirrus RF to the temporal resolution in the air traffic dataset in  
1747 ECHAM5 and CAM, we deduce an uncertainty of about 10%.
- 1748 B5. The estimate of the feedback of natural clouds, due to contrail cirrus changing the water and heat  
1749 budget of the upper troposphere, is very uncertain and has not been properly quantified yet (Burkhardt  
1750 and Kärcher, 2011; Schumann et al., 2015). We assume here the uncertainty related to this estimate to  
1751 be only slightly smaller than the estimate itself, or about 15%.

1 July 2020 Revised

1752 B6. Uncertainty in the RF estimate of Chen and Gettelman (2013) to assumptions in the initial ice-  
1753 crystal radii and contrail cross-sectional areas is about 33%.

1754 We assume independence of the uncertainties except for the dependence of A3 and B3 on the uncertainty  
1755 in B2. The overall uncertainty due to the water budget and the contrail cirrus scheme (including  
1756 uncertainty A3) is about 40% and more than 50% in the case of the Chen and Gettelman (2013). From the  
1757 two different sources of uncertainty (list A, radiative, and list B, contrail cirrus properties, above) we  
1758 calculate an overall contrail cirrus RF uncertainty of about 70%, assuming independence of the overall  
1759 uncertainties described in A and B.

1760 Note that we do not attempt to infer an estimate for the uncertainty of the factor ERF/RF. When  
1761 calculating the contrail cirrus ERF, the error range given refers to the error range of contrail cirrus RF and  
1762 not ERF.

### 1763 F. Emission metrics calculations

1764 We calculate the AGWP and AGTP, and corresponding GWPs and GTPs, for aviation CO<sub>2</sub>, NO<sub>x</sub> (which  
1765 encompasses the ERF of short-term O<sub>3</sub>, CH<sub>4</sub>, CH<sub>4</sub>-induced O<sub>3</sub> and SWV), soot, SO<sub>2</sub>, and contrail cirrus.  
1766 The methodology and analytical expressions for the emissions metrics are described in detail in previous  
1767 literature (e.g., Fuglestedt et al. 2010; Myhre et al. 2013). The impulse response function (IRF) that  
1768 describes the atmospheric decay of CO<sub>2</sub> upon emission is taken from Joos et al. (2013). For the other  
1769 species, the atmospheric decay is given by a constant e-folding time taken as the ‘perturbation lifetime’.  
1770 The lifetimes used here are broadly consistent with Fuglestedt et al. (2010). The radiative efficiency (RE)  
1771 for CO<sub>2</sub> is calculated using year 2018 background concentrations of 407 ppm (annual mean, from monthly  
1772 mean observed concentrations from NOAA GMD -  
1773 [ftp://aftp.cmdl.noaa.gov/products/trends/co2/co2\\_mm\\_gl.txt](ftp://aftp.cmdl.noaa.gov/products/trends/co2/co2_mm_gl.txt)). This yields a RE of  $1.68 \times 10^{-15} \text{ W m}^{-2} \text{ kg}^{-1}$ ,  
1774 4% lower than used in the IPCC Fifth Assessment report (AR5) (Myhre et al., 2013). The climate response  
1775 IRF is taken from Boucher and Reddy (2008). The latter has an inherent equilibrium climate sensitivity  
1776 (ECS) of  $1.06\text{K} (\text{W m}^{-2})^{-1}$ , equivalent to a 3.9K equilibrium response to a doubling of CO<sub>2</sub>.

1777 For the calculation of the average rate of CO<sub>2</sub>-warming-equivalent emissions for aviation non-CO<sub>2</sub> forcings  
1778 ( $E_{\text{CO}_2\text{e}^*}$ ) under the GWP\* metric in **Table 5**, we use the relationship between recent changes in effective  
1779 RF and CO<sub>2</sub>-equivalent emissions from Allen et al. (2018) (or Equation (1) with  $\alpha = 0$ ),

$$1780 \quad E_{\text{CO}_2\text{e}^*} = [\Delta F / \Delta t] \times [H / \text{AGWP}_{\text{H}(\text{CO}_2)}] \quad (\text{F.1})$$

1781 where  $\Delta F$  is the change in ERF over the recent period,  $\Delta t$ , and  $\text{AGWP}_{\text{H}(\text{CO}_2)}$  is the absolute global warming  
1782 potential of CO<sub>2</sub> at time horizon H. We use updated  $\text{AGWP}_{\text{H}(\text{CO}_2)}$  values incorporating the updated  
1783 radiative efficiency of CO<sub>2</sub> as described in the previous paragraph. Allen et al. (2018) used a backward-  
1784 looking period of 20 years as  $\Delta t$ , whereas here we use a backward-looking 18-yr period as our time series  
1785 of ERF components only extends back to 2000.

### 1786 G. List of Acronyms and abbreviations used in tables and figures of the Appendices

1787 ACARE—Advisory Council for Aeronautical Research in Europe  
1788 ACCMIP—Atmospheric Chemistry and Climate Model Intercomparison Project  
1789 AEDT—Aviation Environmental Design Tool  
1790 AEM—Advanced Emission Model  
1791 AERO2K—Global aircraft emissions data project for climate impacts evaluation  
1792 AGAGE—Advanced Global Atmospheric Gases Experiment  
1793 CAM—Community Atmosphere Model  
1794 CCMoD—Contrail Cirrus Module  
1795 CH<sub>3</sub>CCl<sub>3</sub>—Methyl chloroform  
1796 COCIP—Contrail Cirrus Prediction Tool

1 July 2020 Revised

- 1797 CTM—Chemical Transport Model  
1798 ECHAM—European Centre/Hamburg Model  
1799 IPCC—Intergovernmental Panel on Climate Change  
1800 MAGICC—Model for the Assessment of Greenhouse Gas Induced Climate Change  
1801 MOZART—Model for OZone And Related chemical Tracers  
1802 NOAA—National Oceanic and Atmospheric Administration  
1803 QUANTIFY—Quantifying the Climate Impact of Global and European Transport System  
1804 REACT4C—Reducing Emissions from Aviation by Changing Trajectories for the benefit of Climate  
1805 RCP—Representative Concentration Pathway  
1806 SRES—Special Report on Emission Scenarios  
1807 TAR—Third Assessment Report  
1808 TRADEOFF—Aircraft emissions: contribution of different climate components to changes in radiative  
1809 forcing—tradeoff to reduce atmospheric impact  
1810 TROPOS—2D global TROPOSpheric model  
1811 WDCGG—World Data Centre for Greenhouse Gases

1 July 2020 Revised

1812 **Table D.1.** The CH<sub>4</sub> RFs derived for all the aircraft emission  
 1813 inventories that are present in the model ensemble.<sup>a</sup>

Inventories	CH <sub>4</sub> RF, mW m <sup>-2</sup>	
	Old	New
AEDT	-6.67	-8.22
AEM	-6.82	-8.41
AERO2K	-7.09	-8.74
REACT4C	-6.97	-8.59
QUANTIFY	-6.96	-8.58
TRADEOFF	-7.11	-8.76

1814 <sup>a</sup> Values are those represented in the model ensemble based on MOZART-3  
 1815 CTM simulations (Old) and recalculated values using a revised simplified  
 1816 expression for the CH<sub>4</sub> RF (New) as presented by Etmann et al. (2016). The  
 1817 NO<sub>x</sub> emissions of each inventory are normalized so that all RFs are scaled to  
 1818 the same global total emissions (0.71 Tg(N) yr<sup>-1</sup>) as in the REACT4C model.

1819

1820 **Table D.2.** The best NO<sub>x</sub> RFs per unit emission derived for datasets that include and exclude late 1990s  
 1821 numbers and related estimates, see text for details.

Components	Value	Uncertainty*	Value	Uncertainty*
	(mW m <sup>-2</sup> (Tg (N) yr <sup>-1</sup> ) <sup>-1</sup> )			
	with IPCC (1999)		without IPCC (1999)	
Short-term O <sub>3</sub>	25.6	±7.3	25.1	±7.2
CH <sub>4</sub>	-13.8	±4.7	-13.4	±4.5
CH <sub>4</sub> -induced O <sub>3</sub>	-6.9	±2.3	-6.7	±2.3
SWV	-2.1	±0.7	-2.0	±0.7
Net NO <sub>x</sub>	3.9	±5.7	4.0	±5.8

1822 \*Stated uncertainties are one standard deviation (68% confidence interval).

1823



1 July 2020 Revised

1824 **Table D.3.** Methane response in TROPOS and other studies

Variable	Year	2D CTM, TROPOS		Study	Literature		Variable estimate/change
		Transient	Steady-state <sup>a</sup>		Ref	Model/Years	
CH <sub>4</sub> burden, Tg	2000	4770.8	4785.1	IPCC TAR		1998	4850 Tg
				Voulgarakis et al 2013		ACCMIP	4750 <sup>d</sup> Tg
				Dalsøren et al 2016		Oslo CTM3	4560 <sup>d</sup> Tg
				Dalsøren et al 2016		1970–2012	+15 %
				This study <sup>c</sup>			+13 %
	2050	5051.6	5081.4	Voulgarakis et al 2013		ACCMIP	5000 <sup>d</sup> Tg
			Voulgarakis et al 2013		2000–2050	+5.3 <sup>d</sup> %	
			This study <sup>c</sup>			+5.9 %	
CH <sub>4</sub> abundance, ppb	2000	1784.2	1787.5	Observations		NOAA AGAGE WDCGG	1773 ppb 1774 ppb 1783 ppb
	2050	1886.2	1897.6	Meinshausen et al 2011		MAGICC	1833 ppb
CH <sub>4</sub> lifetime (τ <sub>CH<sub>4</sub>+OH</sub> ) <sup>b</sup> , yr	2000	10.6	10.5	Prather et al 2012		CH <sub>3</sub> CCl <sub>3</sub> -based	11.2 ± 1.3 yr
				Voulgarakis et al 2013		ACCMIP	9.8 ± 1.6 yr
				Holmes et al 2013		1980/85–2000/05	-2.2 ± 1.8 %
				This study <sup>c</sup>			-2.06 %
				Voulgarakis et al 2013		1980–2000	-4 %
	This study <sup>c</sup>			-2 %			
2050	11.0	11.0	Voulgarakis et al 2013		2000–2050	+1.0 <sup>d</sup> %	
			This study <sup>c</sup>			+3.5 %	
aircraft CH <sub>4</sub> lifetime (τ <sub>CH<sub>4</sub>+OH</sub> ), yr	2000	-0.137	-0.145	Hoor et al 2009		AERO2K	-1.55 % Tg(N) <sup>-1</sup>
				Myhre et al 2011		QUANTIFY	-1.46 % Tg(N) <sup>-1</sup>
				Holmes et al 2011		Model ensemble	-1.77 % Tg(N) <sup>-1</sup>
				Søvde et al 2014		REACT4C	-1.36 % Tg(N) <sup>-1</sup>
				This study <sup>c</sup>		dE <sub>NO<sub>x</sub></sub> =QUANTIFY	-1.48 % Tg(N) <sup>-1</sup>
	2050	-0.293	-0.311	Hodnebrog et al 2011		SRES B1	-1.61 % Tg(N) <sup>-1</sup>
						B1 ACARE	-1.48 % Tg(N) <sup>-1</sup>
				Hodnebrog et al 2012		SRES A1B	-1.22 % Tg(N) <sup>-1</sup>
				Khodayari et al 2014a		AEDT Scenario1	-1.88 % Tg(N) <sup>-1</sup>
				This study <sup>c</sup>		AEDT Baseline	-1.59 % Tg(N) <sup>-1</sup>
				RCP45	-1.36 % Tg(N) <sup>-1</sup>		

1825

1826

1 July 2020 Revised

1827 **Table D.4.** Calculated CH<sub>4</sub> correction factors

Aviation emissions year	CH <sub>4</sub> correction factors	
	This study	Grewe and Stenke (2008) methodology
2000	0.73	0.65
2005	0.75	0.73
2011	0.78	0.81
2018	0.79	0.86

1828

1829 **Table E.1.** Scaling of contrail cirrus RF and ERF results <sup>a</sup>

Model	Inventory	Representation of flight distance	RF (mW/m <sup>2</sup> )	Scalings	Scaled RF (mW/m <sup>2</sup> ) <sup>b</sup>	Reference
ECHAM4-CCMod	AERO2K 2002	track	38	S <sub>1</sub> , S <sub>2</sub> , S <sub>4</sub>	70	Burkhardt and Kärcher (2011)
ECHAM5-CCMod	AEDT 2006	slant	56	S <sub>3</sub> , S <sub>4</sub>	56	Bock and Burkhardt (2016)
COCIP	AEDT 2006	flight vectors	63	S <sub>4</sub>	72	Schumann et al. (2015)
CAM5	AEDT 2006	slant	13 [57] <sup>c</sup>	S <sub>3</sub> , S <sub>4</sub>	57	Chen and Gettelman (2013)
Best estimate					66 <sup>d</sup>	

1830 <sup>a</sup> Adapted from Table 1 of Bock and Burkhardt (2016).1831 <sup>b</sup> RF that would be expected in 2006 when using slant distance from the AEDT inventory with hourly resolution.1832 <sup>c</sup> An updated simulation (see text) yielded 57 mW m<sup>-2</sup>.1833 <sup>d</sup> The best estimate is of RFs, and excludes the Chen and Gettelman (2013) results since this is closer to an ERF (see main text).

1834

1835

1836

1837

1 July 2020 Revised

1838 **Table F.1a.** Emission metrics and corresponding CO<sub>2</sub>-equivalent emissions for the ERF components of  
 1839 2018 aviation emissions and cloudiness using CO<sub>2</sub> IRF without C-cycle feedbacks from Gasser et al.  
 1840 (2017), and climate IRF from Boucher and Reddy (2008).

1841 **Metrics**

ERF term	GWP <sub>20</sub>	GWP <sub>50</sub>	GWP <sub>100</sub>	GTP <sub>20</sub>	GTP <sub>50</sub>	GTP <sub>100</sub>
CO <sub>2</sub>	1	1	1	1	1	1
Contrail cirrus (Tg CO <sub>2</sub> basis)	2.39	1.15	0.68	0.70	0.11	0.10
Contrail cirrus (km basis)	40	19	11	12	1.9	1.6
Net NO <sub>x</sub>	637	216	122	-231	-75	14
Aerosol-radiation						
Soot emissions	4409	2125	1252	1295	210	177
SO <sub>2</sub> emissions	-856	-412	-243	-251	-41	-34
Water vapor emissions	0.22	0.11	0.06	0.07	0.01	0.009

1842

1843 **Table F.1b.** Emission metrics and corresponding CO<sub>2</sub>-equivalent emissions for the ERF components of  
 1844 2018 aviation emissions and cloudiness using CO<sub>2</sub> IRF without C-cycle feedbacks, and climate IRF from  
 1845 Gasser et al. (2017).

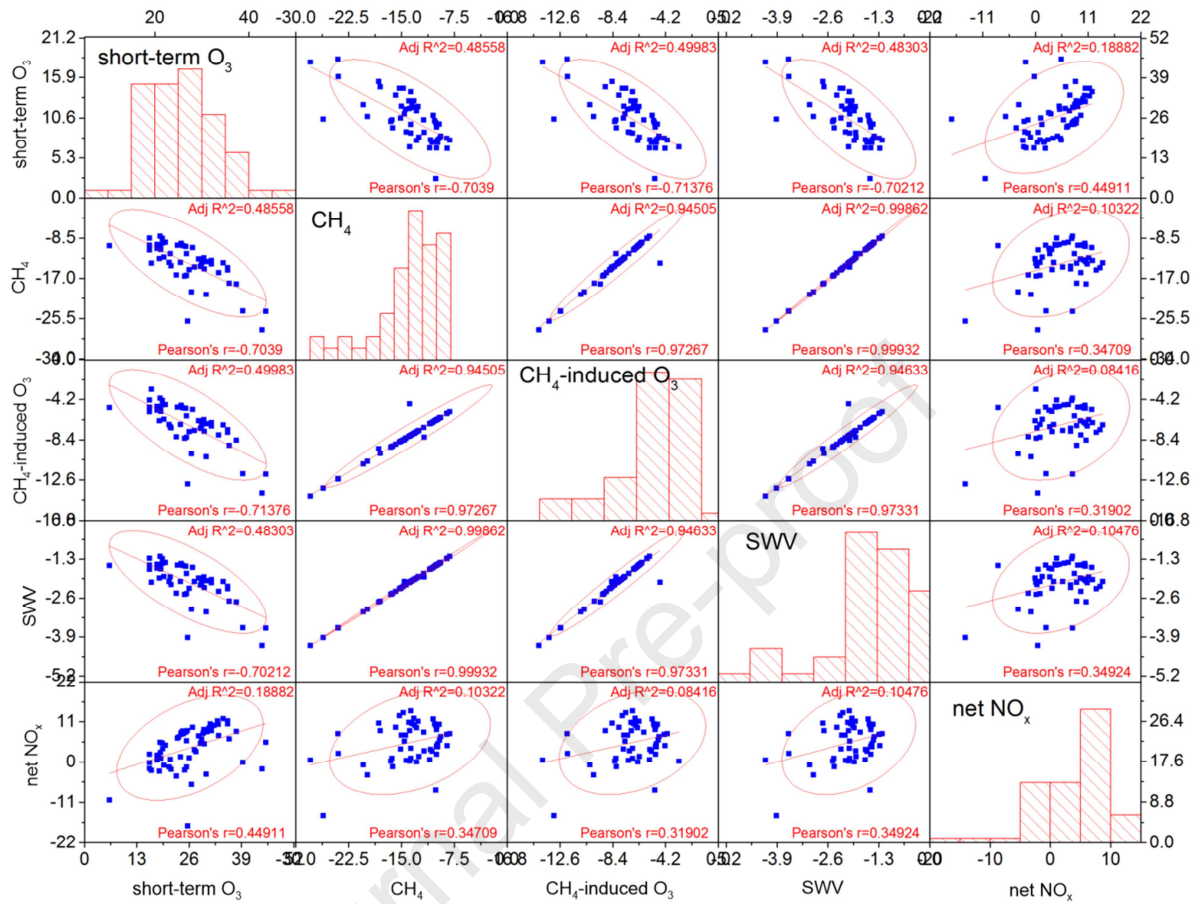
1846 **Metrics**

ERF term	GWP <sub>20</sub>	GWP <sub>50</sub>	GWP <sub>100</sub>	GTP <sub>20</sub>	GTP <sub>50</sub>	GTP <sub>100</sub>
CO <sub>2</sub>	1	1	1	1	1	1
Contrail cirrus (Tg CO <sub>2</sub> basis)	2.39	1.15	0.68	0.3	0.19	0.15
Contrail cirrus (km basis)	40	19	11	4	3.3	2.6
Net NO <sub>x</sub>	637	216	122	-420	-18	22
Aerosol-radiation						
Soot emissions	4409	2125	1252	466	360	284
SO <sub>2</sub> emissions	-856	-412	-243	-90	-70	-55
Water vapor emissions	0.22	0.11	0.06	0.03	0.018	0.014

1847

1 July 2020 Revised

1848

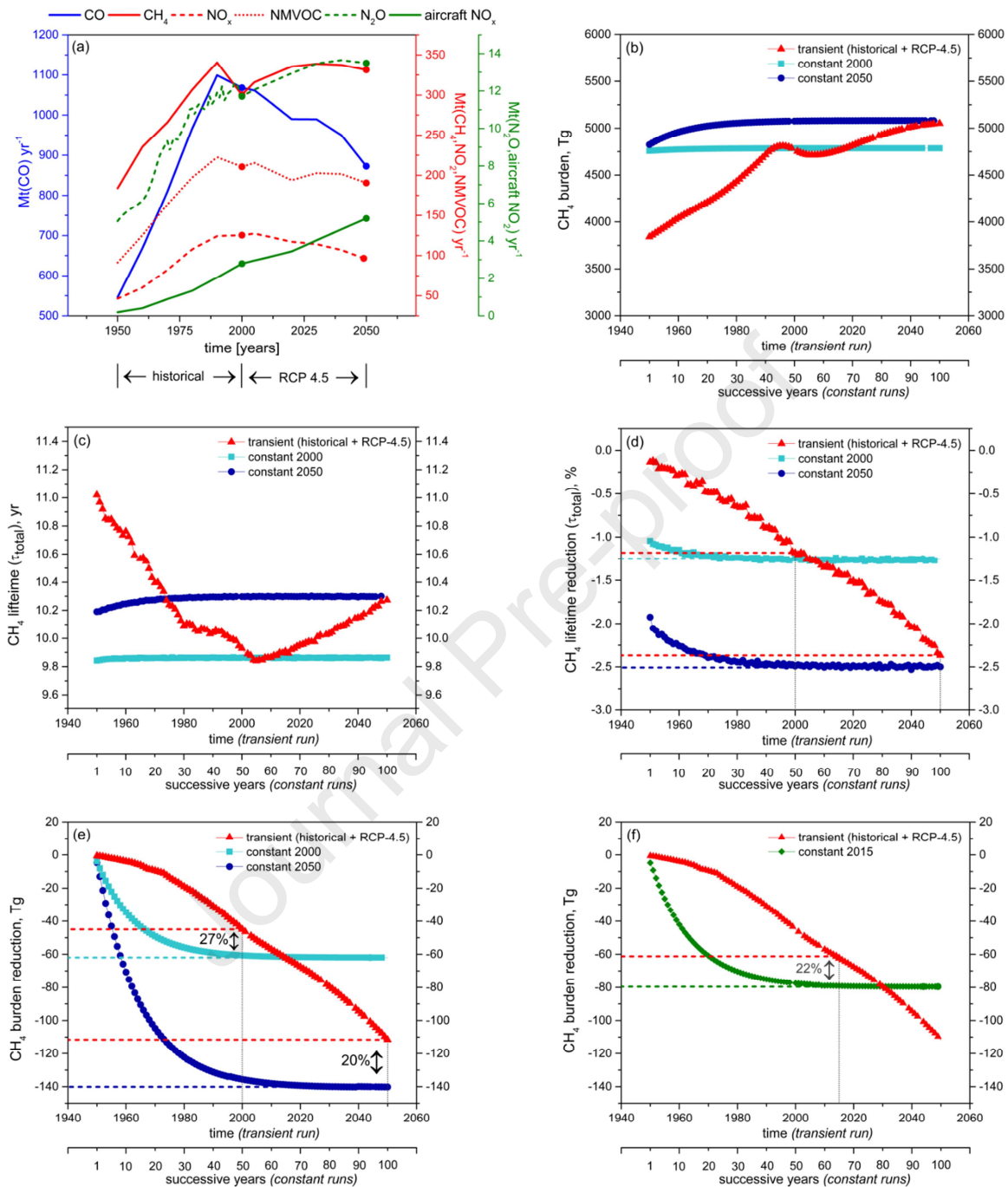


1849

1850 **Figure D.1.** Matrix of pair-wise scatter plots of RF values from NO<sub>x</sub> terms: short-term O<sub>3</sub>, CH<sub>4</sub>, CH<sub>4</sub>-  
 1851 induced O<sub>3</sub>, SWV and net NO<sub>x</sub> (i.e., the sum of all 4 components), all represented as normalized RFs  
 1852 (mW m<sup>-2</sup> (Tg(N)yr<sup>-1</sup>)<sup>-1</sup>) from the ensemble studies (see details in text). The red line is the linear fit, the  
 1853 ellipse shows the 95% confidence level and histograms present frequencies.

1854

1 July 2020 Revised



1855

1856 **Figure D.2.** (a) Past and future anthropogenic emissions of CO, CH<sub>4</sub>, NO<sub>x</sub>, NMVOC, N<sub>2</sub>O and aircraft  
 1857 NO<sub>x</sub> (IIASA RCP Database: <http://www.iiasa.ac.at/web-apps/tnt/RcpDb/>). Dots represent conditions for  
 1858 'constant 2000' and 'constant 2050' simulations.

1859 (b) Evolution of the global CH<sub>4</sub> burden in TROPOS for transient aircraft NO<sub>x</sub> emissions combining  
 1860 historical emissions (1950–2000) and RCP-4.5 emissions (2000–2050); and constant emissions for the  
 1861 years 2000 and 2050.

1 July 2020 Revised

1862 (c) Global CH<sub>4</sub> lifetime due to aircraft NO<sub>x</sub> emissions in TROPOS for transient emissions combining  
1863 historical emissions (1950–2000) and RCP-4.5 emissions (2000–2050); and constant emissions for the  
1864 years 2000 and 2050.

1865 (d) Global CH<sub>4</sub> lifetime reduction due to aircraft NO<sub>x</sub> emissions in TROPOS for transient emissions  
1866 combining historical emissions (1950–2000) and RCP-4.5 emissions (2000–2050); and constant  
1867 emissions for the years 2000 and 2050. The dashed lines represent 2000 and 2050 equilibrium values  
1868 (light and dark blue) and 2000 and 2050 transient values (red).

1869 (e) Global CH<sub>4</sub> burden reduction due to aircraft NO<sub>x</sub> emissions in TROPOS for transient emissions  
1870 combining historical emissions (1950–2000) and RCP-4.5 emissions (2000–2050); and constant  
1871 emissions for the years 2000 and 2050. The dashed lines represent 2000 and 2050 equilibrium values  
1872 (light and dark blue) and 2000 and 2050 transient values (red).

1873 (f) Global CH<sub>4</sub> burden reduction due to aircraft NO<sub>x</sub> emissions in TROPOS for transient emissions  
1874 combining historical emissions (1950–2000) and RCP-4.5 emissions (2000–2050); and constant  
1875 emissions for the year 2018. The dashed lines represent 2018 equilibrium (green) and transient values  
1876 (red).

1877

**Highlights**

- Global aviation warms Earth's surface through both CO<sub>2</sub> and net non-CO<sub>2</sub> contributions.
- Global aviation contributes a few percent to anthropogenic radiative forcing.
- Non-CO<sub>2</sub> impacts comprise about 2/3 of the net radiative forcing.
- Comprehensive and quantitative calculations of aviation effects are presented.
- Data are made available to analyze past, present and future aviation climate forcing.

Journal Pre-proof

**Declaration of competing interest**

The authors\* declare that they have no known competing financial interests or personal relationships that could have appeared to influence the work reported in this paper.

Authors\* **D. S. Lee, D. W. Fahey, A. Skowron, M. R. Allen, U. Burkhardt, Q. Chen, S. J. Doherty, S. Freeman, P.M. Forster, J. Fuglestedt, A. Gettelman, R. R. De León, L. L. Lim, M. T. Lund, R. J. Millar, B. Owen, J. E. Penner, G. Pitari, M. J. Prather, R. Sausen, L. J. Wilcox**